



# CHORUS

This is the accepted manuscript made available via CHORUS. The article has been published as:

## Curvature corrections to the nonlocal interfacial model for short-ranged forces

José M. Romero-Enrique, Alessio Squarcini, Andrew O. Parry, and Paul M. Goldbart

Phys. Rev. E **97**, 062804 — Published 25 June 2018

DOI: [10.1103/PhysRevE.97.062804](https://doi.org/10.1103/PhysRevE.97.062804)

# The non-local interfacial model for short-ranged forces revisited

José M. Romero-Enrique,<sup>1</sup> Alessio Squarcini,<sup>2,3</sup> Andrew O. Parry,<sup>4</sup> and Paul M. Goldbart<sup>5</sup>

<sup>1</sup> *Departamento de Física Atómica, Molecular y Nuclear, Área de Física Teórica, Universidad de Sevilla, Avenida de Reina Mercedes s/n, 41012 Seville, Spain*

<sup>2</sup> *Max-Planck-Institut für Intelligente Systeme, Heisenbergstr. 3, D-70569 Stuttgart, Germany*

<sup>3</sup> *IV. Institut für Theoretische Physik, Universität Stuttgart, Pfaffenwaldring 57, D-70569 Stuttgart, Germany*

<sup>4</sup> *Department of Mathematics, Imperial College London, London SW7 2AZ, United Kingdom*

<sup>5</sup> *School of Physics, Georgia Institute of Technology, 837 State Street, Atlanta, Georgia 30332, USA*

In this paper we revisit the derivation of a non-local interfacial Hamiltonian model for systems with short-ranged intermolecular forces. Starting from a microscopic Landau-Ginzburg-Wilson Hamiltonian with a double parabola potential we reformulate the derivation of the interfacial model using a rigorous boundary integral approach. This is done for three scenarios: a single fluid phase in contact with a non-planar substrate (wall), a free interface separating coexisting fluid (liquid and gas, say) phases, and finally a liquid-gas interface in contact with a non-planar confining wall as applicable to wetting phenomena. For the first two cases our approach identifies the correct form of the curvature corrections to the free energy and, for the case of a free-interface, allows us to recast these as an interfacial self-interaction as has been conjectured previously in the literature. When the interface is in contact with a substrate our approach similarly identifies curvature corrections to the non-local binding potential, describing the interaction of the interface and wall, for which we propose a generalised and improved diagrammatic formulation.

PACS numbers: 02.30.Rz, 05.20.Jj, 68.03.Cd, 68.08.Bc, 68.35.Md

## I. INTRODUCTION

Whilst significant progress has been made in the last few decades in understanding the statistical mechanics of inhomogeneous fluids and related interfacial phenomena [1–4], from a fundamental perspective many challenges remain for theory. Techniques based on molecular methods such as computer simulations [5, 6] and Density Functional Theory [1, 7] are wide spread, but under some circumstances large lengthscales emerge which make the use of mesoscopic models, often referred to as effective interfacial Hamiltonian or capillary-wave models, much more convenient and useful [8–10]. These, in fact, have been pivotal in the development of the fluctuation theory of the thermal-wandering-induced roughness associated with a free or weakly pinned liquid-gas interface [8], and also the classification of critical singularities occurring at continuous surface phase transitions such as wetting [2–4, 11–13] and wedge filling [14–23]. The search for a link between truly microscopic approaches and these mesoscopic descriptions can be traced back to van der Waals [24] and continue to this day, and in the last few years considerable effort has been invested in establishing this connection more rigorously. For example, intrinsic sampling methods use a many-body percolative, approach to identify the interfacial position from the underlying microscopic molecular configurations, and this has been extensively used in simulations [25–38]. A second, related, development has been the attempt to systematically derive an interfacial model for wetting transitions in settings involving short-ranged intermolecular forces from a more microscopic starting point [39–45]. The need for this was originally driven by the significant discrepancy

between initial predictions of strong non-universality for 3D critical wetting, based on renormalization group studies of local, partly phenomenologically justified, interfacial models [11, 12], and the findings of more microscopic Ising model simulation studies, which only reported minor deviations from mean-field-like behaviour [46]. In attempting to explain this, Fisher and Jin [47, 48] set out a very useful systematic basis for the derivation of an interfacial model from an underlying continuum Landau-Ginzburg-Wilson (LGW) Hamiltonian. Their idea was to introduce a constraint that specifies the interfacial configuration [which we denote  $\ell(\mathbf{x})$ ] from that of the more microscopic order parameter  $m(\mathbf{r})$ . Different options are available, such as the crossing criterion, in which  $\ell(\mathbf{x})$  is identified as the surface on which the order parameter takes some specified value or, alternatively, integral criteria which are generalised measures of the local adsorption. Once the interface is defined, the interfacial Hamiltonian  $H[\ell]$  is identified via the partial trace:

$$e^{-\beta H[\ell]} = \int Dm e^{-\beta \mathcal{H}_{LGW}[m]} \approx e^{-\beta \mathcal{H}_{LGW}[m_{\Xi}]}, \quad (1)$$

where  $m_{\Xi}(\mathbf{r})$  is the profile that *minimizes* the LGW Hamiltonian  $\mathcal{H}_{LGW}[m]$ , subject to the constraint and additional boundary conditions. The Fisher-Jin identification [47, 48], generalised to non-planar walls, will be the starting point for our entire investigation. Within this scheme, therefore, all that is required is the determination of the constrained profile  $m_{\Xi}(\mathbf{r})$ , which will be a functional of the interfacial configuration (and wall shape). Fisher and Jin obtained this for a planar wall by considering perturbations about the flat interfacial configuration. However this perturbative approach is inadequate for the purposes at hand because it misidentifies

the structure of corrections to the standard local interfacial model. Indeed, this leads to serious problems when carried forward in renormalization group studies, where it erroneously alters the structure of the well-known global phase diagrams for wetting [49]. Later, it was appreciated that the solutions to the constrained mean-field-like equations for  $m_{\Xi}(\mathbf{r})$  could be reformulated using Green's functions [39, 40]. This highlights immediately the *non-local* nature of the interaction of the interface and substrate, which has a simple diagrammatic representation. Furthermore, it resolves many of the problems associated with the fluctuation theory of critical wetting and, in addition, yields a description of correlation functions fully consistent with exact sum-rules [42, 43]. The predictions of this non-local model are also consistent with more recent Ising model simulations, which reported deviations from mean-field behavior for critical wetting [50]. The non-local decay of order between a fluctuating interface and particles situated away from it, predicted by this approach, has been seen directly, in both Ising model and molecular simulation studies [35, 51].

In this paper we present an alternative and more rigorous derivation of the non-local interfacial model to that presented originally [39, 40], which was still partly physically motivated. Our new derivation is based on exact integral representations of the solutions of linear partial differential equations on a closed domain, which are cast as functionals of the solutions at the boundaries. This method, referred to as the boundary element method, has in fact been applied successfully to numerous engineering problems [52, 53]. Here, we develop an improved perturbative diagrammatic approach, which is related to the multiple reflection method used in the celebrated analysis of the wave equation yielding eigenfrequencies in a closed domain [54–56]. When applying this methodology to the evaluation of the interfacial free energy and order-parameter profile of a fluid phase in contact with a structured substrate or of a constrained liquid-gas configuration, we recover, at leading-order, the previous non-local model but now with curvature corrections. For the case of a constrained liquid-gas interface this leads naturally to an interfacial self-interaction precisely as has been conjectured [57]. The most detailed application of this method involves the rigorous determination of the binding potential functional for wetting films in contact with a non-planar wall. Here, we identify an additional series of diagrams, not present in the original formulation, which arise when the substrate and liquid-gas interface are not parallel. These diagrams are re-summed to obtain a new version of the non-local model which recovers the original version of the non-local model in certain limits.

Our paper is arranged as follows: In Section II we present the theoretical framework and recall the mathematical tools used in our approach. In Section III we apply this to a single phase, which we take to be liquid, in contact with a wall to determine the mean-field excess free-energy functional  $F_{wl}[\psi]$ , which is a functional

of the wall shape  $\psi$ . In Section IV we extend this to a free liquid-gas interface, and determine the interfacial Hamiltonian  $H[\ell]$ , which is a functional of the (constrained) interfacial configuration  $\ell$ . Finally, we consider the most involved situation, in which a constrained wetting film located near to a non-planar wall, and we determine the binding potential  $W[\ell, \psi]$ , which is a functional of both the interface and the wall shapes.

## II. THEORETICAL FRAMEWORK

Consider the LGW Hamiltonian defined on a domain  $\Omega$ :

$$\mathcal{H}_{LGW}[m] = \int_{\Omega} d\mathbf{r} \left\{ \frac{1}{2} (\nabla m)^2 + \Delta\phi(m) \right\} + \int_{\partial\Omega} \Phi_s(\mathbf{s}) ds, \quad (2)$$

where the shifted potential  $\Delta\phi(m)$  corresponds to the excess contribution, with respect to the bulk, of the free-energy density, and  $\Phi_s$  is a surface potential defined on the domain boundary  $\partial\Omega$ . Typically,  $\Phi_s$  is taken to be a quadratic function of  $m(\mathbf{s})$ , i.e.,

$$\Phi_s(\mathbf{s}) = -\frac{g}{2} \left[ m(\mathbf{s}) + \frac{h_1}{g} \right]^2, \quad (3)$$

where  $h_1$  and  $g$  are a local field and an enhancement parameter, respectively, modelling the coupling to the substrate (i.e., wall). Usually, these quantities are taken to be equal to their flat-wall counterparts, although additional curvature-induced terms may be included phenomenologically. Finally, we note that fixed (i.e., Dirichlet) boundary conditions correspond to the limit  $h_1 \rightarrow \infty$ ,  $g \rightarrow -\infty$  with  $-h_1/g = m_1$  where  $m_1$  is the fixed value of the order parameter at the wall.

In zero external field (i.e.,  $h = 0$ ) and below the bulk critical temperature  $T_c$ , the shifted potential  $\Delta\phi$  has a familiar double-well structure, which we capture via the simple double-parabola (DP) approximation:

$$\Delta\phi(m) = \frac{\kappa^2}{2} (|m| - m_0)^2, \quad (4)$$

where  $\kappa$  is the inverse bulk correlation length and  $m_0$  is the bulk order parameter. In this description, therefore, there are two bulk phases having order-parameter values  $-m_0$  (which we regard as the gas phase) and  $+m_0$  (which we regard as the liquid phase). For a general inhomogeneous situation, we will identify the phase at any point via the sign of the order parameter. Consequently, we shall refer to the phase as gas if  $m < 0$  and liquid otherwise. Finally, we adopt a simple crossing criterion of a constrained interfacial configuration, whereby the interface is defined as the surface on which the order parameter vanishes, i.e.,  $m = 0$  [47, 48].

As the constrained profile  $m_\Xi$  minimizes the LGW Hamiltonian, it satisfies the mean-field like Euler-Lagrange equation:

$$\nabla^2 m_\Xi = \kappa^2(m_\Xi - m_b), \quad (5)$$

where  $m_b = \pm m_0$ , depending on whether the bulk phase is liquid or gas. This partial differential equation is to be solved subject to the natural boundary condition

$$\mathbf{n} \cdot \nabla m_\Xi(\mathbf{s}) = h_1 + g m_\Xi(\mathbf{s}), \quad (6)$$

where  $\mathbf{n}$  is the outward normal to the boundary of the integration domain  $\Omega$ . If fixed boundary condition are applied on  $\mathbf{s}$ , we simply set  $m_\Xi(\mathbf{s}) = m_1$  instead of imposing Eq. (6).

In order to obtain the mean-field free energy, we first consider the situation where there is only one phase in the integration domain. Multiplying Eq. (5) by  $(m_\Xi - m_b)/2$ , and integrating over the domain  $\Omega$  we get

$$\int_\Omega d\mathbf{r} \frac{(m_\Xi - m_b) \nabla^2 m_\Xi}{2} = \int_\Omega \frac{\kappa^2}{2} (m_\Xi - m_b)^2. \quad (7)$$

We now use the identity  $u \nabla^2 u + \nabla u \cdot \nabla u = \nabla \cdot (u \nabla u)$  with  $u = m_\Xi - m_b$  and apply the divergence theorem to obtain

$$\begin{aligned} \int_\Omega d\mathbf{r} \left\{ \frac{1}{2} (\nabla m_\Xi)^2 + \frac{\kappa^2}{2} (m_\Xi - m_b)^2 \right\} \\ = \oint_{\partial\Omega} ds \frac{m_\Xi(\mathbf{s}) - m_b}{2} (\mathbf{n} \cdot \nabla m_\Xi(\mathbf{s})). \end{aligned} \quad (8)$$

Next, we make use of Eq. (6) to re-write the surface contribution to Eq. (2) using

$$\begin{aligned} \Phi_s(\mathbf{s}) &= -\frac{1}{2} \left( m_\Xi(\mathbf{s}) + \frac{h_1}{g} \right) (\mathbf{n} \cdot \nabla m_\Xi(\mathbf{s})) \\ &= - \left[ \frac{m_\Xi(\mathbf{s}) - m_b}{2} + \frac{h_1 + g m_b}{2g} \right] (\mathbf{n} \cdot \nabla m_\Xi(\mathbf{s})). \end{aligned} \quad (9)$$

Hence, when evaluated at the equilibrium profile  $m_\Xi$  the LGW Hamiltonian identifies the free energy as

$$\begin{aligned} \mathcal{H}_{LGW}[m_\Xi] &= \int_\Omega d\mathbf{r} \left\{ \frac{1}{2} (\nabla m_\Xi)^2 + \frac{\kappa^2}{2} (m_\Xi - m_b)^2 \right\} \\ &\quad + \oint_{\partial\Omega} \Phi_s(\mathbf{s}) ds, \end{aligned} \quad (10)$$

and reduces to

$$\mathcal{H}_{LGW}[m_\Xi] = -\frac{h_1 + g m_b}{2g} \oint_{\partial\Omega} ds \mathbf{n} \cdot \nabla m_\Xi(\mathbf{s}), \quad (11)$$

a result that will be central to our method.

In the presence of a wetting layer of a different phase that intrudes between the wall and the bulk (see Fig. 1) the domain  $\Omega$  must be considered to be the union  $\Omega = \cup_i \Omega_i$ , where each appropriate sub-domain  $\Omega_i$  has boundaries  $\partial\Omega_i$  that lie either on the substrate surface or at

the liquid-gas interface. We denote  $\partial\Omega_i = \partial\Omega_{1,i} \cup \partial\Omega_{2,i}$ , where the boundary condition Eq. (6) is satisfied in  $\partial\Omega_{1,i}$  and  $\partial\Omega_{2,i}$  corresponds to the gas-liquid interface. For this case, the generalization of Eq. (8) identifies the constrained free-energy functional for a given interfacial configuration as

$$\begin{aligned} \mathcal{H}_{LGW}[m_\Xi] &= \\ &= \sum_i \left[ \int_{\Omega_i} d\mathbf{r} \left\{ \frac{1}{2} (\nabla m_\Xi)^2 + \frac{\kappa^2}{2} (m_\Xi - (m_b)_i)^2 \right\} \right. \\ &\quad \left. + \int_{\partial\Omega_{1,i}} ds \Phi_s(\mathbf{s}) \right], \end{aligned} \quad (12)$$

which reduces to

$$\begin{aligned} \mathcal{H}_{LGW}[m_\Xi] &= \sum_i \left[ -\frac{h_1 + g m_b}{2g} \int_{\partial\Omega_{1,i}} ds \mathbf{n} \cdot \nabla m_\Xi(\mathbf{s}) \right. \\ &\quad \left. - \frac{(m_b)_i}{2} \int_{\partial\Omega_{2,i}} ds (\mathbf{n} \cdot \nabla m_\Xi(\mathbf{s})) \right] \end{aligned} \quad (13)$$

The mean-field free energy corresponds to the interfacial configuration that gives the least free energy. In this sense, the free energy becomes a functional of the interfacial profile.

The above results demonstrate that, for the potential, the equilibrium free energy of an interfacial configuration may be determined in terms of the normal derivatives of the order parameter at the substrate and liquid-gas interface (if present). This simplification is not so surprising, given that, for the DP potential, the whole order parameter profile can be obtained formally in terms of the values at the boundaries. To see this, let us consider the (rescaled) Green's function that solves

$$\mathcal{L}K(\mathbf{r}, \mathbf{r}_0) \equiv (-\nabla_{\mathbf{r}}^2 + \kappa^2) K(\mathbf{r}, \mathbf{r}_0) = 2\kappa \delta(\mathbf{r} - \mathbf{r}_0), \quad (14)$$

and which vanishes as  $|\mathbf{r} - \mathbf{r}_0| \rightarrow \infty$ . The subscript in  $\nabla_{\mathbf{r}}^2$  denotes that the nabla operator acts on the argument  $\mathbf{r}$  of  $K$ . Its solution is the Ornstein-Zernike correlation function

$$K(\mathbf{r}, \mathbf{r}_0) = \frac{\kappa \exp(-\kappa|\mathbf{r} - \mathbf{r}_0|)}{2\pi |\mathbf{r} - \mathbf{r}_0|}. \quad (15)$$

The second Green's identity for the Hermitian operator  $\mathcal{L}$  states that

$$\int_\Omega d\mathbf{r} [v \mathcal{L}u - u \mathcal{L}v] = - \int_{\partial\Omega} [v(\mathbf{n} \cdot \nabla u) - u(\mathbf{n} \cdot \nabla v)] ds \quad (16)$$

for any domain  $\Omega$  with boundary  $\partial\Omega$ , where the outward normal is  $\mathbf{n}$  and  $u$  and  $v$  are arbitrary functions. If we choose  $u(\mathbf{r}) = K(\mathbf{r}, \mathbf{r}_0)/2\kappa$  and  $v(\mathbf{r}) = m_\Xi(\mathbf{r}) - m_b$ , and taking into account Eqs. (5) and (14), then

$$\begin{aligned} (m_\Xi(\mathbf{r}) - m_b) \Theta_\Omega(\mathbf{r}) &= \frac{1}{2\kappa} \int_{\partial\Omega} ds K(\mathbf{s}, \mathbf{r}) (\mathbf{n} \cdot \nabla m_\Xi(\mathbf{s})) \\ &\quad - \frac{1}{2\kappa} \int_{\partial\Omega} ds (m_\Xi(\mathbf{s}) - m_b) (\mathbf{n} \cdot \nabla_{\mathbf{s}} K(\mathbf{s}, \mathbf{r})), \end{aligned} \quad (17)$$

where  $\Theta_\Omega(\mathbf{r})$  is the characteristic function of the set  $\Omega$ , i.e.,  $\Theta_\Omega(\mathbf{r}) = 1$  if  $\mathbf{r} \in \Omega$ , and  $\Theta_\Omega(\mathbf{r}) = 0$  otherwise (excluding in both cases the boundary  $\partial\Omega$ ). As before,  $\partial\Omega_1$  refers to the portion of the boundary where the Eq. (6) is satisfied, whilst  $\partial\Omega_2$  lies on the appropriate side of gas-liquid interface (see Fig. 1). We can then recast Eq. (17) as

$$\begin{aligned}
(m_\Xi(\mathbf{r}) - m_b)\Theta_\Omega(\mathbf{r}) &= \frac{1}{2\kappa} \int_{\partial\Omega_1} ds \left( \frac{h_1}{g} + m_b \right) \partial_n K(\mathbf{s}, \mathbf{r}) \\
&+ \frac{m_b}{2\kappa} \int_{\partial\Omega_2} ds \partial_n K(\mathbf{s}, \mathbf{r}) \\
&+ \frac{1}{2\kappa} \int_{\partial\Omega_1} ds \left( K(\mathbf{s}, \mathbf{r}) - \frac{1}{g} \partial_n K(\mathbf{s}, \mathbf{r}) \right) \partial_n m_\Xi(\mathbf{s}) \\
&+ \frac{1}{2\kappa} \int_{\partial\Omega_2} ds K(\mathbf{s}, \mathbf{r}) \partial_n m_\Xi(\mathbf{s}), \tag{18}
\end{aligned}$$

where  $\partial_n$  denotes the normal derivative  $\mathbf{n} \cdot \nabla_{\mathbf{s}}$ .

What remains is the determination of the normal derivative  $\partial_n m_\Xi$  at each point along the sub-domain boundaries. However, Eq. (18) itself cannot be used to determine these, and we must use a technique to modify this appropriately. To this end, we first place  $\mathbf{r}$  at a boundary point *and* deform the boundary near it by by cutting a circular hole of radius  $\epsilon$  and adding a hemispherical cap atop it, so that the point is again inside the sub-domain under consideration. We then evaluate the order parameter at  $\mathbf{r}$ , and finally take the limit  $\epsilon \rightarrow 0$ . Assuming the interfaces are smooth, we obtain the following integral equation within each domain:

$$\begin{aligned}
\frac{m_\Xi(\mathbf{s}_0) - m_b}{2} &= \frac{1}{2\kappa} \int_{\partial\Omega_1} ds \left( \frac{h_1}{g} + m_b \right) \partial_n K(\mathbf{s}, \mathbf{s}_0) \\
&+ \frac{m_b}{2\kappa} \int_{\partial\Omega_2} ds \partial_n K(\mathbf{s}, \mathbf{s}_0) \\
&+ \frac{1}{2\kappa} \int_{\partial\Omega_1} ds \left( K(\mathbf{s}, \mathbf{s}_0) - \frac{1}{g} \partial_n K(\mathbf{s}, \mathbf{s}_0) \right) \partial_n m_\Xi(\mathbf{s}) \\
&+ \frac{1}{2\kappa} \int_{\partial\Omega_2} ds K(\mathbf{s}, \mathbf{s}_0) \partial_n m_\Xi(\mathbf{s}), \tag{19}
\end{aligned}$$

where the normal derivative of the Green's function  $K$  acts on its first argument, and integration must be interpreted as its Cauchy principal value. Consequently, if  $\mathbf{s}_0 \in \partial\Omega_1$  Eq. (19) can be written as

$$\begin{aligned}
&\frac{1}{2\kappa} \int_{\partial\Omega_1} ds \left( \frac{h_1}{g} + m_b \right) (\partial_n K(\mathbf{s}, \mathbf{s}_0) + \kappa \delta(\mathbf{s} - \mathbf{s}_0)) \\
&+ \frac{1}{2\kappa} \int_{\partial\Omega_1} ds \left( K(\mathbf{s}, \mathbf{s}_0) - \frac{1}{g} \partial_n K(\mathbf{s}, \mathbf{s}_0) \right. \\
&- \left. \frac{\kappa}{g} \delta(\mathbf{s} - \mathbf{s}_0) \right) \partial_n m_\Xi(\mathbf{s}) + \frac{m_b}{2\kappa} \int_{\partial\Omega_2} ds \partial_n K(\mathbf{s}, \mathbf{s}_0) \\
&+ \frac{1}{2\kappa} \int_{\partial\Omega_2} ds K(\mathbf{s}, \mathbf{s}_0) \partial_n m_\Xi(\mathbf{s}) = 0. \tag{20}
\end{aligned}$$

Similarly if  $\mathbf{s}_0 \in \partial\Omega_2$ , Eq. (19) reads

$$\begin{aligned}
&\frac{1}{2\kappa} \int_{\partial\Omega_1} ds \left( \frac{h_1}{g} + m_b \right) \partial_n K(\mathbf{s}, \mathbf{s}_0) \\
&+ \frac{m_b}{2\kappa} \left( \kappa + \int_{\partial\Omega_2} ds \partial_n K(\mathbf{s}, \mathbf{s}_0) \right) \\
&+ \frac{1}{2\kappa} \int_{\partial\Omega_1} ds \left( K(\mathbf{s}, \mathbf{s}_0) - \frac{1}{g} \partial_n K(\mathbf{s}, \mathbf{s}_0) \right) \partial_n m_\Xi(\mathbf{s}) \\
&+ \frac{1}{2\kappa} \int_{\partial\Omega_2} ds K(\mathbf{s}, \mathbf{s}_0) \partial_n m_\Xi(\mathbf{s}) = 0. \tag{21}
\end{aligned}$$

Under some circumstances, e.g., for certain boundary conditions, Eqs. (20) and (21) are not the most convenient representations of the constrained order-parameter profile. Another possible representation is the single-layer potential. Let us assume that the order parameter on the boundary  $\partial\Omega$  is known. Now we determine the solutions to the Helmholtz equation inside and outside  $\Omega$  with the same Dirichlet boundary conditions. We can use Eq. (17) for these problems, keeping in mind that the normal derivatives are different in each problem. Adding these equations, we find the following representation, valid everywhere in space:

$$m_\Xi(\mathbf{r}) = m_b + \frac{1}{2\kappa} \int_{\partial\Omega} ds K(\mathbf{s}, \mathbf{r}) \Psi(\mathbf{s}), \tag{22}$$

where  $\Psi(\mathbf{s}) = (\partial_n m_\Xi(\mathbf{s}))^+ - (\partial_n m_\Xi(\mathbf{s}))^-$ , with the plus (minus) sign standing for the interior (exterior) problem to  $\Omega$ , and  $\mathbf{n}(\mathbf{s})$  is the outward normal from  $\Omega$ . The auxiliary function  $\Psi(\mathbf{s})$  can be obtained from the boundary integral equation

$$m_\Xi(\mathbf{s}) = m_b + \frac{1}{2\kappa} \int_{\partial\Omega} ds_0 K(\mathbf{s}_0, \mathbf{s}) \Psi(\mathbf{s}_0). \tag{23}$$

The normal derivatives of the order-parameter profile on the boundary can be related to  $\Psi$  as

$$(\partial_n m_\Xi(\mathbf{s}))^\pm = \pm \frac{\Psi(\mathbf{s})}{2} + \frac{1}{2\kappa} \int_{\partial\Omega} ds_0 \mathbf{n}(\mathbf{s}) \cdot \nabla_{\mathbf{s}} K(\mathbf{s}_0, \mathbf{s}) \Psi(\mathbf{s}_0). \tag{24}$$

Alternatively, a double-layer potential representation of the order-parameter profile can be obtained if the normal derivative of the order parameter on the boundary  $\partial\Omega$  is known. We use Eq. (17) for the solutions to the Helmholtz equation inside and outside  $\Omega$  with opposite Neumann boundary conditions. Note that the outward normal for every domain is the inwards normal for the other one. By adding these equations we again obtain a representation that is valid everywhere in space:

$$\delta m_\Xi(\mathbf{r}) = \frac{1}{2\kappa} \int_{\partial\Omega} ds \mathbf{n}(\mathbf{s}) \cdot \nabla_{\mathbf{s}} K(\mathbf{s}, \mathbf{r}) \bar{\Psi}(\mathbf{s}), \tag{25}$$

where  $\delta m_\Xi(\mathbf{r}) \equiv m_\Xi(\mathbf{r}) - m_b$  and  $m_b = \pm m_0$  is the appropriate bulk order parameter in the region containing  $\mathbf{r}$ . Here, the modified auxiliary function  $\bar{\Psi}(\mathbf{s}) =$

$(\delta m_{\Xi}(\mathbf{s}))^- - (\delta m_{\Xi}(\mathbf{s}))^+$ . The limits of the order parameter on each side of  $\partial\Omega$  are related to  $\bar{\Psi}$  as

$$\delta m_{\Xi}(\mathbf{s}^{\pm}) = \mp \frac{\bar{\Psi}(\mathbf{s})}{2} + \frac{1}{2\kappa} \int_{\partial\Omega} d\mathbf{s}_0 \mathbf{n}(\mathbf{s}_0) \cdot \nabla_{\mathbf{s}_0} K(\mathbf{s}_0, \mathbf{s}) \bar{\Psi}(\mathbf{s}_0). \quad (26)$$

On the other hand,  $\partial_n m_{\Xi}(\mathbf{s}) \equiv \mathbf{n}(\mathbf{s}) \cdot \nabla_{\mathbf{s}} m_{\Xi}$  is continuous on  $\partial\Omega$ :

$$\partial_n m_{\Xi}(\mathbf{s}) = \mathbf{n}(\mathbf{s}) \cdot \nabla_{\mathbf{s}} \left[ \int_{\partial\Omega} d\mathbf{s}_0 \bar{\Psi}(\mathbf{s}_0) \mathbf{n}(\mathbf{s}_0) \cdot \nabla_{\mathbf{s}_0} \frac{K(\mathbf{s}_0, \mathbf{s})}{2\kappa} \right] \quad (27)$$

Finally, we provide some additional relations which will be useful later. On using the Green's identity Eq. (16) for two Green's functions, it follows that

$$\int_{\partial\Omega} d\mathbf{s} K(\mathbf{s}, \mathbf{r}) \mathbf{n}(\mathbf{s}) \cdot \nabla_{\mathbf{s}} K(\mathbf{s}, \mathbf{r}') = \int_{\partial\Omega} d\mathbf{s} K(\mathbf{s}, \mathbf{r}') \mathbf{n}(\mathbf{s}) \cdot \nabla_{\mathbf{s}} K(\mathbf{s}, \mathbf{r}), \quad (28)$$

where  $\mathbf{r}$  and  $\mathbf{r}'$  are positions inside the domain  $\Omega$ . If  $\mathbf{r}' \rightarrow \mathbf{s}'$  on the boundary  $\partial\Omega$  then Eq. (28) leads to

$$\int_{\partial\Omega} d\mathbf{s} K(\mathbf{s}, \mathbf{s}') \mathbf{n}(\mathbf{s}) \cdot \nabla_{\mathbf{s}} K(\mathbf{s}, \mathbf{r}) = -\kappa K(\mathbf{s}', \mathbf{r}) + \int_{\partial\Omega} d\mathbf{s} K(\mathbf{s}, \mathbf{r}) \mathbf{n}(\mathbf{s}) \cdot \nabla_{\mathbf{s}} K(\mathbf{s}, \mathbf{s}'). \quad (29)$$

Finally, if  $\mathbf{r} \rightarrow \mathbf{s}$  on  $\partial\Omega$  then

$$\int_{\partial\Omega} d\mathbf{s} K(\mathbf{s}_0, \mathbf{s}) \mathbf{n}(\mathbf{s}_0) \cdot \nabla_{\mathbf{s}_0} K(\mathbf{s}_0, \mathbf{s}') = \int_{\partial\Omega} d\mathbf{s}_0 K(\mathbf{s}_0, \mathbf{s}') \mathbf{n}(\mathbf{s}_0) \cdot \nabla_{\mathbf{s}_0} K(\mathbf{s}_0, \mathbf{s}). \quad (30)$$

In the next sections we apply this formalism to obtain the interfacial free-energies relevant to wetting phenomena: (i) the interfacial free energy of a non-wetting bulk phase in contact with a rough substrate; (ii) the self-interaction corresponding to a free liquid-gas interface; and, finally, (iii) the binding potential for a wetting film configuration (see Fig. 1).

### III. INTERFACIAL FREE ENERGY OF A LIQUID PHASE IN CONTACT WITH A NON-PLANAR WALL

The first system that we consider is the simple case of a bulk phase in contact with a non-planar wall when a wetting film is absent. The local height of the wall, above some reference plane (often taken to be the plane  $z = 0$ ) is written  $\psi(\mathbf{x})$ , where  $\mathbf{x} = (x, y)$  is the parallel displacement. Without loss of generality, we concentrate on the wall-liquid interface, supposing that the local surface field  $h_1$  is positive, so that the order parameter has the same (positive) value throughout. In this case, the domain  $\Omega$  is just the set of points for which  $z > \psi(\mathbf{x})$ .

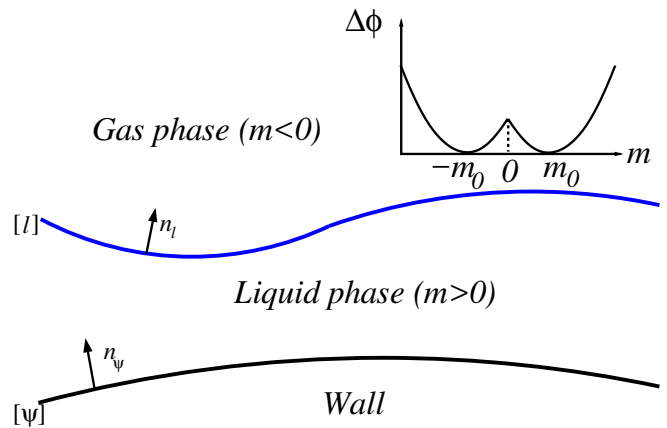


FIG. 1: Schematic illustration of a non-planar interfacial configuration for a constrained wetting film of liquid at a non-planar wall (black line). Conventions for the surface normals are shown. Inset: the double-parabola approximation for  $\Delta\phi(m)$ .

In addition, we suppose that the substrate is chemically homogeneous, so that  $h_1$  and  $g$  do not vary with position. The equilibrium mean-field configuration  $m_{\Xi}(\mathbf{r})$  follows from the simple minimization of the LGW Hamiltonian, resulting in the Helmholtz equation Eq. (5) and the boundary conditions

$$\begin{aligned} \mathbf{n}_{\psi} \cdot \nabla m_{\Xi}(\mathbf{r}) &= -h_1 - g m_{\Xi}(\mathbf{r}), \quad \text{for } \mathbf{r} = (\mathbf{x}, \psi(\mathbf{x})) \\ m_{\Xi}(z) &\rightarrow m_b, \quad \text{for } z \rightarrow +\infty, \end{aligned} \quad (32)$$

where the bulk magnetization for the liquid phase is  $m_b = m_0$ . Similar results apply to the wall-gas interface, for which  $h_1$  is negative and  $m_b = -m_0$ . Here,  $\mathbf{n}_{\psi}$  denotes the *inward* normal to the wall. Since the order parameter does not change sign in  $\Omega$ , Eq. (20) can be recast as

$$\begin{aligned} \int_{\psi} d\mathbf{s} \left[ K(\mathbf{s}, \mathbf{s}') + \frac{1}{g} \partial_n K(\mathbf{s}, \mathbf{s}') - \frac{\kappa}{g} \delta(\mathbf{s} - \mathbf{s}') \right] q(\mathbf{s}) \\ = \left( \frac{-h_1}{g} - m_b \right) \left[ -\kappa + \int_{\psi} d\mathbf{s} \partial_n K(\mathbf{s}, \mathbf{s}') \right], \end{aligned} \quad (33)$$

where the integration  $\int_{\psi}$  is over the substrate surface,  $\partial_n(\mathbf{s})$  is a shorthand for  $\mathbf{n}(\mathbf{s}) \cdot \nabla_{\mathbf{s}}$ ,  $q \equiv \partial_n \delta m_{\Xi}$ , and  $\delta m_{\Xi} \equiv m_{\Xi} - m_b$ . Equation (33) can only be solved exactly in few exceptional circumstances, such as when symmetry arguments can be applied; these include planar, cylindrical, or spherical substrates, all of which have constant curvature. For example, for a planar substrate  $q$  is constant over the surface, and has the value

$$q = -\frac{\kappa(h_1 + g m_b)}{\kappa - g}. \quad (34)$$

However, the generic solution of Eq. (33) must include the *local* curvature of the substrate, and it is natural to look for a perturbative solution when the deviations from the flat case are small. To this end, let us introduce the principal curvatures  $k_1(\mathbf{s})$  and  $k_2(\mathbf{s})$  at a point

$\mathbf{s} = (\mathbf{x}, \psi(\mathbf{x}))$  on the surface.  $R_i = 1/\kappa_i$  are the corresponding radii of curvature, and it is convenient to recall that  $K_G = k_1 k_2$  is the Gaussian curvature and  $H = (k_1 + k_2)/2$  is the mean curvature (or half of the total curvature). Let us denote by  $R$  the minimum of  $|R_1|$  and  $|R_2|$ , so that  $H \sim R^{-1}$ . Far from the bulk critical point the bulk correlation length  $\kappa^{-1}$  is microscopically small, so the substrate can be considered flat over several correlation lengths provided that  $\kappa R \gg 1$ .

### A. Perturbative approach

We now set out our perturbative analysis of Eq. (33). The idea is to expand all elementary building blocks of Eq. (33) [the Ornstein-Zernike (OZ) kernel, its normal derivative,  $q$ , and  $d\mathbf{s}$ ] on the LHS and RHS of Eq. (33) in powers of the curvature  $H$ , which can then be equated, term by term. We suppose that locally the surface is well approximated by a paraboloid in a neighbourhood of  $\mathbf{s}'$ , where we locate the origin of the coordinates. Consider now a point on the substrate surface  $\mathbf{s} = (\mathbf{x}, \psi(\mathbf{x}))$ . The vertical displacement of  $\mathbf{s}$  with respect to the horizontal plane is

$$\Delta\psi(\mathbf{r}_\perp) \equiv \frac{1}{2}k_1 x^2 + \frac{1}{2}k_2 y^2 + \dots, \quad (35)$$

where we have written  $\mathbf{r}_\perp = \mathbf{x} - \mathbf{x}_0 \equiv (x, y)$  for the projection of the vector  $\mathbf{s} - \mathbf{s}'$  onto the horizontal plane  $\pi_0$ , tangent to the graph of  $\psi(\mathbf{x})$  in  $\mathbf{s}'$ . With this parametrization, the coefficients  $k_i$  are exactly the principal curvatures  $k_i(\mathbf{s}')$  evaluated at  $\mathbf{s}'$ . The ellipses in Eq. (35) stand for higher-order terms in  $x, y$ , which are coupled to higher-orders of the local curvatures as well. We assume that the Taylor coefficients associated to terms  $x^m y^{n-m}$  (with  $0 \leq m \leq n$  and  $n > 3$ ) scale as  $R^{-n+1}$ . With this property, close to the origin  $\Delta\psi(\mathbf{r}_\perp) = R\Delta\bar{\psi}(\mathbf{r}_\perp R^{-1})$ , i.e.,  $R$  is the only relevant lengthscale for the substrate shape.

Let us consider first the OZ kernel. The two points are separated by the distance  $|\mathbf{s} - \mathbf{s}'| = \sqrt{\mathbf{r}_\perp^2 + (\Delta\psi(\mathbf{r}_\perp))^2}$ , and for small curvatures we can Taylor expand around the flat configuration to express the OZ kernel as a power series in the curvature:

$$K(\mathbf{s}, \mathbf{s}') = \mathcal{K}(r_\perp) \left[ 1 - \frac{1}{2}(1 + \kappa r_\perp) \left( \frac{\Delta\psi(\mathbf{r}_\perp)}{r_\perp} \right)^2 + \mathcal{O}(R^{-4}) \right], \quad (36)$$

where  $\mathcal{K}(x) = \kappa e^{-\kappa x}/2\pi x$ . As the kernel  $\mathcal{K}$  decays exponentially with a lengthscale  $\kappa^{-1}$ , Eq. (36) is a faithful representation of  $K(\mathbf{s}, \mathbf{s}')$  around  $\mathbf{s}'$  if  $\kappa R \gg 1$ . For the normal derivative of the kernel we have

$$\partial_n K(\mathbf{s}, \mathbf{s}') = \mathbf{n}(\mathbf{s}) \cdot \nabla_{\mathbf{s}} K(\mathbf{s}, \mathbf{s}') = \mathbf{n}(\mathbf{s}) \cdot \frac{\mathbf{s} - \mathbf{s}'}{|\mathbf{s} - \mathbf{s}'|} \frac{\partial \mathcal{K}(|\mathbf{s} - \mathbf{s}'|)}{\partial |\mathbf{s} - \mathbf{s}'|}. \quad (37)$$

The Monge parametrization of the normal vector is

$$\mathbf{n}(\mathbf{s}) = \frac{(-\nabla_\perp \Delta\psi(\mathbf{r}_\perp), 1)}{\sqrt{1 + (\nabla_\perp \Delta\psi(\mathbf{r}_\perp))^2}}, \quad (38)$$

where  $\nabla_\perp \equiv (\partial_x, \partial_y)$ . Then, following the above ideas we can show that

$$\partial_n K(\mathbf{s}, \mathbf{s}') = \frac{1 + \kappa r_\perp}{r_\perp} \mathcal{K}(r_\perp) \left( \frac{\mathbf{r}_\perp \cdot \nabla_\perp \Delta\psi - \Delta\psi}{r_\perp} \right) + \mathcal{O}(R^{-3}), \quad (39)$$

where the term in parentheses is  $\mathcal{O}(R^{-1})$  [see Eq. (35)]. The surface element  $d\mathbf{s} = \sqrt{1 + (\nabla_\perp \Delta\psi)^2} d\mathbf{r}_\perp = (1 + (\nabla_\perp \Delta\psi)^2/2) d\mathbf{r}_\perp + \mathcal{O}(R^{-4})$ . The normal derivative of the order parameter can be expanded in a similar way; thus,  $q(\mathbf{s}) = \sum_{n=1}^{\infty} q_n(\mathbf{s})$ , where  $q_n = \mathcal{O}(R^{-n})$ . Plugging the above relations into Eq. (33) and identifying the corresponding terms, order by order, we find a recursive chain of integral equations for  $q_n(\mathbf{s})$  of the form (see App. A):

$$\int_{\mathbb{R}^2} d\mathbf{r}_\perp q_n(\mathbf{r}_\perp) \left[ \mathcal{K}(r_\perp) - \frac{\kappa}{g} \delta(\mathbf{r}_\perp) \right] = f_n[q_0, \dots, q_{n-1}], \quad (40)$$

where we have extended the integral to  $\mathbb{R}^2$ , ignoring terms exponentially decaying in  $\kappa R$ . In general,  $f_n$  is a functional of  $q_i$  for  $i < n$ . For  $n = 0$ ,  $f_0 = \kappa(h_1 + gm_b)/g$ , which is independent of  $\mathbf{s}'$ , so  $q_0(\mathbf{s})$  is given by Eq. (34) everywhere on the substrate. Following the procedure outlined in App. A, we find for the next-order terms

$$q_1 = q_0 \frac{g}{\kappa - g} \frac{H}{\kappa}, \quad (41)$$

$$q_2 = q_0 \frac{g}{\kappa - g} \left( \frac{H^2}{2\kappa^2} \left( 1 + \frac{2\kappa}{\kappa - g} \right) - \frac{K_G}{2\kappa^2} \right). \quad (42)$$

We are now in the position to estimate the interfacial thermodynamic properties and the order-parameter profile. The interfacial free energy  $\mathcal{F}_{wl}$  of the wall-liquid interface is obtained from Eq. (11) as

$$\mathcal{F}_{wl} = \frac{h_1 + gm_b}{2g} \int_{\psi} d\mathbf{s} q(\mathbf{s}) = \sigma_{wl} \mathcal{A} + \Delta\mathcal{F}_{wl}[\psi], \quad (43)$$

where  $\sigma_{wl} \equiv (\kappa/2)(h_1 + gm_b)^2/[g(g - \kappa)]$  is the surface tension defined for a planar wall-liquid interface, and  $\mathcal{A}$  is the total substrate area. Thus, the increment  $\Delta\mathcal{F}_{wl}[\psi]$  accounts for all the curvature-related terms. For large  $\kappa R$ ,  $\Delta\mathcal{F}_{wl}$  can be expressed as

$$\begin{aligned} \frac{\Delta\mathcal{F}_{wl}}{\sigma_{wl} \mathcal{A}} &= \frac{g}{\kappa - g} \frac{\overline{H}}{\kappa} + \frac{1}{2} \left( \frac{g}{\kappa - g} \right) \left( 1 + \frac{2\kappa}{\kappa - g} \right) \frac{\overline{H^2}}{\kappa^2} \\ &\quad - \frac{1}{2} \left( \frac{g}{\kappa - g} \right) \frac{\overline{K_G}}{\kappa^2} + \dots, \end{aligned} \quad (44)$$

where  $\overline{H}$ ,  $\overline{H^2}$  and  $\overline{K_G}$  are the averages over the substrate of the mean curvature, its square, and the Gaussian curvature, respectively. The leading order is consistent with

the expression obtained in Refs. [40, 41]. Finally, the ellipses correspond to higher-order curvature contributions which, in general, are non-vanishing. This feature, as well as the contribution being proportional to  $\overline{H^2}$ , is nonzero, implies that the DP model does not satisfy the morphological thermodynamics hypothesis for confined fluids of hard bodies [58] (see also Ref. [59] for a critical review of this proposal).

Diagrammatically, the interfacial free energy can be represented as

$$\mathcal{F}_{wl} = \sigma_{wl} \left[ \begin{array}{c} \text{---}\bullet\text{---} + \left(\frac{g}{\kappa - g}\right) \text{---}\blacktriangle\text{---} \\ + \frac{1}{2} \left(\frac{g}{\kappa - g}\right) \left(1 + \frac{2\kappa}{\kappa - g}\right) \text{---}\blacksquare\text{---} \\ - \frac{1}{2} \left(\frac{g}{\kappa - g}\right) \text{---}\blacklozenge\text{---} + \dots \end{array} \right], \quad (45)$$

where the wavy line corresponds to the substrate surface, the black circle means that one must integrate over all the positions on that surface with the appropriate infinitesimal area element. The filled triangle corresponds to integration over the surface, weighted by the local mean curvature in units of  $\kappa$  (our notation for this symbol differs from that used in Ref. [41] by a factor of  $1/2$ ). Finally, for the filled square and the rhombus the weight function for the surface integrations are the squared mean curvature and the Gaussian curvature, respectively, in units of  $\kappa^2$ . The present treatment highlights non-zero bending rigidity and saddle-splay coefficients, which were missing in the original formulation of the non-local model [40, 41]. The values of these are in agreement with those obtained from the exact solutions for the free energy of a fluid outside or inside a spherical or a cylindrical surface of radius  $R$  within the DP model [60] (see also App. D).

## B. General diagrammatic approach

We can go beyond the approach presented in the previous section and obtain formally the full expansion of the interfacial free energy in powers of substrate curvatures. For this purpose, we return to Eq. (33). The integral-equation kernel can be formally inverted as

$$\begin{aligned} X(\mathbf{s}, \mathbf{s}') &\equiv \left( K(\mathbf{s}, \mathbf{s}') + \frac{1}{g} \partial_n K(\mathbf{s}, \mathbf{s}') - \frac{\kappa}{g} \delta(\mathbf{s} - \mathbf{s}') \right)^{-1} \\ &= \frac{g}{g - \kappa} \delta(\mathbf{s} - \mathbf{s}') \\ &\quad - \frac{g}{g - \kappa} \int_{\psi} d\mathbf{s}_1 X(\mathbf{s}, \mathbf{s}_1) \left( U(\mathbf{s}_1, \mathbf{s}') + \frac{1}{g} \partial_{n_1} K(\mathbf{s}_1, \mathbf{s}') \right), \end{aligned} \quad (46)$$

where  $U(\mathbf{s}, \mathbf{s}') \equiv K(\mathbf{s}, \mathbf{s}') - \delta(\mathbf{s} - \mathbf{s}')$  is the barred kernel introduced in Ref. [57], and  $\partial_{n_1} \equiv \mathbf{n}(\mathbf{s}_1) \cdot \nabla_{\mathbf{s}_1}$ . This expression can be iterated, so we obtain the following

formal expansion for  $X$ :

$$\begin{aligned} X(\mathbf{s}, \mathbf{s}') &= \frac{g}{g - \kappa} \delta(\mathbf{s} - \mathbf{s}') \\ &\quad - \left( \frac{g}{g - \kappa} \right)^2 \left( U(\mathbf{s}, \mathbf{s}') + \frac{1}{g} \partial_n K(\mathbf{s}, \mathbf{s}') \right) \\ &\quad + \left( \frac{g}{g - \kappa} \right)^3 \int_{\psi} d\mathbf{s}_1 \left( U(\mathbf{s}, \mathbf{s}_1) + \frac{1}{g} \partial_n K(\mathbf{s}, \mathbf{s}_1) \right) \\ &\quad \times \left( U(\mathbf{s}_1, \mathbf{s}') + \frac{1}{g} \partial_{n_1} K(\mathbf{s}_1, \mathbf{s}') \right) + \dots \end{aligned} \quad (47)$$

The solution to Eq. (33) can be expressed as

$$\begin{aligned} q(\mathbf{s}) &= - \frac{\kappa(h_1 + gm_b)}{\kappa - g} \left[ 1 - \int_{\psi} d\mathbf{s}_1 d\mathbf{s}_2 X(\mathbf{s}, \mathbf{s}_1) U(\mathbf{s}_1, \mathbf{s}_2) \right. \\ &\quad \left. - \int_{\psi} d\mathbf{s}_1 d\mathbf{s}_2 X(\mathbf{s}, \mathbf{s}_1) \frac{1}{\kappa} \partial_{n_1} K(\mathbf{s}_1, \mathbf{s}_2) \right]. \end{aligned} \quad (48)$$

When the expansion Eq. (47) is introduced in the previous expression, we arrive at a formal series for  $q$ , where each term is proportional to the convolution of  $n$  functions, each being either  $U$  or  $(\partial_n K)/\kappa$ . We introduce the following diagrammatic representation:

$$U(\mathbf{s}, \mathbf{s}') = \text{---}\bullet\text{---} \quad ; \quad \frac{1}{\kappa} \partial_n K(\mathbf{s}, \mathbf{s}') = \text{---}\bullet\text{---}\text{---}\circ\text{---}, \quad (49)$$

where in the latter diagram the arrow points to the position where the normal derivative is taken. In this way, the expansion terms appearing in  $q$  can be represented as chain-like diagrams. For example:

$$\int_{\psi} d\mathbf{s}_1 d\mathbf{s}_2 U(\mathbf{s}, \mathbf{s}_1) \frac{1}{\kappa} \partial_{n_1} K(\mathbf{s}_1, \mathbf{s}_2) = \text{---}\bullet\text{---}\text{---}\bullet\text{---}\text{---}\circ\text{---}, \quad (50)$$

where a filled circle corresponds to an integrated position and the open circle represents the point  $\mathbf{s}$  where  $q$  is evaluated. Thus, from Eq. (48) we have

$$\begin{aligned} q(\mathbf{s}) &= - \frac{\kappa(h_1 + gm_b)}{\kappa - g} \left[ 1 + \frac{g}{\kappa - g} \text{---}\bullet\text{---} \right. \\ &\quad + \frac{g}{\kappa - g} \text{---}\bullet\text{---}\text{---}\circ\text{---} + \frac{g}{\kappa - g} \frac{\kappa}{\kappa - g} \text{---}\bullet\text{---}\text{---}\bullet\text{---}\text{---}\circ\text{---} \\ &\quad + \frac{g}{\kappa - g} \frac{\kappa}{\kappa - g} \text{---}\bullet\text{---}\text{---}\bullet\text{---}\text{---}\bullet\text{---}\text{---}\circ\text{---} \\ &\quad \left. + \left( \frac{g}{\kappa - g} \right)^2 \left( \text{---}\bullet\text{---}\text{---}\bullet\text{---}\text{---}\bullet\text{---}\text{---}\text{---}\circ\text{---} + \text{---}\bullet\text{---}\text{---}\text{---}\bullet\text{---}\text{---}\text{---}\bullet\text{---}\text{---}\text{---}\circ\text{---} \right) + \dots \right]. \end{aligned} \quad (51)$$

Here, each diagram with  $n$  bonds (of which  $m$  are of  $(\partial_n K)/\kappa$ -type) must be multiplied by a factor

$$\left( \frac{g}{\kappa - g} \right)^n \left( \frac{\kappa}{g} \right)^{m - m_0}, \quad (52)$$

where the index  $m_0$  is either 0 or 1, depending whether the first bond on the left (i.e., the one that emerges from



the filled extreme circle) is of  $U$  or  $(\partial_n K)/\kappa$  type, respectively. The connection with the curvature expansion is evident as, taking into account Eqs. (36) and (39), we find that

$$\text{Diagram 1} \equiv \text{Diagram 2} - 1 \quad (53)$$

$$= \frac{1}{2} \left[ \text{Diagram 3} - \text{Diagram 4} \right] + \mathcal{O}(R^{-4})$$

$$\text{Diagram 1} = \text{Diagram 5} + \mathcal{O}(R^{-3}), \quad (54)$$

where by the open symbols we denote the evaluation of the corresponding weight functions at  $\mathbf{s}$ . Thus, a diagram with  $n$   $U$ -type and  $m$   $(\partial_n K)/\kappa$ -type bonds is of order of  $R^{-(2n+m)}$ . This demonstrates that in order to obtain the corrections to  $q$  to order  $R^{-2}$ , only the first three diagrams in Eq. (51) are needed.

By substituting Eq. (51) into Eq. (43) we obtain the following diagrammatic expansion of the interfacial free energy:

$$\mathcal{F}_{wl} = \sigma_{wl} \left[ \text{Diagram 1} + \left( \frac{g}{\kappa - g} \right) (\text{Diagram 2} + \text{Diagram 3}) + \frac{g}{\kappa - g} \frac{\kappa}{\kappa - g} \text{Diagram 4} + \dots \right] \quad (55)$$

which coincides with our previous result Eq. (45) up to  $R^{-2}$  corrections. In this expansion, the factors that multiply each diagram are the same as those that multiply the corresponding diagrams in Eq. (51).

### C. Evaluation of the order-parameter profile

As for the interfacial free energy, we can obtain a formally exact expression for the order-parameter profile from Eq. (18):

$$\delta m_{\Xi}(\mathbf{r}) = -\frac{1}{2\kappa} \int_{\psi} ds K(\mathbf{s}, \mathbf{r}) q(\mathbf{s}) - \frac{1}{2\kappa} \int_{\psi} ds \left( \frac{h_1}{g} + m_b + \frac{q(\mathbf{s})}{g} \right) \partial_n K(\mathbf{s}, \mathbf{r}) \quad (56)$$

or, equivalently,

$$\delta m_{\Xi}(\mathbf{r}) = -\frac{1}{2} \int_{\psi} ds K(\mathbf{s}, \mathbf{r}) \left( \frac{h_1}{g} + m_b + \frac{\kappa + g}{\kappa g} q(\mathbf{s}) \right) - \frac{1}{2\kappa} \int_{\psi} ds \left( \frac{h_1}{g} + m_b + \frac{q(\mathbf{s})}{g} \right) \times (\partial_n K(\mathbf{s}, \mathbf{r}) - \kappa K(\mathbf{s}, \mathbf{r})) \quad (57)$$

by substitution of the expansion (51) for  $q(\mathbf{s})$ . However, it is more convenient to use the single-layer potential representation, Eq. (22). Note that, once we know  $q$ , the order parameter on the substrate can be obtained from Eq. (31) as  $-h_1/g - m_b - q/g$ . It is instructive to derive the order parameter starting from the perturbative

approach by expanding  $\Psi$  in powers of the local curvature. The derivation proceeds along the same steps as the previous sections (see App. A). After substitution of the expansion of  $\Psi$  into Eq. (22), we find the following diagrammatic representation of the order parameter:

$$\delta m_{\Xi} \approx \frac{h_1 + gm_b}{\kappa - g} \left[ \text{Diagram 1} + \frac{\kappa}{\kappa - g} \text{Diagram 2} + \left( \frac{1}{2} \frac{g}{\kappa - g} + \frac{\kappa^2}{(\kappa - g)^2} \right) \text{Diagram 3} - \frac{1}{2} \frac{g}{\kappa - g} \text{Diagram 4} \right]. \quad (58)$$

The presence of the curvature correction terms, which are not accounted for in the original non-local *ansatz*, can be checked again with the exact solutions known for spherical and cylindrical substrates (see App. D).

As for the free energy, we can also generate a general diagrammatic approach to the curvature corrections. For this purpose, Eq. (23) can be formally solved as

$$\Psi(\mathbf{s}) = 2\kappa \int_{\psi} ds_0 K^{-1}(\mathbf{s}, \mathbf{s}_0) \left( -\frac{h_1 + gm_b}{g} - \frac{q(\mathbf{s}_0)}{g} \right), \quad (59)$$

where  $K^{-1}(\mathbf{s}, \mathbf{s}_0) = \lim_{g \rightarrow \infty} X(\mathbf{s}, \mathbf{s}_0)$ , i.e.,

$$K^{-1}(\mathbf{s}, \mathbf{s}_0) = \delta(\mathbf{s} - \mathbf{s}_0) - U(\mathbf{s}, \mathbf{s}_0) + \int_{\psi} ds_1 U(\mathbf{s}, \mathbf{s}_1) U(\mathbf{s}_1, \mathbf{s}_0) - \dots \quad (60)$$

Substituting the expansions Eqs. (51) and (60) into Eq. (59), and back into Eq. (22), we obtain the following expansion for the order-parameter profile:

$$\delta m_{\Xi} = \frac{h_1 + gm_b}{\kappa - g} \left[ \text{Diagram 1} + \frac{\kappa}{\kappa - g} \text{Diagram 2} + \frac{g}{\kappa - g} \text{Diagram 3} + \left( \frac{\kappa}{\kappa - g} \right)^2 \text{Diagram 4} + \dots \right] \quad (61)$$

The diagrams of this expansion are obtained by convolution of a chain-like diagram of  $q$  from Eq. (51) and the Green's function  $K(\mathbf{s}, \mathbf{r})$ . The factor associated with each diagram [except for the first one in Eq. (61)] is given by the product of two terms: the factor associated to the  $q$  diagram, Eq. (52), and either 1 (if the chainlike diagram has only  $U$ -type bonds) or  $[1 - (1 - \kappa/g)^{l+1}]$  otherwise, with  $l$  being the number of  $U$ -type bonds from the last  $(\partial_n K)/\kappa$ -type bond to the extreme where the Green's function  $K(\mathbf{s}, \mathbf{r})$  emerges. By using (53) and (54), the diagrammatic expansion (61) reduces to (58) up to  $R^{-3}$  corrections.

### D. Summary and remarks

So far we have done two things. First, we devised a perturbative approach based on a small-curvature expansion

of surfaces and we have applied this to a (non-wetting) bulk phase in contact with a substrate. The free energy (45) contains curvature corrections that we have identified exactly at the leading (nontrivial) order. The curvature expansions are, however, quite cumbersome, and to this end we developed a more fundamental approach, based on the formal inversion of integral equations satisfied by the order-parameter field. By using a diagrammatic approach we have found a formal expansion of the interfacial free energy [see Eq. (55)]. By following this approach we have also derived the order-parameter profile in the bulk phase; see Eq. (58). For small interfacial/surface curvatures, the wetting diagrams entering into the formal expansions simplify, and they reveal the curvature corrections in terms of local Gaussian and average curvatures; this property will be analyzed in detail in the next section for the case of an isolated liquid-gas interface.

#### IV. THE FREE INTERFACE AND ITS SELF-INTERACTION ENERGY FUNCTIONAL

Next, we turn our attention to the liquid-gas interface. This is free in the sense that it is isolated, infinitely far from any confining walls but *constrained* so that the surface of zero magnetization adopts a given, smooth, non-planar configuration  $\ell(\mathbf{x})$ . Overhangs are excluded and, again, we shall suppose that the curvature is small everywhere. We follow the prescription set out by Fisher and Jin [47, 48], where by the effective interfacial model is identified as the minimum of the LGW model subject to this cross-criterion constraint together with the appropriate bulk boundary conditions, viz., that  $m_{\Xi}(\mathbf{r}) \rightarrow \mp m_0$  as  $z \rightarrow \pm\infty$ , i.e., gas is above and liquid is below the interface corresponding to the two domains  $\Omega_1$  and  $\Omega_2$ . These regions are uncoupled, and in each the equilibrium *constrained* profile satisfies the Helmholtz equation (13) subject to the above boundary conditions. In this case, the solution to Eq. (20) can be written as

$$\int_{\ell} ds K(\mathbf{s}, \mathbf{s}') q^{\pm}(\mathbf{s}) = -m_0 \left( \kappa \mp \int_{\ell} ds \partial_n K(\mathbf{s}, \mathbf{s}') \right), \quad (62)$$

where  $\mathbf{n}$  is the interface normal towards the gas phase. This relation tells us that, given the interfacial profile  $\ell(\mathbf{x})$  as a background, the order parameter can be found from knowledge of  $q^{\pm}(\mathbf{s}_{\ell}) = \partial_{n_{\ell}} \delta m_{\Xi}(\mathbf{s}_{\ell}^{\pm})$ , where  $\delta m_{\Xi} = m(\mathbf{r}) \pm m_0$  for  $\mathbf{r}$  lying above/below the interface. Notice that the order parameter is a function of the position but also a *functional* of the interfacial shape  $\ell(\mathbf{x})$ . Our main goal is to determine this functional dependence.

##### A. Perturbative approach

If we assume that the local interfacial curvatures are small, we can proceed in a similar way to the previ-

ous section. The normal derivative of the order parameter can be expanded in powers of the minimum local curvature radius  $R$ ; thus  $q^{\pm}(\mathbf{s}_{\ell}) = \sum_{n=1}^{\infty} q_n^{\pm}(\mathbf{s}_{\ell})$ , where  $q_n = \mathcal{O}(R^{-n})$ . It follows that for a flat interface  $q_n = 0$  (for  $n \geq 1$ ), and the series reduces to  $q^{\pm}(\mathbf{s}_{\ell}) = q_0(\mathbf{s}_{\ell})$ . Inserting the above relations into Eq. (62) and identifying the corresponding terms, order by order, we find a recursive chain of equations for the  $q_n$ 's. Following the scheme used in the previous section, we can solve up to  $\mathcal{O}(R^{-3})$  and obtain the desired  $q$ 's (see App. A). The DP potential allows us to write the LGW Hamiltonian in terms of surface integrals only, viz.,

$$\mathcal{H}_{LGW}[m_{\Xi}] \equiv H[\ell] = -\frac{m_0}{2} \int_{\ell} ds_{\ell} (q^+(\mathbf{s}_{\ell}) + q^-(\mathbf{s}_{\ell})), \quad (63)$$

where  $H[\ell]$  is the interfacial Hamiltonian. This functional can be evaluated with the perturbative expansion for  $q^{\pm}$  mentioned above and, consequently, it leads to a similar expansion of the Hamiltonian that we cast in the form  $H[\ell] = \sigma \mathcal{A}_{I_g} + \Delta H[\ell]$ , where

$$\Delta H[\ell] \equiv -\sigma \sum_{n=2}^{\infty} (-1)^n \omega_n[\ell], \quad (64)$$

is the self-interaction contribution [57],  $\sigma = \kappa m_0^2$  is the surface tension, and  $\mathcal{A}_{I_g}$  the interfacial area. The functionals  $\omega_n[\ell]$  are (assured to be) of order  $\mathcal{O}(R^{-2(n-1)})$ . Having in mind the approximate solutions for  $q$  just derived, we find that

$$H[\ell] = \kappa m_0^2 \int_{\ell} ds_{\ell} - \frac{m_0}{2} \int_{\ell} ds_{\ell} (q_2^+(\mathbf{s}_{\ell}) + q_2^-(\mathbf{s}_{\ell})) + \mathcal{O}(R^{-3}). \quad (65)$$

Thus we immediately recover that  $H[\ell] = \sigma \int_{\ell} ds_{\ell} + \dots$  which is just the standard capillary-wave Hamiltonian. The ellipses stand for the energy corrections due to the self-interaction: the first of these corrections is

$$-\sigma \omega_2[\ell] = -\frac{m_0}{2} \int_{\ell} ds_{\ell} (q_2^+(\mathbf{s}_{\ell}) + q_2^-(\mathbf{s}_{\ell})) \quad (66)$$

or, more explicitly, using Eq. (A16),

$$H[\ell] \approx \sigma \int_{\ell} ds_{\ell} - \frac{\sigma}{8} \int_{\ell} ds_{\ell} \left( \frac{k_1(\mathbf{s}_{\ell}) - k_2(\mathbf{s}_{\ell})}{\kappa} \right)^2. \quad (67)$$

We use the symbol  $\approx$  to mean that relationships hold up to  $\mathcal{O}(R^{-3})$  corrections. The absence of a  $1/R$  contribution, i.e., the vanishing of the Tolman length, is due to the Ising symmetry of the DP model. In the theory of lipid membranes the above functional the functional (67) is commonly expressed in terms of the Gaussian and extrinsic curvatures of the interface, following Helfrich [61]

$$H[\ell] \approx \sigma \mathcal{A}_{\ell} + \int_{\ell} ds_{\ell} (\kappa_B H^2 + \kappa_G K_G), \quad (68)$$

where the coupling constants are the bending rigidity

$$\kappa_B = -\frac{\sigma}{2\kappa^2} \quad (69)$$

and the saddle-splay rigidity

$$\kappa_G = \frac{\sigma}{2\kappa^2}. \quad (70)$$

Using the diagrammatic notation introduced in the previous section, the full  $H[\ell]$  can be expressed as

$$H[\ell] = \sigma \left[ \text{---}\bullet\text{---} - \frac{1}{2} \left( \text{---}\blacksquare\text{---} - \text{---}\blacklozenge\text{---} \right) + \dots \right]. \quad (71)$$

The constrained order-parameter profiles in the gas and liquid phases can be obtained from Eq. (18) as

$$\delta m_{\Xi}(\mathbf{r}) \equiv m_{\Xi}(\mathbf{r}) \mp m_0 = \mp \frac{1}{2\kappa} \int_{\ell} ds K(\mathbf{s}, \mathbf{r}) q^{\pm}(\mathbf{s}) + \frac{m_0}{2\kappa} \int_{\ell} ds \partial_n K(\mathbf{s}, \mathbf{r}), \quad (72)$$

where the upper (lower) sign must be selected when  $\mathbf{r}$  is in the gas (liquid) region. Proceeding in a similar way as in the previous section, the constrained order-parameter profiles can be expressed in the gas phase as

$$\delta m_{\Xi} \approx m_0 \left[ \text{---}\bullet\text{---} - \frac{1}{2} \left( \text{---}\blacksquare\text{---} - \text{---}\blacklozenge\text{---} \right) \right] \quad (73)$$

and in the liquid phase as

$$\delta m_{\Xi} \approx -m_0 \left[ \text{---}\bullet\text{---} - \frac{1}{2} \left( \text{---}\blacksquare\text{---} - \text{---}\blacklozenge\text{---} \right) \right]. \quad (74)$$

## B. General diagrammatic approach

We can go beyond this perturbative approach, and obtain the full set of functionals  $\omega_n$ . For this purpose, we define  $\bar{q}(\mathbf{s})$  to be  $(q^+(\mathbf{s}) + q^-(\mathbf{s}))/2$ . Note that the interfacial Hamiltonian (63) is proportional to the surface integral of  $\bar{q}$ . From Eq. (62) it follows that  $\bar{q}$  satisfies the integral equation

$$\bar{q}(\mathbf{s}_{\ell}) = -\kappa m_0 - \int_{\ell} ds U(\mathbf{s}_{\ell}, \mathbf{s}) \bar{q}(\mathbf{s}). \quad (75)$$

Formally, this equation can be solved iteratively as

$$\bar{q}(\mathbf{s}_{\ell}) = -\kappa m_0 \left( 1 - \int_{\ell} ds U(\mathbf{s}_{\ell}, \mathbf{s}) + \int_{\ell} ds ds' U(\mathbf{s}_{\ell}, \mathbf{s}) U(\mathbf{s}, \mathbf{s}') - \dots \right), \quad (76)$$

where the  $n^{\text{th}}$  term involves the convolution of  $n$   $U$ -type functions on the interface. Upon substituting this expres-

sion into Eq. (63) we are lead to the following expansion:

$$H[\ell] = \sigma \left( 1 - \int_{\ell} ds_1 ds_2 U(\mathbf{s}_1, \mathbf{s}_2) + \int_{\ell} ds_1 ds_2 ds_3 U(\mathbf{s}_1, \mathbf{s}_2) U(\mathbf{s}_2, \mathbf{s}_3) - \dots \right) \quad (77)$$

or, diagrammatically,

$$H[\ell] = \sigma \left[ \text{---}\bullet\text{---} - \text{---}\bullet\text{---}\bullet\text{---}\bullet\text{---} + \text{---}\bullet\text{---}\bullet\text{---}\bullet\text{---}\bullet\text{---} + \dots \right]. \quad (78)$$

From this expression, we obtain that

$$\omega_n = \int_{\ell} ds_1 \dots ds_n U(\mathbf{s}_1, \mathbf{s}_2) U(\mathbf{s}_2, \mathbf{s}_3) \dots U(\mathbf{s}_{n-1}, \mathbf{s}_n) \quad (79)$$

which is the expression obtained in Ref. [57]. In general, from Eq. (53) we get that  $\omega_n \sim R^{-2(n-1)}$ , which connects the self-interaction contributions to the curvature corrections to the free energy. We note that this expression is general, so it is also valid for spherical bubbles, for which  $\omega_n = \exp(2(n-1)\kappa R)$  [57] because  $H^2 = K_G$ . We can also obtain the order-parameter profiles by considering in Eq. (61) the limit  $h_1 = 0$ ,  $g \rightarrow -\infty$ ,  $m_b = -m_0$  (or  $+m_0$ ) for the gas (or liquid) phase, respectively. Thus, the order-parameter profile in the gas phase has the expansion

$$\delta m_{\Xi} = m_0 \left[ \text{---}\bullet\text{---} - \text{---}\bullet\text{---}\bullet\text{---}\bullet\text{---} + \text{---}\bullet\text{---}\bullet\text{---}\bullet\text{---}\bullet\text{---} - \dots \right] \quad (80)$$

and in the liquid phase has the expansion

$$\delta m_{\Xi} = -m_0 \left[ \text{---}\bullet\text{---} - \text{---}\bullet\text{---}\bullet\text{---}\bullet\text{---} + \text{---}\bullet\text{---}\bullet\text{---}\bullet\text{---}\bullet\text{---} - \dots \right] \quad (81)$$

Again, these equations reduce to Eqs. (73) and (74) upon using Eq. (53) up to  $R^{-3}$  corrections.

Once we have established the connection between the self-interaction of the fluid interface and the curvature corrections to the interfacial free energy, we can find the full functional of the interfacial shape. This task can be pursued to any desired accuracy in the curvature, which we leave at  $\mathcal{O}(R^{-3})$ . Leaving the technical aspects aside here (see App. B for details) we find that Eq. (68) reduces to the interfacial Hamiltonian

$$H[\ell] \approx \sigma \mathcal{A}_{\pi} + \frac{\sigma}{2} \int d\mathbf{x}_1 d\mathbf{x}_2 \mathcal{W}(x_{12}) (\ell(\mathbf{x}_2) - \ell(\mathbf{x}_1))^2, \quad (82)$$

where the self-interaction is described by the function

$$\mathcal{W}(x) \equiv \frac{\kappa}{2\pi} \frac{1 + \kappa x}{x^3} e^{-\kappa x} = \frac{1 + \kappa x}{x^2} \mathcal{K}(x), \quad (83)$$

thus rigorously re-deriving the result first obtained in Ref. [57]. Clearly, for a flat interface  $H[\ell] = \sigma \mathcal{A}_{\pi}$  with

$\mathcal{A}_\pi$  being the planar (projected) area. As shown in Ref. [57], when the gradient is small we can expand as  $\ell(\mathbf{x}_2) \simeq \ell(\mathbf{x}_1) + \mathbf{x}_{21} \cdot \nabla \ell(\mathbf{x}_1) + \dots$ , in which case Eq. (82) reduces to

$$H[\ell] \approx \sigma \mathcal{A}_\pi + \frac{\sigma}{2} \int d\mathbf{x} (\nabla \ell(\mathbf{x}))^2, \quad (84)$$

thus recovering the standard mesoscopic capillary-wave Hamiltonian, which can now be seen as a particular *local* small-gradient limit of the *non-local* functional (82). The present derivation of the non-local self-interaction improves on that presented in Ref. [57] inasmuch as it systematically and rigorously accounts for all curvature corrections.

### C. Summary and remarks

In this section we considered an isolated liquid-gas interface and solved the Helmholtz equations required to identify the free energy of a constrained interfacial configuration defined by a crossing criterion. We first implemented a direct perturbation expansion in the local curvature, obtaining the Helfrich-like corrections to the surface tension term and identifying the values of bending and saddle-splay rigidities for the DP potential. We then refined this expansion by considering the order-parameter profile around the interface in which the curvature corrections are explicit [see Eqs. (73) and (74)]. This leads us naturally to express the free energy as an interfacial self-interaction that can be neatly expressed that involves a formally exact way using a diagrammatic expansion. Finally, in the limit of small curvatures this non-local interaction recovers the standard local capillary-wave model.

## V. BINDING ENERGY FOR A WETTING FILM CONFIGURATION

Having examined the wall-liquid and free (but constrained) liquid-gas interfaces, we turn to the case of a wall-gas interface where an intruding wetting layer of liquid, with positive order parameter (i.e.,  $m > 0$ ) intrudes between the substrate and the bulk gas (where the order parameter is set to  $-m_0$ ). The wall is again described by a height function  $\psi(\mathbf{x})$ , and the liquid-gas interface (i.e., the surface on which  $m = 0$ ) is constrained to lie along  $\ell(\mathbf{x})$ . No overhangs of either the interface or substrate occur; nor do these two surfaces touch. The minimum of the LGW Hamiltonian (2) subject to the substrate, bulk, and crossing-criterion boundary conditions

$$\mathbf{n}_\psi \cdot \nabla m_\Xi(\mathbf{r}) = -h_1 - gm_\Xi(\mathbf{r}), \text{ for } \mathbf{r} = (\mathbf{x}, \psi(\mathbf{x})); \quad (85)$$

$$m_\Xi(z) \rightarrow -m_0, \quad \text{for } z \rightarrow +\infty; \quad (86)$$

$$m_\Xi(\mathbf{r}) = 0, \text{ for } \mathbf{r} = (\mathbf{x}, \ell(\mathbf{x})) \quad (87)$$

defines a constrained excess free energy for the wall-gas interface, which by Eq. (13) can be recast as

$$\mathcal{F}_{wg}[\ell, \psi] = -\frac{m_0}{2} \int_\ell ds [q_\ell^+(\mathbf{s}) + q_\ell^-(\mathbf{s})] + \frac{h_1 + gm_0}{2g} \int_\psi ds q_\psi(\mathbf{s}), \quad (88)$$

where  $q_\ell^\pm(\mathbf{s}) \equiv \mathbf{n}_\ell(\mathbf{s}) \cdot \nabla_{\mathbf{s}} \delta m^\pm(\mathbf{s})$  for  $\mathbf{s}$  on the liquid-gas interface, and  $q_\psi \equiv \mathbf{n}_\psi(\mathbf{s}) \cdot \nabla_{\mathbf{s}} \delta m(\mathbf{s})$  on the substrate.

The next step is to define and identify the binding potential  $W[\ell, \psi]$ . By analogy with isolated interfaces, the free energy of a wetting layer can be expressed as a functional of the normal derivatives of the order parameter computed at the layer boundaries. The binding potential takes into account the interaction of the interface with the wall, and is determined by subtracting the contributions arising from the isolated wall-liquid and constrained but free liquid-gas interfaces, which we have already determined. Therefore, before presenting the final result for  $W[\ell, \psi]$  and its diagrammatic formulation, we need to consider the fundamental relations obeyed by the order parameter in a wetting layer. In order to do so we need some technical preliminaries.

### A. Technical preliminaries

From Eqs. (20) and (21) it follows that the functions  $q_\ell^+(\mathbf{s})$ ,  $q_\ell^-(\mathbf{s})$ , and  $q_\psi(\mathbf{s})$  satisfy the coupled integral equations

$$\begin{aligned} \int_\psi ds \left[ K(\mathbf{s}_\psi, \mathbf{s}) + \frac{1}{g} \partial_n K(\mathbf{s}_\psi, \mathbf{s}) - \frac{\kappa}{g} \delta(\mathbf{s} - \mathbf{s}_\psi) \right] q_\psi(\mathbf{s}) \\ - \int_\ell ds K(\mathbf{s}_\psi, \mathbf{s}) q_\ell^-(\mathbf{s}) \\ = \left( \frac{-h_1}{g} - m_0 \right) \left( -\kappa + \int_\psi ds \partial_n K(\mathbf{s}_\psi, \mathbf{s}) \right) \\ + m_0 \int_\ell ds \partial_n K(\mathbf{s}_\psi, \mathbf{s}); \quad (89) \end{aligned}$$

$$\begin{aligned} \int_\psi ds \left[ K(\mathbf{s}_\ell, \mathbf{s}) + \frac{1}{g} \partial_n K(\mathbf{s}_\ell, \mathbf{s}) \right] q_\psi(\mathbf{s}) \\ - \int_\ell ds K(\mathbf{s}_\ell, \mathbf{s}) q_\ell^-(\mathbf{s}) = m_0 \left( \kappa + \int_\ell ds \partial_n K(\mathbf{s}_\ell, \mathbf{s}) \right) \\ + \left( \frac{-h_1}{g} - m_0 \right) \int_\psi ds \partial_n K(\mathbf{s}_\ell, \mathbf{s}) \quad (90) \end{aligned}$$

and

$$\int_\ell ds K(\mathbf{s}_\ell, \mathbf{s}) q_\ell^+(\mathbf{s}) = -m_0 \left( \kappa - \int_\ell ds \partial_n K(\mathbf{s}_\ell, \mathbf{s}) \right), \quad (91)$$

where  $\mathbf{s}_\ell$  and  $\mathbf{s}_\psi$  are on the liquid-gas interface and on the substrate, respectively. Note that these equations are linear in  $q$ . In order to extract the interaction between the surfaces, we obtain the equations in

terms of the new fields  $\Delta q_\ell^\pm(\mathbf{s}) \equiv q_\ell^\pm(\mathbf{s}) - q_\ell^{0,\pm}(\mathbf{s})$ , and  $\Delta q_\psi(\mathbf{s}) \equiv q_\psi(\mathbf{s}) - q_\psi^0(\mathbf{s})$ , where the 0-superscript means that the corresponding normal derivative is evaluated on its isolated interface.  $q_\psi^0$  and  $q_\ell^{0,\pm}$  satisfy Eqs. (33) and (62), respectively. Note that  $\Delta q_\ell^{0,+} \equiv 0$  (because the gas domain is shielded from influence of the wall) and Eqs. (89) and (90) can be recast as

$$\begin{aligned} & \int_\psi ds \left[ K(\mathbf{s}_\psi, \mathbf{s}) + \frac{1}{g} \partial_n K(\mathbf{s}_\psi, \mathbf{s}) \right. \\ & \left. - \frac{\kappa}{g} \delta(\mathbf{s}_\psi - \mathbf{s}) \right] \Delta q_\psi(\mathbf{s}) - \int_\ell ds K(\mathbf{s}_\psi, \mathbf{s}) \Delta q_\ell^-(\mathbf{s}) \\ & = m_0 \int_\ell ds \partial_n K(\mathbf{s}_\psi, \mathbf{s}) + \int_\ell ds K(\mathbf{s}_\psi, \mathbf{s}) q_\ell^{0,-}(\mathbf{s}) \\ & \equiv 2\kappa \delta m_\Xi^{0,l}(\mathbf{s}_\psi) \end{aligned} \quad (92)$$

and

$$\begin{aligned} & \int_\psi ds \left[ K(\mathbf{s}_\ell, \mathbf{s}) + \frac{1}{g} \partial_n K(\mathbf{s}_\ell, \mathbf{s}) \right] \Delta q_\psi(\mathbf{s}) \\ & - \int_\ell ds K(\mathbf{s}_\ell, \mathbf{s}) \Delta q_\ell(\mathbf{s}) \\ & = \left( \frac{-h_1}{g} - m_0 \right) \int_\psi ds \partial_n K(\mathbf{s}_\ell, \mathbf{s}) \\ & - \int_\psi ds \left[ K(\mathbf{s}_\ell, \mathbf{s}) + \frac{1}{g} \partial_n K(\mathbf{s}_\ell, \mathbf{s}) \right] q_\psi^0(\mathbf{s}) \\ & \equiv 2\kappa \delta m_\Xi^{0,\psi}(\mathbf{s}_\ell), \end{aligned} \quad (93)$$

where we have identified the RHS of both equations as the order-parameter profile  $\delta m_\Xi^{0,l(\psi)}(\mathbf{s})$  at the boundary point  $\mathbf{s}$  due to the presence of an isolated liquid-gas (wall) interface, respectively [see Eqs. (57) and (72)]. Equations (92) and (93) are the basis of our perturbative approach, as we can expand  $\Delta q_\psi$  and  $\Delta q_\ell^-$  in powers of  $K(\mathbf{s}_\ell, \mathbf{s}_\psi)$  as  $\Delta q_\psi = \sum_{i=1}^{\infty} \Delta q_{i,\psi}$  and  $\Delta q_\ell = \sum_{i=1}^{\infty} \Delta q_{i,\ell}$ . Each term of this expansion can be formally solved as follows. At the wall,

$$\Delta q_{1,\psi}(\mathbf{s}_\psi) = \int_\psi ds X_\psi(\mathbf{s}_\psi, \mathbf{s}) 2\kappa \delta m_\Xi^{0,\ell}(\mathbf{s}), \quad (94)$$

and, otherwise,

$$\Delta q_{i>1,\psi}(\mathbf{s}_\psi) = \int_\psi ds \int_\ell ds' X_\psi(\mathbf{s}_\psi, \mathbf{s}) K(\mathbf{s}, \mathbf{s}') \Delta q_{i-1,\ell}(\mathbf{s}'). \quad (95)$$

Similarly, at the interface

$$\Delta q_{1,\ell}(\mathbf{s}_\ell) = - \int_\ell ds K_\ell^{-1}(\mathbf{s}_\ell, \mathbf{s}) 2\kappa \delta m_\Xi^{0,\psi}(\mathbf{s}), \quad (96)$$

and, otherwise,

$$\begin{aligned} \Delta q_{i>1,\ell}(\mathbf{s}_\ell) & = \int_\ell ds \int_\psi ds' K_\ell^{-1}(\mathbf{s}_\ell, \mathbf{s}) \left( K(\mathbf{s}, \mathbf{s}') \right. \\ & \left. + \frac{1}{g} \partial_{n'} K(\mathbf{s}, \mathbf{s}') \right) \Delta q_{i-1,\psi}(\mathbf{s}'), \end{aligned} \quad (97)$$

where  $X_\psi$  is the operator on the substrate defined by Eq. (47), and  $K_\ell^{-1}$  is the inverse operator of  $K$  on the liquid-gas interface.

Now using the Green's identities (28)-(30), it follows that

$$\begin{aligned} \Delta q_{i>1,\ell}(\mathbf{s}_\ell) & = \int_\ell ds \int_\psi ds' \int_\psi ds'' K_\ell^{-1}(\mathbf{s}_\ell, \mathbf{s}) \\ & \times K(\mathbf{s}, \mathbf{s}') \left( \delta(\mathbf{s}' - \mathbf{s}'') + \frac{\kappa}{g} K_\psi^{-1}(\mathbf{s}', \mathbf{s}'') \right) \Delta q_{i-1,\psi}(\mathbf{s}'') \\ & + \frac{\kappa}{g} \int_\ell ds \int_\psi ds' \int_\psi ds'' \int_\psi ds''' K_\ell^{-1}(\mathbf{s}_\ell, \mathbf{s}) K(\mathbf{s}, \mathbf{s}') \\ & \times \frac{1}{\kappa} \partial_{n'} K(\mathbf{s}', \mathbf{s}'') K_\psi^{-1}(\mathbf{s}'', \mathbf{s}''') \Delta q_{i-1,\psi}(\mathbf{s}'''), \end{aligned} \quad (98)$$

where  $K_\psi^{-1}$  is the inverse operator of  $K$  on the substrate, i.e.,  $X_\psi$  in the limit  $g \rightarrow -\infty$ . Taking into account the expansions (47), (60), (61) and (81), we obtain a diagrammatic expansion for  $\Delta q_\ell$  and  $\Delta q_\psi$ :

$$\begin{aligned} \Delta q_\psi(\mathbf{s}) & = -2\kappa m_0 \left[ \frac{g}{g-\kappa} \left( \text{diagram 1} - \text{diagram 2} + \dots \right) \right. \\ & \left. + \frac{\kappa}{\kappa-g} \text{diagram 3} + \dots - \frac{\kappa}{\kappa-g} \text{diagram 4} \right] \\ & \left( \frac{g}{g-\kappa} \right)^2 \left( 1 + \frac{\kappa}{g} \text{diagram 5} + \dots \right) \\ & + 2\kappa \frac{h_1 + gm_0}{g} \left[ \left( \frac{g}{g-\kappa} \right)^2 \left( \text{diagram 6} \right) \right. \\ & \left. + \frac{g}{\kappa-g} \text{diagram 7} + \dots \right] + \dots \end{aligned} \quad (99)$$

and

$$\begin{aligned} \Delta q_\ell^-(\mathbf{s}) & = 2\kappa \frac{h_1 + gm_0}{g} \left[ \frac{g}{g-\kappa} \left( \text{diagram 8} \right) \right. \\ & \left. - \text{diagram 9} + \frac{g}{\kappa-g} \text{diagram 10} + \dots \right] \\ & - 2\kappa m_0 \left[ \frac{g+\kappa}{g-\kappa} \text{diagram 11} + \dots \right] + \dots \end{aligned} \quad (100)$$

where the symbols have the meanings as described above. The diagrams in this expansion have segments on alternating interfaces connected via  $K$  kernels, so they can be

regarded as decorated versions of the zig-zag diagrams of the original non-local model. The segments on the substrate correspond to convolution products of  $U$  and  $(\partial_n K)/\kappa$ -type bonds on this surface, while on the liquid-gas interface only  $U$ -type bonds are involved. The filled extreme, which by convention we place on the left, provides the factor  $-2\kappa m_0$  or  $-2\kappa(h_1 + gm_0)/g$ , depending on whether it is located on the liquid-gas interface or on the substrate, respectively. On the other hand, the interface on which the open extreme resides indicates whether the diagram contributes to  $\Delta q_\psi$  (if it is on the substrate) or  $\Delta q_\ell^-$  (otherwise). The factor that multiplies each diagram can be obtained as the product of terms associated to each segment. The segments on the liquid-gas interface have a factor  $(-1)^n$ , where  $n$  is the number of bonds (of  $U$ -type) in the segment. The contribution of the segments on the substrate depend on their positions. Let  $n$  be the total number of bonds in the segment, and  $m$  be the number of  $(\partial_n K)/\kappa$  bonds. If the segment contains the filled extreme, its contribution is given by

$$-\left(\frac{g}{\kappa - g}\right)^{n+1} \left(\frac{\kappa}{g}\right)^{m-m_0} \left[1 - (1 - \delta_{m,0}) \left(1 - \frac{\kappa}{g}\right)^{l+1}\right] \quad (101)$$

where  $\delta_{i,j}$  is the Kronecker symbol, the index  $m_0$  is either 0 or 1 (depending on the first bond being of  $U$ -type or  $(\partial_n K)/\kappa$ -type, respectively), and  $l$  is the number of  $U$ -type bonds after the last  $(\partial K)/\kappa$ -type bond. Note that this expression is the factor that multiplies the diagrams in the expansion (61) for the order-parameter profile above the substrate, multiplied by  $g/(g - \kappa)$ . The contribution of a segment on the substrate that contains the open extreme is

$$-\left(\frac{g}{\kappa - g}\right)^{n+1} \left(\frac{\kappa}{g}\right)^m. \quad (102)$$

Finally, any other segment on the substrate will provide the following factor: either

$$-\left(\frac{g}{\kappa - g}\right)^{n+1} \left(\frac{\kappa}{g}\right)^m \left[2 - \left(1 - \frac{\kappa}{g}\right)^{l+1}\right], \quad (103)$$

if the last bond is of  $U$ -type, or

$$-\left(\frac{g}{\kappa - g}\right)^{n+1} \left(\frac{\kappa}{g}\right)^m \left[2 - \frac{g}{\kappa} + \frac{\kappa}{g} - \left(1 - \frac{g}{\kappa}\right) \left(1 - \frac{\kappa}{g}\right)^{l+1}\right], \quad (104)$$

with  $l$  being the number of consecutive  $U$ -type bonds in the rightmost sequence in the segment.

## B. Binding potential functional and order parameter

With these preliminaries behind us, we are now in a position to obtain the diagrammatic representation of the binding potential and the order-parameter profile. The binding potential functional  $W[\ell, \psi]$  is defined as the substrate-interface interaction in the excess free energy:

$$\mathcal{F}_{wg} = \mathcal{F}_{wl}[\psi] + H[\ell] + W[\ell, \psi], \quad (105)$$

where  $\mathcal{F}_{wl}[\psi]$  is the free energy of the wall-liquid interface and  $H[\ell]$  is the free liquid-gas interfacial Hamiltonian, which we have already determined. So, in terms of  $\Delta q_\ell^-$  and  $\Delta q_\psi$ , we have

$$W[\ell, \psi] = -\frac{m_0}{2} \int_\ell ds \Delta q_\ell^-(\mathbf{s}) + \frac{h_1 + gm_0}{2g} \int_\psi ds \Delta q_\psi(\mathbf{s}). \quad (106)$$

Substituting the expansions (99) and (100) into this expression, we arrive at the following diagrammatic expansion for the binding potential functional:

$$W[\ell, \psi] = \sum_{n=1}^{\infty} \left( -\kappa m_0 \frac{h_1 + gm_0}{g} \Omega_n^n + \kappa m_0^2 \Omega_n^{n+1} + \kappa \left(\frac{h_1 + gm_0}{g}\right)^2 \Omega_{n+1}^n \right), \quad (107)$$

where  $\Omega_i^j$  is the sum of all the independent diagrams that have  $i$  segments on the substrate and  $j$  segments on the liquid-gas interface. Note that these diagrams correspond to those obtained previously for  $\Delta q_\psi$  and  $\Delta q_\ell^-$ , but integrating over the positions of  $\mathbf{s}$ , i.e., with a filled right extreme. For the first terms we have:

$$\begin{aligned} \Omega_1^1 = & \frac{g}{g - \kappa} \left( 2 \begin{array}{c} \text{---} \bullet \text{---} \\ \text{---} \bullet \text{---} \end{array} - 2 \begin{array}{c} \text{---} \bullet \text{---} \\ \text{---} \bullet \text{---} \end{array} \right) \\ & + \frac{\kappa}{\kappa - g} \begin{array}{c} \text{---} \bullet \text{---} \\ \text{---} \bullet \text{---} \end{array} + \frac{g}{\kappa - g} \begin{array}{c} \text{---} \bullet \text{---} \\ \text{---} \bullet \text{---} \end{array} \\ & - \frac{\kappa}{\kappa - g} \begin{array}{c} \text{---} \bullet \text{---} \\ \text{---} \bullet \text{---} \end{array} + \dots \end{aligned} \quad (108)$$

while

$$\begin{aligned} \Omega_1^2 = & \frac{g}{g - \kappa} \left( \frac{\kappa + g}{g} \begin{array}{c} \text{---} \bullet \text{---} \\ \text{---} \bullet \text{---} \end{array} - 2 \frac{\kappa + g}{g} \begin{array}{c} \text{---} \bullet \text{---} \\ \text{---} \bullet \text{---} \end{array} + \frac{\kappa + g}{g} \begin{array}{c} \text{---} \bullet \text{---} \\ \text{---} \bullet \text{---} \end{array} \right) \\ & + \frac{2\kappa}{g} \begin{array}{c} \text{---} \bullet \text{---} \\ \text{---} \bullet \text{---} \end{array} + \dots \end{aligned} \quad (109)$$

and

$$\Omega_2^1 = \left( \frac{g}{g-\kappa} \right)^2 \left( \begin{array}{c} \text{Diagram 1} \\ \text{Diagram 2} \\ \text{Diagram 3} \\ \text{Diagram 4} \\ \text{Diagram 5} \\ \text{Diagram 6} \\ \text{Diagram 7} \\ \text{Diagram 8} \\ \text{Diagram 9} \\ \text{Diagram 10} \\ \text{Diagram 11} \\ \text{Diagram 12} \\ \text{Diagram 13} \\ \text{Diagram 14} \\ \text{Diagram 15} \\ \text{Diagram 16} \\ \text{Diagram 17} \\ \text{Diagram 18} \\ \text{Diagram 19} \\ \text{Diagram 20} \\ \text{Diagram 21} \\ \text{Diagram 22} \\ \text{Diagram 23} \\ \text{Diagram 24} \\ \text{Diagram 25} \\ \text{Diagram 26} \\ \text{Diagram 27} \\ \text{Diagram 28} \\ \text{Diagram 29} \\ \text{Diagram 30} \\ \text{Diagram 31} \\ \text{Diagram 32} \\ \text{Diagram 33} \\ \text{Diagram 34} \\ \text{Diagram 35} \\ \text{Diagram 36} \\ \text{Diagram 37} \\ \text{Diagram 38} \\ \text{Diagram 39} \\ \text{Diagram 40} \\ \text{Diagram 41} \\ \text{Diagram 42} \\ \text{Diagram 43} \\ \text{Diagram 44} \\ \text{Diagram 45} \\ \text{Diagram 46} \\ \text{Diagram 47} \\ \text{Diagram 48} \\ \text{Diagram 49} \\ \text{Diagram 50} \\ \text{Diagram 51} \\ \text{Diagram 52} \\ \text{Diagram 53} \\ \text{Diagram 54} \\ \text{Diagram 55} \\ \text{Diagram 56} \\ \text{Diagram 57} \\ \text{Diagram 58} \\ \text{Diagram 59} \\ \text{Diagram 60} \\ \text{Diagram 61} \\ \text{Diagram 62} \\ \text{Diagram 63} \\ \text{Diagram 64} \\ \text{Diagram 65} \\ \text{Diagram 66} \\ \text{Diagram 67} \\ \text{Diagram 68} \\ \text{Diagram 69} \\ \text{Diagram 70} \\ \text{Diagram 71} \\ \text{Diagram 72} \\ \text{Diagram 73} \\ \text{Diagram 74} \\ \text{Diagram 75} \\ \text{Diagram 76} \\ \text{Diagram 77} \\ \text{Diagram 78} \\ \text{Diagram 79} \\ \text{Diagram 80} \\ \text{Diagram 81} \\ \text{Diagram 82} \\ \text{Diagram 83} \\ \text{Diagram 84} \\ \text{Diagram 85} \\ \text{Diagram 86} \\ \text{Diagram 87} \\ \text{Diagram 88} \\ \text{Diagram 89} \\ \text{Diagram 90} \\ \text{Diagram 91} \\ \text{Diagram 92} \\ \text{Diagram 93} \\ \text{Diagram 94} \\ \text{Diagram 95} \\ \text{Diagram 96} \\ \text{Diagram 97} \\ \text{Diagram 98} \\ \text{Diagram 99} \\ \text{Diagram 100} \end{array} \right). \quad (110)$$

These diagrams are all decorated versions of the diagrams in the original non-local model. They are multiplied by a factor that is the same as the corresponding coefficient for the associated  $\Delta q$  diagram with open right extreme, provided the diagram either contains  $(\partial_n K)/\kappa$ -type bonds or is symmetric under a mirror reflection, i.e., it is the same when read from left to right or the reverse. Otherwise, the factor is twice the coefficient for the associated  $\Delta q$  diagram. The reason for this is that two different  $\Delta q$  diagrams lead to the same contribution to  $W[\ell, \psi]$ . In this sense we mean that only independent diagrams are taken into account in the diagrammatic expansion of  $W[\ell, \psi]$ , because we discard one of the two equivalent diagrams, which are related via a mirror reflection.

Now we turn to the order-parameter profile. Above the liquid-gas interface the profile is uninfluenced by the presence of the substrate, so it has a diagrammatic expansion given by Eq. (80). On the other hand, the order-parameter profile within the adsorbed liquid layer is influenced by the proximity of both the wall and the liquid-gas interface, and has the representation

$$\begin{aligned} \delta m_{\Xi}(\mathbf{r}) &= -\frac{1}{2\kappa} \int_{\psi} ds K(\mathbf{s}, \mathbf{r}) q_{\psi}(\mathbf{s}) \\ &\quad - \frac{1}{2\kappa} \int_{\psi} ds \left( \frac{h_1}{g} + m_b + \frac{q_{\psi}(\mathbf{s})}{g} \right) \partial_n K(\mathbf{s}, \mathbf{r}) \\ &\quad + \frac{1}{2\kappa} \int_{\ell} ds K(\mathbf{s}, \mathbf{r}) q_{\ell}^{-}(\mathbf{s}) \\ &\quad + \frac{m_0}{2\kappa} \int_{\ell} ds \partial_n K(\mathbf{s}, \mathbf{r}). \end{aligned} \quad (111)$$

Now, writing  $q_{\psi} = q_{\psi}^0 + \Delta q_{\psi}$  and  $q_{\ell}^{-} = q_{\ell}^{0,-} + \Delta q_{\ell}^{-}$ , and making use of Eqs. (57) and (72), we obtain the following expression for the order parameter in the liquid layer:

$$\begin{aligned} \delta m_{\Xi}(\mathbf{r}) &= \delta m_{\Xi}^{0,\psi}(\mathbf{r}) + \delta m_{\Xi}^{0,\ell}(\mathbf{r}) \\ &\quad + \frac{1}{2\kappa} \int_{\ell} ds K(\mathbf{s}, \mathbf{r}) \Delta q_{\ell}^{-}(\mathbf{s}) \\ &\quad - \frac{1}{2\kappa} \int_{\psi} ds \left( K(\mathbf{s}, \mathbf{r}) + \frac{1}{g} \partial_n K(\mathbf{s}, \mathbf{r}) \right) \Delta q_{\psi}(\mathbf{s}), \end{aligned} \quad (112)$$

where the kernel connecting the substrate to the position  $\mathbf{r}$  in the last term can be related to  $K$  using Eq. (29). Taking into account the expansions (99) and (100), we find that the order-parameter profile in the liquid layer

has the following expansion:

$$\begin{aligned} \delta m_{\Xi} &= -m_0 \left[ \begin{array}{c} \text{Diagram 1} \\ \text{Diagram 2} \\ \text{Diagram 3} \\ \text{Diagram 4} \\ \text{Diagram 5} \\ \text{Diagram 6} \\ \text{Diagram 7} \\ \text{Diagram 8} \\ \text{Diagram 9} \\ \text{Diagram 10} \\ \text{Diagram 11} \\ \text{Diagram 12} \\ \text{Diagram 13} \\ \text{Diagram 14} \\ \text{Diagram 15} \\ \text{Diagram 16} \\ \text{Diagram 17} \\ \text{Diagram 18} \\ \text{Diagram 19} \\ \text{Diagram 20} \\ \text{Diagram 21} \\ \text{Diagram 22} \\ \text{Diagram 23} \\ \text{Diagram 24} \\ \text{Diagram 25} \\ \text{Diagram 26} \\ \text{Diagram 27} \\ \text{Diagram 28} \\ \text{Diagram 29} \\ \text{Diagram 30} \\ \text{Diagram 31} \\ \text{Diagram 32} \\ \text{Diagram 33} \\ \text{Diagram 34} \\ \text{Diagram 35} \\ \text{Diagram 36} \\ \text{Diagram 37} \\ \text{Diagram 38} \\ \text{Diagram 39} \\ \text{Diagram 40} \\ \text{Diagram 41} \\ \text{Diagram 42} \\ \text{Diagram 43} \\ \text{Diagram 44} \\ \text{Diagram 45} \\ \text{Diagram 46} \\ \text{Diagram 47} \\ \text{Diagram 48} \\ \text{Diagram 49} \\ \text{Diagram 50} \\ \text{Diagram 51} \\ \text{Diagram 52} \\ \text{Diagram 53} \\ \text{Diagram 54} \\ \text{Diagram 55} \\ \text{Diagram 56} \\ \text{Diagram 57} \\ \text{Diagram 58} \\ \text{Diagram 59} \\ \text{Diagram 60} \\ \text{Diagram 61} \\ \text{Diagram 62} \\ \text{Diagram 63} \\ \text{Diagram 64} \\ \text{Diagram 65} \\ \text{Diagram 66} \\ \text{Diagram 67} \\ \text{Diagram 68} \\ \text{Diagram 69} \\ \text{Diagram 70} \\ \text{Diagram 71} \\ \text{Diagram 72} \\ \text{Diagram 73} \\ \text{Diagram 74} \\ \text{Diagram 75} \\ \text{Diagram 76} \\ \text{Diagram 77} \\ \text{Diagram 78} \\ \text{Diagram 79} \\ \text{Diagram 80} \\ \text{Diagram 81} \\ \text{Diagram 82} \\ \text{Diagram 83} \\ \text{Diagram 84} \\ \text{Diagram 85} \\ \text{Diagram 86} \\ \text{Diagram 87} \\ \text{Diagram 88} \\ \text{Diagram 89} \\ \text{Diagram 90} \\ \text{Diagram 91} \\ \text{Diagram 92} \\ \text{Diagram 93} \\ \text{Diagram 94} \\ \text{Diagram 95} \\ \text{Diagram 96} \\ \text{Diagram 97} \\ \text{Diagram 98} \\ \text{Diagram 99} \\ \text{Diagram 100} \end{array} \right] \\ &\quad - \frac{\kappa+g}{g-\kappa} \left[ \begin{array}{c} \text{Diagram 101} \\ \text{Diagram 102} \\ \text{Diagram 103} \\ \text{Diagram 104} \\ \text{Diagram 105} \\ \text{Diagram 106} \\ \text{Diagram 107} \\ \text{Diagram 108} \\ \text{Diagram 109} \\ \text{Diagram 110} \\ \text{Diagram 111} \\ \text{Diagram 112} \\ \text{Diagram 113} \\ \text{Diagram 114} \\ \text{Diagram 115} \\ \text{Diagram 116} \\ \text{Diagram 117} \\ \text{Diagram 118} \\ \text{Diagram 119} \\ \text{Diagram 120} \\ \text{Diagram 121} \\ \text{Diagram 122} \\ \text{Diagram 123} \\ \text{Diagram 124} \\ \text{Diagram 125} \\ \text{Diagram 126} \\ \text{Diagram 127} \\ \text{Diagram 128} \\ \text{Diagram 129} \\ \text{Diagram 130} \\ \text{Diagram 131} \\ \text{Diagram 132} \\ \text{Diagram 133} \\ \text{Diagram 134} \\ \text{Diagram 135} \\ \text{Diagram 136} \\ \text{Diagram 137} \\ \text{Diagram 138} \\ \text{Diagram 139} \\ \text{Diagram 140} \\ \text{Diagram 141} \\ \text{Diagram 142} \\ \text{Diagram 143} \\ \text{Diagram 144} \\ \text{Diagram 145} \\ \text{Diagram 146} \\ \text{Diagram 147} \\ \text{Diagram 148} \\ \text{Diagram 149} \\ \text{Diagram 150} \\ \text{Diagram 151} \\ \text{Diagram 152} \\ \text{Diagram 153} \\ \text{Diagram 154} \\ \text{Diagram 155} \\ \text{Diagram 156} \\ \text{Diagram 157} \\ \text{Diagram 158} \\ \text{Diagram 159} \\ \text{Diagram 160} \\ \text{Diagram 161} \\ \text{Diagram 162} \\ \text{Diagram 163} \\ \text{Diagram 164} \\ \text{Diagram 165} \\ \text{Diagram 166} \\ \text{Diagram 167} \\ \text{Diagram 168} \\ \text{Diagram 169} \\ \text{Diagram 170} \\ \text{Diagram 171} \\ \text{Diagram 172} \\ \text{Diagram 173} \\ \text{Diagram 174} \\ \text{Diagram 175} \\ \text{Diagram 176} \\ \text{Diagram 177} \\ \text{Diagram 178} \\ \text{Diagram 179} \\ \text{Diagram 180} \\ \text{Diagram 181} \\ \text{Diagram 182} \\ \text{Diagram 183} \\ \text{Diagram 184} \\ \text{Diagram 185} \\ \text{Diagram 186} \\ \text{Diagram 187} \\ \text{Diagram 188} \\ \text{Diagram 189} \\ \text{Diagram 190} \\ \text{Diagram 191} \\ \text{Diagram 192} \\ \text{Diagram 193} \\ \text{Diagram 194} \\ \text{Diagram 195} \\ \text{Diagram 196} \\ \text{Diagram 197} \\ \text{Diagram 198} \\ \text{Diagram 199} \\ \text{Diagram 200} \end{array} \right] \\ &\quad - \frac{h_1 + gm_0}{g} \left[ \begin{array}{c} \text{Diagram 201} \\ \text{Diagram 202} \\ \text{Diagram 203} \\ \text{Diagram 204} \\ \text{Diagram 205} \\ \text{Diagram 206} \\ \text{Diagram 207} \\ \text{Diagram 208} \\ \text{Diagram 209} \\ \text{Diagram 210} \\ \text{Diagram 211} \\ \text{Diagram 212} \\ \text{Diagram 213} \\ \text{Diagram 214} \\ \text{Diagram 215} \\ \text{Diagram 216} \\ \text{Diagram 217} \\ \text{Diagram 218} \\ \text{Diagram 219} \\ \text{Diagram 220} \\ \text{Diagram 221} \\ \text{Diagram 222} \\ \text{Diagram 223} \\ \text{Diagram 224} \\ \text{Diagram 225} \\ \text{Diagram 226} \\ \text{Diagram 227} \\ \text{Diagram 228} \\ \text{Diagram 229} \\ \text{Diagram 230} \\ \text{Diagram 231} \\ \text{Diagram 232} \\ \text{Diagram 233} \\ \text{Diagram 234} \\ \text{Diagram 235} \\ \text{Diagram 236} \\ \text{Diagram 237} \\ \text{Diagram 238} \\ \text{Diagram 239} \\ \text{Diagram 240} \\ \text{Diagram 241} \\ \text{Diagram 242} \\ \text{Diagram 243} \\ \text{Diagram 244} \\ \text{Diagram 245} \\ \text{Diagram 246} \\ \text{Diagram 247} \\ \text{Diagram 248} \\ \text{Diagram 249} \\ \text{Diagram 250} \\ \text{Diagram 251} \\ \text{Diagram 252} \\ \text{Diagram 253} \\ \text{Diagram 254} \\ \text{Diagram 255} \\ \text{Diagram 256} \\ \text{Diagram 257} \\ \text{Diagram 258} \\ \text{Diagram 259} \\ \text{Diagram 260} \\ \text{Diagram 261} \\ \text{Diagram 262} \\ \text{Diagram 263} \\ \text{Diagram 264} \\ \text{Diagram 265} \\ \text{Diagram 266} \\ \text{Diagram 267} \\ \text{Diagram 268} \\ \text{Diagram 269} \\ \text{Diagram 270} \\ \text{Diagram 271} \\ \text{Diagram 272} \\ \text{Diagram 273} \\ \text{Diagram 274} \\ \text{Diagram 275} \\ \text{Diagram 276} \\ \text{Diagram 277} \\ \text{Diagram 278} \\ \text{Diagram 279} \\ \text{Diagram 280} \\ \text{Diagram 281} \\ \text{Diagram 282} \\ \text{Diagram 283} \\ \text{Diagram 284} \\ \text{Diagram 285} \\ \text{Diagram 286} \\ \text{Diagram 287} \\ \text{Diagram 288} \\ \text{Diagram 289} \\ \text{Diagram 290} \\ \text{Diagram 291} \\ \text{Diagram 292} \\ \text{Diagram 293} \\ \text{Diagram 294} \\ \text{Diagram 295} \\ \text{Diagram 296} \\ \text{Diagram 297} \\ \text{Diagram 298} \\ \text{Diagram 299} \\ \text{Diagram 300} \end{array} \right] \\ &\quad - \left( \frac{g}{\kappa-g} \right)^2 \left[ \begin{array}{c} \text{Diagram 301} \\ \text{Diagram 302} \\ \text{Diagram 303} \\ \text{Diagram 304} \\ \text{Diagram 305} \\ \text{Diagram 306} \\ \text{Diagram 307} \\ \text{Diagram 308} \\ \text{Diagram 309} \\ \text{Diagram 310} \\ \text{Diagram 311} \\ \text{Diagram 312} \\ \text{Diagram 313} \\ \text{Diagram 314} \\ \text{Diagram 315} \\ \text{Diagram 316} \\ \text{Diagram 317} \\ \text{Diagram 318} \\ \text{Diagram 319} \\ \text{Diagram 320} \\ \text{Diagram 321} \\ \text{Diagram 322} \\ \text{Diagram 323} \\ \text{Diagram 324} \\ \text{Diagram 325} \\ \text{Diagram 326} \\ \text{Diagram 327} \\ \text{Diagram 328} \\ \text{Diagram 329} \\ \text{Diagram 330} \\ \text{Diagram 331} \\ \text{Diagram 332} \\ \text{Diagram 333} \\ \text{Diagram 334} \\ \text{Diagram 335} \\ \text{Diagram 336} \\ \text{Diagram 337} \\ \text{Diagram 338} \\ \text{Diagram 339} \\ \text{Diagram 340} \\ \text{Diagram 341} \\ \text{Diagram 342} \\ \text{Diagram 343} \\ \text{Diagram 344} \\ \text{Diagram 345} \\ \text{Diagram 346} \\ \text{Diagram 347} \\ \text{Diagram 348} \\ \text{Diagram 349} \\ \text{Diagram 350} \\ \text{Diagram 351} \\ \text{Diagram 352} \\ \text{Diagram 353} \\ \text{Diagram 354} \\ \text{Diagram 355} \\ \text{Diagram 356} \\ \text{Diagram 357} \\ \text{Diagram 358} \\ \text{Diagram 359} \\ \text{Diagram 360} \\ \text{Diagram 361} \\ \text{Diagram 362} \\ \text{Diagram 363} \\ \text{Diagram 364} \\ \text{Diagram 365} \\ \text{Diagram 366} \\ \text{Diagram 367} \\ \text{Diagram 368} \\ \text{Diagram 369} \\ \text{Diagram 370} \\ \text{Diagram 371} \\ \text{Diagram 372} \\ \text{Diagram 373} \\ \text{Diagram 374} \\ \text{Diagram 375} \\ \text{Diagram 376} \\ \text{Diagram 377} \\ \text{Diagram 378} \\ \text{Diagram 379} \\ \text{Diagram 380} \\ \text{Diagram 381} \\ \text{Diagram 382} \\ \text{Diagram 383} \\ \text{Diagram 384} \\ \text{Diagram 385} \\ \text{Diagram 386} \\ \text{Diagram 387} \\ \text{Diagram 388} \\ \text{Diagram 389} \\ \text{Diagram 390} \\ \text{Diagram 391} \\ \text{Diagram 392} \\ \text{Diagram 393} \\ \text{Diagram 394} \\ \text{Diagram 395} \\ \text{Diagram 396} \\ \text{Diagram 397} \\ \text{Diagram 398} \\ \text{Diagram 399} \\ \text{Diagram 400} \end{array} \right] \\ &\quad - \frac{g}{g-\kappa} \left[ \begin{array}{c} \text{Diagram 401} \\ \text{Diagram 402} \\ \text{Diagram 403} \\ \text{Diagram 404} \\ \text{Diagram 405} \\ \text{Diagram 406} \\ \text{Diagram 407} \\ \text{Diagram 408} \\ \text{Diagram 409} \\ \text{Diagram 410} \\ \text{Diagram 411} \\ \text{Diagram 412} \\ \text{Diagram 413} \\ \text{Diagram 414} \\ \text{Diagram 415} \\ \text{Diagram 416} \\ \text{Diagram 417} \\ \text{Diagram 418} \\ \text{Diagram 419} \\ \text{Diagram 420} \\ \text{Diagram 421} \\ \text{Diagram 422} \\ \text{Diagram 423} \\ \text{Diagram 424} \\ \text{Diagram 425} \\ \text{Diagram 426} \\ \text{Diagram 427} \\ \text{Diagram 428} \\ \text{Diagram 429} \\ \text{Diagram 430} \\ \text{Diagram 431} \\ \text{Diagram 432} \\ \text{Diagram 433} \\ \text{Diagram 434} \\ \text{Diagram 435} \\ \text{Diagram 436} \\ \text{Diagram 437} \\ \text{Diagram 438} \\ \text{Diagram 439} \\ \text{Diagram 440} \\ \text{Diagram 441} \\ \text{Diagram 442} \\ \text{Diagram 443} \\ \text{Diagram 444} \\ \text{Diagram 445} \\ \text{Diagram 446} \\ \text{Diagram 447} \\ \text{Diagram 448} \\ \text{Diagram 449} \\ \text{Diagram 450} \\ \text{Diagram 451} \\ \text{Diagram 452} \\ \text{Diagram 453} \\ \text{Diagram 454} \\ \text{Diagram 455} \\ \text{Diagram 456} \\ \text{Diagram 457} \\ \text{Diagram 458} \\ \text{Diagram 459} \\ \text{Diagram 460} \\ \text{Diagram 461} \\ \text{Diagram 462} \\ \text{Diagram 463} \\ \text{Diagram 464} \\ \text{Diagram 465} \\ \text{Diagram 466} \\ \text{Diagram 467} \\ \text{Diagram 468} \\ \text{Diagram 469} \\ \text{Diagram 470} \\ \text{Diagram 471} \\ \text{Diagram 472} \\ \text{Diagram 473} \\ \text{Diagram 474} \\ \text{Diagram 475} \\ \text{Diagram 476} \\ \text{Diagram 477} \\ \text{Diagram 478} \\ \text{Diagram 479} \\ \text{Diagram 480} \\ \text{Diagram 481} \\ \text{Diagram 482} \\ \text{Diagram 483} \\ \text{Diagram 484} \\ \text{Diagram 485} \\ \text{Diagram 486} \\ \text{Diagram 487} \\ \text{Diagram 488} \\ \text{Diagram 489} \\ \text{Diagram 490} \\ \text{Diagram 491} \\ \text{Diagram 492} \\ \text{Diagram 493} \\ \text{Diagram 494} \\ \text{Diagram 495} \\ \text{Diagram 496} \\ \text{Diagram 497} \\ \text{Diagram 498} \\ \text{Diagram 499} \\ \text{Diagram 500} \end{array} \right] \\ &\quad + \left( \frac{g}{g-\kappa} \right) \left( \frac{\kappa+g}{g-\kappa} \right)^2 \left[ \begin{array}{c} \text{Diagram 501} \\ \text{Diagram 502} \\ \text{Diagram 503} \\ \text{Diagram 504} \\ \text{Diagram 505} \\ \text{Diagram 506} \\ \text{Diagram 507} \\ \text{Diagram 508} \\ \text{Diagram 509} \\ \text{Diagram 510} \\ \text{Diagram 511} \\ \text{Diagram 512} \\ \text{Diagram 513} \\ \text{Diagram 514} \\ \text{Diagram 515} \\ \text{Diagram 516} \\ \text{Diagram 517} \\ \text{Diagram 518} \\ \text{Diagram 519} \\ \text{Diagram 520} \\ \text{Diagram 521} \\ \text{Diagram 522} \\ \text{Diagram 523} \\ \text{Diagram 524} \\ \text{Diagram 525} \\ \text{Diagram 526} \\ \text{Diagram 527} \\ \text{Diagram 528} \\ \text{Diagram 529} \\ \text{Diagram 530} \\ \text{Diagram 531} \\ \text{Diagram 532} \\ \text{Diagram 533} \\ \text{Diagram 534} \\ \text{Diagram 535} \\ \text{Diagram 536} \\ \text{Diagram 537} \\ \text{Diagram 538} \\ \text{Diagram 539} \\ \text{Diagram 540} \\ \text{Diagram 541} \\ \text{Diagram 542} \\ \text{Diagram 543} \\ \text{Diagram 544} \\ \text{Diagram 545} \\ \text{Diagram 546} \\ \text{Diagram 547} \\ \text{Diagram 548} \\ \text{Diagram 549} \\ \text{Diagram 550} \\ \text{Diagram 551} \\ \text{Diagram 552} \\ \text{Diagram 553} \\ \text{Diagram 554} \\ \text{Diagram 555} \\ \text{Diagram 556} \\ \text{Diagram 557} \\ \text{Diagram 558} \\ \text{Diagram 559} \\ \text{Diagram 560} \\ \text{Diagram 561} \\ \text{Diagram 562} \\ \text{Diagram 563} \\ \text{Diagram 564} \\ \text{Diagram 565} \\ \text{Diagram 566} \\ \text{Diagram 567} \\ \text{Diagram 568} \\ \text{Diagram 569} \\ \text{Diagram 570} \\ \text{Diagram 571} \\ \text{Diagram 572} \\ \text{Diagram 573} \\ \text{Diagram 574} \\ \text{Diagram 575} \\ \text{Diagram 576} \\ \text{Diagram 577} \\ \text{Diagram 578} \\ \text{Diagram 579} \\ \text{Diagram 580} \\ \text{Diagram 581} \\ \text{Diagram 582} \\ \text{Diagram 583} \\ \text{Diagram 584} \\ \text{Diagram 585} \\ \text{Diagram 586} \\ \text{Diagram 587} \\ \text{Diagram 588} \\ \text{Diagram 589} \\ \text{Diagram 590} \\ \text{Diagram 591} \\ \text{Diagram 592} \\ \text{Diagram 593} \\ \text{Diagram 594} \\ \text{Diagram 595} \\ \text{Diagram 596} \\ \text{Diagram 597} \\ \text{Diagram 598} \\ \text{Diagram 599} \\ \text{Diagram 600} \end{array} \right]. \end{aligned} \quad (113)$$

Note that, once again, these diagrams are decorated versions of those obtained in the original non-local model. Their prefactors are either  $-m_0$  (if the left extreme is on the liquid-gas interface) or  $-h_1/g - m_0$  (if it is on the substrate). The coefficient that multiplies each diagram is the product of  $(-1)^k$ , with  $k$  being the number of  $K$ -type bonds that connect both interfaces, and the factors associated with the segments with each substrate. Sections with  $n$  of the  $U$ -type bonds on the liquid-gas interface contribute with a factor  $(-1)^n$ . A segment on the substrate has a factor given by Eq. (101) if it contains the left diagram extreme, and otherwise by Eq. (103) or (104), depending on the nature of the rightmost bond in the segment.

### C. Resummation of wetting diagrams

As we pointed out in the previous sections, the curvature expansion for isolated interfaces is actually connected to the formal diagrammatic method we have developed. This connection also persists for a wetting film configuration; but it is not at all explicit. The aim of this section is to illustrate how the perturbative scheme emerges from the diagrammatic one. However, the connection is actually far from trivial. The reason is that, although the  $(\partial K)/\kappa$ -type bonds are of order  $R^{-1}$  [see Eq. (39)], this is not the case for the  $U$ -type bonds: its integral with respect to one argument is of order of  $R^{-2}$ , but  $U$  is of order of unity for  $\kappa|\mathbf{s}-\mathbf{s}'| \sim 1$ . So, if we convolute  $U$  with a function that varies on a lengthscale much larger than  $\kappa^{-1}$ , this is not a problem. However, in the case considered in the present section, we usually convolute  $U$  with a kernel  $K$  connecting both interfaces, which varies on the same lengthscale (i.e.,  $\kappa^{-1}$ ) as  $U$ . However,

we shall see that it is possible to resum the diagrams to obtain a diagrammatic representation of the zeroth-order (in curvature) corrections. By Eq. (36),  $K(\mathbf{s}, \mathbf{s}') - \mathcal{K}(r_\perp)$  is of order  $R^{-2}$ , where  $\mathbf{r}_\perp$  is the projection of  $\mathbf{s} - \mathbf{s}'$  on the plane tangent to the interface at  $\mathbf{s}'$ . Thus, we can neglect diagrams that present  $(\partial_n K)/\kappa$ -type bonds, and we replace  $K(\mathbf{s}, \mathbf{s}')$  by  $\mathcal{K}(r_\perp)$  in the  $U$ -type bonds.

First, we consider the convolution of  $K(\mathbf{r}, \mathbf{s})$  with  $K(\mathbf{s}, \mathbf{s}')$ , where  $\mathbf{s}$  and  $\mathbf{s}'$  are on the same interface and  $\mathbf{r}$  is either above or below this interface. We place the origin at  $\mathbf{s}'$ , neglect curvature corrections and, finally, assume that  $\kappa r \gg 1$ . Then we have

$$\int d\mathbf{s} K(\mathbf{s}, \mathbf{0}) K(\mathbf{s}, \mathbf{r}) \approx \left(\frac{\kappa}{2\pi}\right)^2 \int_0^\infty ds e^{-\kappa s} \quad (114)$$

$$\times \int_0^{2\pi} d\theta \frac{\exp[-\kappa\sqrt{r^2 + s^2 - 2sr \sin \alpha \cos \theta}]}{\sqrt{r^2 + s^2 - 2sr \sin \alpha \cos \theta}},$$

where  $\alpha$  is the angle between  $\mathbf{r}$  and the surface normal at the origin  $\mathbf{n}(\mathbf{0})$ . As  $\kappa r \gg 1$  but  $\kappa s \lesssim 1$ , we expand the distance between  $\mathbf{r}$  and  $\mathbf{s}$  in powers of  $s/r$ , so in the first approximation we have

$$\int d\mathbf{s} K(\mathbf{s}, \mathbf{0}) K(\mathbf{s}, \mathbf{r}) \approx \quad (115)$$

$$\frac{\kappa e^{-\kappa r}}{2\pi r} \int_0^\infty \kappa ds e^{-\kappa s} \frac{1}{2\pi} \int_0^{2\pi} d\theta \exp[\kappa s \sin \alpha \cos \theta].$$

The modified Bessel function of zeroth order and first kind  $I_0$  has the integral representation

$$I_0(x) = \frac{1}{2\pi} \int_0^{2\pi} d\theta \exp[x \cos \theta]. \quad (116)$$

Therefore

$$\int d\mathbf{s} K(\mathbf{s}, \mathbf{0}) K(\mathbf{s}, \mathbf{r}) \approx \frac{\kappa e^{-\kappa r}}{2\pi r} \int_0^\infty \kappa ds e^{-\kappa s} I_0(\kappa s \sin \alpha)$$

$$= \frac{\kappa e^{-\kappa r}}{2\pi r} \frac{1}{|\cos \alpha|}, \quad (117)$$

and thus

$$\int d\mathbf{s}_0 U(\mathbf{s}, \mathbf{s}_0) K(\mathbf{s}_0, \mathbf{r}) \approx K(\mathbf{s}, \mathbf{r}) \left( \frac{|\mathbf{r} - \mathbf{s}|}{|\mathbf{n}(\mathbf{s}) \cdot (\mathbf{r} - \mathbf{s})|} - 1 \right), \quad (118)$$

up to corrections in powers of  $(\kappa R)^{-1}$  and  $(\kappa r)^{-1}$ . Eq. (118) vanishes if  $\mathbf{r}$  is on the normal direction to the substrate at  $\mathbf{s}$ . As a consequence, when the liquid-gas interface is parallel to the substrate (e.g., for parallel planes or concentric spheres or cylinders), the non-local model *ansatz* is a good approximation to the full solution when curvature corrections are neglected [40, 60] (see also App. D). On the other hand, a saddle-point analysis of the binding potential shows that the maximum contribution to the multiple integrals associated with each diagram in Eq. (107) arises from the neighbourhood of the closest pair of points located on different interfaces, which would lie on a normal direction common to both

substrates. In this sense, the binding-potential representation shown above is extremely non-local: in leading order only the shape of the substrate and the liquid-gas interfaces around their closest positions features. However, this is not true for the order-parameter profile at an arbitrary position  $\mathbf{r}$ ; and, in general, corrections beyond  $\delta m_\Xi^{0,\ell} + \delta m_\Xi^{0,\psi}$  will be incorrect with the original non-local model *ansatz*, even neglecting curvature corrections.

In order to obtain a more local representation of the binding potential and the order-parameter profile, we note that the structure of the diagrams shows  $K$  bonds that connect both interfaces, followed by a segment of diagram on one interface. The idea is to resum the convolutions of a  $K$  bond connecting the wall and the gas-liquid interface with all the possible segments either on the liquid-gas interface or on the substrate. If this is done to zeroth-order in the curvature, we obtain renormalized bonds between the wall and the gas-liquid interface. For example, a renormalized bond between a (left) position on the substrate and a (right) position on the gas-liquid interface would be:

$$K_{\psi \rightarrow \ell}(\mathbf{s}, \mathbf{r}) = K(\mathbf{s}, \mathbf{r}) + \sum_{i=1}^{\infty} (-1)^i$$

$$\times \int_\ell d\mathbf{s}_1 \cdots d\mathbf{s}_i U(\mathbf{s}, \mathbf{s}_1) \cdots U(\mathbf{s}_{i-1}, \mathbf{s}_i) K(\mathbf{s}_i, \mathbf{r}), \quad (119)$$

which is approximately given by

$$K_{\psi \rightarrow \ell}(\mathbf{s}, \mathbf{r}) \approx K(\mathbf{s}, \mathbf{r}) \sum_{i=0}^{\infty} \left( 1 - \frac{1}{|\cos \alpha|} \right)^i$$

$$= K(\mathbf{s}, \mathbf{r}) |\cos \alpha|, \quad (120)$$

and hence

$$K_{\psi \rightarrow \ell}(\mathbf{s}, \mathbf{r}) \approx -\frac{1}{\kappa} \partial_n K(\mathbf{s}, \mathbf{r}), \quad (121)$$

where  $\partial_n K(\mathbf{s}, \mathbf{r}) = \mathbf{n}(\mathbf{s}) \cdot \nabla_{\mathbf{s}} K(\mathbf{s}, \mathbf{r})$ . On the other hand, a renormalized bond between a (left) position on the gas-liquid interface and a (right) position on the substrate would be given by

$$K_{\ell \rightarrow \psi}(\mathbf{s}, \mathbf{r}) = \frac{g + \kappa}{g - \kappa} K(\mathbf{s}, \mathbf{r})$$

$$- \sum_{i=1}^{\infty} \left[ 2 \left( \frac{g}{\kappa - g} \right)^{i+1} + (-1)^i \right]$$

$$\times \int_\psi d\mathbf{s}_1 \cdots d\mathbf{s}_i U(\mathbf{s}, \mathbf{s}_1) \cdots U(\mathbf{s}_{i-1}, \mathbf{s}_i) K(\mathbf{s}_i, \mathbf{r}) \quad (122)$$

which is approximately

$$K_{\ell \rightarrow \psi}(\mathbf{s}, \mathbf{r}) \approx -K(\mathbf{s}, \mathbf{r}) \sum_{i=0}^{\infty} \left( 1 - \frac{1}{|\cos \alpha|} \right)^i$$

$$+ 2 \frac{g}{g - \kappa} K(\mathbf{s}, \mathbf{r}) \sum_{i=0}^{\infty} \left[ \left( \frac{g}{\kappa - g} \right) \left( \frac{1}{|\cos \alpha|} - 1 \right) \right]^i \quad (123)$$



Hence, at leading order,

$$K_{\ell \rightarrow \psi}(\mathbf{s}, \mathbf{r}) = K(\mathbf{s}, \mathbf{r}) \left| \cos \alpha \frac{g + \kappa |\cos \alpha|}{g - \kappa |\cos \alpha|} \right| \quad (124)$$

or, equivalently,

$$K_{\ell \rightarrow \psi}(\mathbf{s}, \mathbf{r}) \approx \frac{1}{\kappa} \partial_n K(\mathbf{s}, \mathbf{r}) \frac{g + \kappa |\cos \alpha|}{g - \kappa |\cos \alpha|}, \quad (125)$$

if a new  $K$ -type bond between the wall and the gas-liquid interface emerges from the right extreme of the diagram on the substrate segment. Otherwise

$$K'_{\ell \rightarrow \psi}(\mathbf{s}, \mathbf{r}) = \frac{g}{g - \kappa} \left[ K(\mathbf{s}, \mathbf{r}) + \sum_{i=1}^{\infty} \left( \frac{g}{\kappa - g} \right)^i \times \int_{\psi} ds_1 \cdots ds_i U(\mathbf{s}, \mathbf{s}_1) \cdots U(\mathbf{s}_{i-1}, \mathbf{s}_i) K(\mathbf{s}_i, \mathbf{r}) \right] \quad (126)$$

which is approximately given by

$$K'_{\ell \rightarrow \psi}(\mathbf{s}, \mathbf{r}) \approx \frac{g}{g - \kappa} K(\mathbf{s}, \mathbf{r}) \sum_{i=0}^{\infty} \left[ \left( \frac{g}{\kappa - g} \right) \left( \frac{1}{|\cos \alpha|} - 1 \right) \right]^i \quad (127)$$

Hence, we have

$$K'_{\ell \rightarrow \psi}(\mathbf{s}, \mathbf{r}) \approx K(\mathbf{s}, \mathbf{r}) \frac{g |\cos \alpha|}{g - \kappa |\cos \alpha|} \quad (128)$$

and, finally,

$$K'_{\ell \rightarrow \psi}(\mathbf{s}, \mathbf{r}) \approx \frac{1}{\kappa} \partial_n K(\mathbf{s}, \mathbf{r}) \frac{g}{g - \kappa |\cos \alpha|}. \quad (129)$$

It follows that in the limit of small curvatures we can perform a resummation of a rather generic convolution of wetting diagram, the ones above providing the most important examples. The resulting diagrams, which are proportional to  $\kappa^{-1}(\partial_n K)$ , are the basic ingredients entering in the binding potential for fixed boundary conditions (i.e., where  $g \rightarrow \infty$ ); this is what we are going to prove in the next section.

#### D. Alternative representation of the binding potential functional for fixed boundary conditions

It is possible to systematically explore the curvature corrections to the binding potential through the consideration of connecting the interface and those interfacial segments involving three types of bonds:  $U_{\pi} \equiv \mathcal{K}(\mathbf{r}_{\perp}) - \delta(\mathbf{r}_{\perp})$ ,  $\partial_n K/\kappa$  (only on the substrate), and  $\tilde{U} = K(\mathbf{s}, \mathbf{s}') - \mathcal{K}(\mathbf{r}_{\perp})$ , which are of order 1,  $(\kappa R)^{-1}$  and  $(\kappa R)^{-2}$ , respectively. However, to simplify the discussion we restrict ourselves to the case in which the order parameter is fixed, to a value  $m_1$ , on substrate. This will allow us to make the connection with the original non-local

model formulation more easily. This case corresponds to the limit  $g \rightarrow -\infty$  and  $-h_1/g - m_0 \rightarrow \delta m_1 \equiv m_1 - m_0$ . Thus, the expansions (108), (109), (110) and (113) only include diagrams that do not present  $(\partial_n K)/\kappa$  bonds. On the other hand, the contributions to the coefficients of the segments on the interfaces now become  $(-1)^n$ , with  $n$  being the number of  $U$ -type bonds of the diagram segment, regardless of whether or not it lies on the liquid-gas interface or substrate. This diagrammatic representation presents the same problems as mentioned above for the finite- $g$  case. However, we can rationalise them using the identities

$$\int_{\psi} ds_0 K_{\psi}^{-1}(\mathbf{s}, \mathbf{s}_0) K(\mathbf{s}_0, \mathbf{r}) = \int_{\psi} ds_0 \left( \delta(\mathbf{s} - \mathbf{s}_0) + \frac{1}{\kappa} \partial_n K(\mathbf{s}, \mathbf{s}_0) \right)^{-1} \frac{1}{\kappa} \partial_{n_0} K(\mathbf{s}_0, \mathbf{r}), \quad (130)$$

and

$$\int_{\ell} ds_0 K_{\ell}^{-1}(\mathbf{s}, \mathbf{s}_0) K(\mathbf{s}_0, \mathbf{r}) = \int_{\ell} ds_0 \left( \delta(\mathbf{s} - \mathbf{s}_0) - \frac{1}{\kappa} \partial_n K(\mathbf{s}, \mathbf{s}_0) \right)^{-1} \frac{1}{\kappa} \partial_{n_0} K(\mathbf{s}_0, \mathbf{r}), \quad (131)$$

where  $\partial_n K(\mathbf{s}, \mathbf{s}_0) \equiv \mathbf{n}(\mathbf{s}) \cdot \nabla_{\mathbf{s}} K(\mathbf{s}, \mathbf{s}_0)$  and  $\partial_{n_0} K(\mathbf{s}_0, \mathbf{r}) \equiv \mathbf{n}(\mathbf{s}_0) \cdot \nabla_{\mathbf{s}_0} K(\mathbf{s}_0, \mathbf{r})$ . These identities arise from Eq. (29) or, alternatively, from the equivalence of the single- and double-layer potentials Eqs. (22) and (25) for given Dirichlet boundary conditions; see Eqs. (23) and (26). By using the fundamental relations  $\int \mathcal{O} \mathcal{O}^{-1} = \delta$  for the inverse operators  $(\delta \pm \partial K/\kappa)^{-1}$  we obtain

$$\left( \delta(\mathbf{s} - \mathbf{s}_0) \pm \frac{1}{\kappa} \partial_n K(\mathbf{s}, \mathbf{s}_0) \right)^{-1} = \delta(\mathbf{s} - \mathbf{s}_0) \mp \int ds_1 \left( \delta(\mathbf{s} - \mathbf{s}_1) \pm \frac{1}{\kappa} \partial_n K(\mathbf{s}, \mathbf{s}_1) \right)^{-1} \frac{1}{\kappa} \partial_{n_1} K(\mathbf{s}_1, \mathbf{s}_0), \quad (132)$$

which formally can be represented as

$$\left( \delta(\mathbf{s} - \mathbf{s}_0) \pm \frac{1}{\kappa} \partial_n K(\mathbf{s}, \mathbf{s}_0) \right)^{-1} = \delta(\mathbf{s} - \mathbf{s}_0) \mp \frac{1}{\kappa} \partial_n K(\mathbf{s}, \mathbf{s}_0) + \int ds_1 \frac{1}{\kappa} \partial_n K(\mathbf{s}, \mathbf{s}_1) \frac{1}{\kappa} \partial_{n_1} K(\mathbf{s}_1, \mathbf{s}_0) + \cdots, \quad (133)$$

it is straightforward to recognize that Eqs. (130) and (131) can be represented diagrammatically as

$$= - \left[ \text{wavy line with circle} - \text{wavy line with circle and dashed line} + \text{wavy line with circle and two dashed lines} - \cdots \right] \quad (134)$$

$$= \left[ \text{wavy line with circle} - \text{wavy line with circle and dashed line} + \text{wavy line with circle and two dashed lines} - \cdots \right], \quad (135)$$

where the bonds carrying arrows linking both interfaces are  $(\partial_n K)/\kappa$  functions, and the arrow indicates the position where the normal derivative is applied. Note that the right-hand sides of these equations correspond to an expansion in powers of  $(\kappa R)^{-1}$ , as  $\partial_n K/\kappa \sim (\kappa R)^{-1}$ . On the other hand, the leading-order contributions are consistent with the renormalized bonds obtained previously [Consider the limit  $g \rightarrow -\infty$  in Eqs. (121), (125) and (129).] On using Eqs. (134) and (135), we obtain the following alternative representation of the binding potential:

$$\frac{W[l, \psi]}{\kappa m_0^2} = \sum_{n=1}^{\infty} \left( \frac{\delta m_1}{m_0} \Omega_n^n + \Omega_n^{n+1} + \left( \frac{\delta m_1}{m_0} \right)^2 \Omega_n^{n+1} \right), \quad (136)$$

which is now similar to the structure of the original non-local treatment. For example, the leading-order contribution, viz.,

$$\Omega_1^1 = - \begin{array}{c} \text{Diagram 1} \\ \text{Diagram 2} \\ \text{Diagram 3} \\ \text{Diagram 4} \\ \text{Diagram 5} \end{array} + \dots, \quad (137)$$

whilst

$$\Omega_1^2 = - \begin{array}{c} \text{Diagram 1} \\ \text{Diagram 2} \\ \text{Diagram 3} \\ \text{Diagram 4} \\ \text{Diagram 5} \end{array} + \dots, \quad (138)$$

and

$$\Omega_2^1 = - \begin{array}{c} \text{Diagram 1} \\ \text{Diagram 2} \\ \text{Diagram 3} \\ \text{Diagram 4} \\ \text{Diagram 5} \end{array} + \dots, \quad (139)$$

and so on. Each diagram has segments on each interface connected via  $(\partial_n K)/\kappa$ -type bonds that link the wall and the gas-liquid interface. The leftmost segment can only contain  $U$ -type bonds (independent of the surface on which it lies). Otherwise, they only have  $\partial K/\kappa$  bonds. The coefficient associated with each diagram is now  $(-1)^{l+m+o}$ , with  $l$  being the total number of  $U$ -bonds in the leftmost segment,  $m$  is the total number of  $(\partial_n K)/\kappa$ -type bonds on the substrate (not on

the liquid-gas interface), and  $o$  is the number of  $(\partial K)/\kappa$  bonds between the wall and the gas-liquid interface that emerge from the substrate and point to the gas-liquid interface.

Similarly, the order-parameter profile has an alternative diagrammatic expansion:

$$\delta m_{\Xi} = -m_0 \left[ \begin{array}{c} \text{Diagram 1} \\ \text{Diagram 2} \\ \text{Diagram 3} \\ \text{Diagram 4} \\ \text{Diagram 5} \\ \text{Diagram 6} \\ \text{Diagram 7} \\ \text{Diagram 8} \\ \text{Diagram 9} \\ \text{Diagram 10} \end{array} \right] + \delta m_1 \left[ \begin{array}{c} \text{Diagram 11} \\ \text{Diagram 12} \\ \text{Diagram 13} \\ \text{Diagram 14} \\ \text{Diagram 15} \\ \text{Diagram 16} \\ \text{Diagram 17} \\ \text{Diagram 18} \\ \text{Diagram 19} \\ \text{Diagram 20} \end{array} \right] + \dots \quad (140)$$

The diagrams start with a (left) segment either on the substrate or on the liquid-gas interface, which only can have  $U$ -type bonds. After that, there are  $(\partial_n K)/\kappa$ -type bonds connecting the wall and the gas-liquid interface, followed by segments on the corresponding interface that can only have  $(\partial_n K)/\kappa$ -bonds. Finally, there is a  $K$ -type bond connecting one interface to the position  $\mathbf{r}$ . Now the sign in front of each diagram is  $(-1)^{l+m+o'}$ , with  $l$  being the number of  $U$ -type bonds on the leftmost segment,  $m$  is the number of  $(\partial_n K)/\kappa$ -type bonds on the substrate, and  $o'$  is the number of  $\partial_n K/\kappa$  bonds that emerge from the liquid-gas interface and point to the substrate.

### E. Flat substrates

In the previous sections we pointed out that the decorated diagrams constitute the novel features of the new formulation of the non-local model. In order to better appreciate these aspects, we consider the binding potential for the case of a flat substrate. The exact binding potential admits a curvature expansion, but even at leading order it differs slightly from the binding potential functional of the original formulation. We start by considering the diagrams contained in  $\Omega_1^1$ . From the results of the previous sections we have that

$$\Omega_1^1 = - \begin{array}{c} \text{Diagram 1} \\ \text{Diagram 2} \\ \text{Diagram 3} \\ \text{Diagram 4} \\ \text{Diagram 5} \\ \text{Diagram 6} \\ \text{Diagram 7} \\ \text{Diagram 8} \\ \text{Diagram 9} \\ \text{Diagram 10} \end{array} + \dots, \quad (141)$$

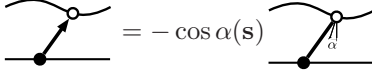
where the flatness of the substrate has enormously simplified the diagrammatic structure. This simplification is due to the vanishing of a large class of wetting diagrams, and can be summarized by the following reduction lemmas.

**Lemma 1**



$$(142)$$

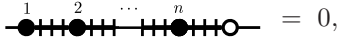
**Lemma 2**




$$(143)$$

where  $\alpha(\mathbf{s})$  is the angle formed by the normal vector and the vertical direction.

**Lemma 3**

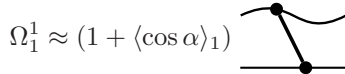


$$(144)$$



$$(145)$$

In addition to these rules, we recall that the decorated diagrams contribute higher-order corrections in the curvature expansion. In particular, a wetting diagram with a chain of  $n$   $U$ -type bonds on the fluid interface belongs to  $\mathcal{O}(R^{-2n})$ , whilst instead a chain of  $m$  arrow diagrams along the substrate belongs to  $\mathcal{O}(R^{-m})$ , where  $R$  is a typical radius of curvature. Therefore, at the leading order of a curvature expansion only the first two addends survive in Eq. (141). Then, thanks to Lemmas 1 and 2, we can further simplify the leading term and we are left with



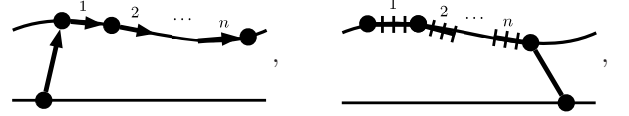
$$(146)$$

where

$$\langle \cos \alpha \rangle_n \equiv \frac{\int_{\ell} d\mathbf{s} \cos \alpha(\mathbf{s}) e^{-n\kappa\ell(\mathbf{s})}}{\int_{\ell} d\mathbf{s} e^{-n\kappa\ell(\mathbf{s})}}, \quad (147)$$

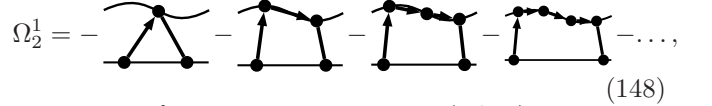
with  $\ell(\mathbf{s})$  being the vertical distance from  $\mathbf{s}$  to the substrate. Already at leading order we can appreciate the novel features of this exact formulation. Indeed, in the original formulation the expansion (141) starts with the same diagram entering in (146) but with a factor 2 in front. The factor  $1 + \cos \alpha(\mathbf{s})$  strongly depends on the local orientation of the interface with respect to the planar wall, and it is clear that the two formulations coincide only for parallel interfaces. However, for interfacial configurations that have a minimum height  $\bar{\ell}$  with respect to the substrate, the weighted average (147) is near to unity. More precisely, a saddle-point calculation shows that  $\langle \cos \alpha \rangle_1 \sim 1 - (\bar{H}/\kappa)$ , where  $\bar{H}$  is the mean curvature at the interfacial position nearest to the substrate.

It then is straightforward to prove, using the above lemmas, that the next-to-leading diagrams appearing in (146) are of the form



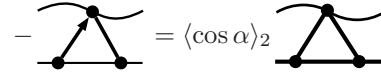
with a prefactor  $-1$  and  $(-1)^n$ , respectively, at the order  $\mathcal{O}(R^{-n})$  and  $\mathcal{O}(R^{-2n})$ , respectively.

These considerations apply also for the remaining classes of diagrams; in particular for  $\Omega_2^1$  we have



$$(148)$$

where the  $n^{\text{th}}$  diagram belongs to  $\mathcal{O}(R^{1-n})$ . Again, by using the previous lemmas, the leading term of  $\Omega_2^1$  can be written as



$$(149)$$


where  $\langle \cos \alpha \rangle_2 \sim 1 - (\bar{H}/2\kappa)$  by a saddle-point calculation.

The effect of the reduction is less effective for the class  $\Omega_2^2$ , for which the segments are located on the fluid interface. However, again a saddle-point calculation shows that, up to  $\mathcal{O}(R^{-1})$  terms,




$$(150)$$

recovering the original formulation of the non-local model. However, we should stress that this is a highly non-local formulation in the sense that the total binding potential between the wall and the gas-liquid interface is obtained. However, if we would like to characterize the influence of the substrate *locally* on a portion of the liquid-gas interface, we have to resort to the new non-local model presented in this Paper. In particular, the functionals  $\Omega_1^1$  and  $\Omega_2^1$  are local, so their contribution to the binding potential arises from

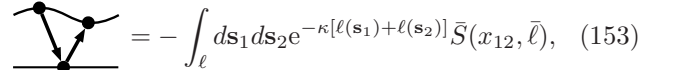


$$(151)$$



$$(152)$$

where now the integration on the liquid-gas interface is restricted to the portion of the gas-liquid interface in which the binding potential is evaluated. A new feature, absent in the original formulation, emerges due to a coupling between the interface position and its orientation. However, as in the original formulation, the  $\Omega_1^2$  functional is highly non-local and has the following representation:



$$(153)$$

where  $x_{12}$  is the projection of  $\mathbf{s}_2 - \mathbf{s}_1$  onto the substrate plane, and  $\bar{S}$  is the effective two-body interaction between the interfacial area elements located around  $\mathbf{s}_1$  and  $\mathbf{s}_2$ . As the corresponding interaction  $S \equiv S(x_{12}, \bar{\ell})$  in the original non-local model [39, 42, 43],  $\bar{S}$  depends on the interfacial heights via  $\bar{\ell} \equiv [\ell(\mathbf{s}_1) + \ell(\mathbf{s}_2)]/2$ , which can be analysed by using the same renormalization-group (RG) flow equations derived in Refs. [39, 42, 43]. More specifically,

$$\bar{S}(x_{12}, \bar{\ell}) = \frac{e^{2\kappa\bar{\ell}}}{\kappa} \mathbf{n}(\mathbf{s}_2) \cdot \nabla_2 \mathcal{K} \left( \sqrt{x_{12}^2 + (2\bar{\ell})^2} \right) \quad (154)$$

where  $\nabla_2$  is the 3D gradient acting on the liquid-gas interfacial position  $\mathbf{r}_2 = (\mathbf{s}_2, \ell(\mathbf{s}_2))$ . For large  $\ell$ , a saddle-point calculation shows that

$$\bar{S}(x_{12}, \bar{\ell}) \approx -\frac{\kappa \cos \alpha_2}{2\pi\bar{\ell}} e^{-\frac{\kappa x_{12}^2}{2\bar{\ell}}} = -\cos \alpha_2 S(x_{12}, \bar{\ell}) \quad (155)$$

where  $\alpha_2$  is the angle formed by the normal vector and the vertical direction at the liquid-gas interface position  $\mathbf{r}_2$ . Thus, as  $S$ , the two-body interaction  $\bar{S}$  has a Gaussian form, with the non-local length  $\xi_{NL} = \sqrt{\bar{\ell}}/\kappa$  precisely as identified in the original formulation [42, 43]. However, our improved formulation introduces as a new feature the coupling of the two-body interaction to the surface orientation through the factor  $\cos \alpha_2$ . A detailed comparison of the RG flows of this effective two-body repulsion within the original and present, exact, formulations in the context of critical wetting will be discussed elsewhere.

## F. Summary and remarks

In this section we have applied the boundary integral diagrammatic method to determine the binding potential functional and order-parameter configuration when a wetting layer intrudes between the bulk phase and the wall. Our results are decorated versions of those appearing in the original formulation and, in particular, contain  $U$ -type kernels on the fluid interface, whilst on the substrate they show  $U$ -type and  $\kappa^{-1}(\partial_n K)$ -type bonds. The effect of the new diagrams can be readily understood for small curvature, where the pertinent multiply embedded convolutions can be re-summed, leading to renormalized diagrams involving the orientation of the surface. In this way, the full non-locality is replaced by a weaker version, which can be used to build a more readily usable effective binding potential functional.

As expected, the new formulation reveals curvature corrections to the original formulation that are reliable when the substrate and fluid interfacial configurations are parallel or concentric, as in the case of spherical and cylindrical symmetry. Strictly speaking, when the interfaces are non-parallel the present improved formulation must be used — the analysis of filling transitions for fluids adsorbed in wedge geometries is a natural place for investigating this.

When the surface order parameter at the wall is fixed (i.e., Dirichlet boundary conditions), and the system is at the location of the critical wetting transition ( $m_1 = m_0$ ), as pertinent to the critical isotherm, the only diagram of relevance remaining is  $\Omega_1^2$ . This term is strongly non-local, and has a structure very similar to that appearing in the original non-local formulation. Once again, this highlights the influence of an effective two-body Gaussian interfacial interaction controlled by a non-local length  $\xi_{NL} = \sqrt{\bar{\ell}}/\kappa$  that is missing entirely from the original local effective Hamiltonian treatments of the critical wetting phase transition.

## VI. CONCLUSIONS

In this paper we have presented a rigorous derivation of the non-local effective interfacial Hamiltonian model for interfaces and wetting in systems possessing short-ranged forces. The present derivation, which is based on a boundary integral formulation, improves on the one given originally, because the boundary conditions at the interface and wall are now handled exactly rather than approximately. The first point to emphasise is that this systematic analysis can indeed be done at all — at least using a simple DP potential, and the crossing criterion definition of the interface position (to which we shall return, later).

This new analysis can also be expressed diagrammatically; a glossary of the elementary diagrams from which all other diagrams follow is given in App. C, together with their algebraic expressions. As with the original formulation each diagram containing a line that spans the liquid wetting layer, thus connecting the liquid-gas interface and wall, can be thought of as an interaction between these surfaces mediated by a bulk-like correlation. Amongst other things, this rigorous formulation allows us to consider, in a systematic fashion, the nature of the curvature corrections appearing in the appropriate free energy. More specifically, we applied the boundary integral method to three situations with the following conclusions:

- *The wall-single phase interface.* First we considered a non-planar wall-liquid interface, where a wetting layer is absent. We showed that the leading-order curvature corrections to the surface tension term involve the local mean and Gaussian curvatures, in the spirit of the Helfrich free energy, with bending and saddle-splay rigidity coefficients, respectively, the values of which are identified. However, the curvature expansion does not truncate at this, or indeed any, order, and the free energy does not conform to the morphological thermodynamics hypothesis [58].
- *The free liquid-gas interface.* Extending this analysis to the free (but constrained) liquid-gas interface we showed that the curvature corrections can

be expressed more precisely as an interfacial self-interaction, the form of which is identical to that proposed in Ref. [57] using less rigorous methods. Indeed, the order-parameter profiles are also identical, lending strong support to the approximate methods used previously to discuss non-locality.

- *The binding potential functional.* For the case in which a wetting layer is present we have derived a generalised diagrammatic representation of the binding potential and order parameter, which contains decorated versions of those diagrams appearing in the original formulation. These generate, in addition to curvature corrections, a coupling between the interfacial orientation and position, which is missing entirely in the original theory. Indeed, strictly speaking, even for small curvatures the diagrams do not converge to those of the original formulation, *unless* the interfacial configurations are nearly parallel to the substrate. However, when the new formulation of the non-local model is applied to a flat substrate, we find features that are very similar to the original version of the non-local model. In particular, the contributions  $\Omega_1^1$  and  $\Omega_2^1$  to the binding potential functional are local, whilst the  $\Omega_1^2$  contribution remains *non-local* and can be expressed as a two-body Gaussian interfacial self-interaction, mediated by the substrate, having a lateral range given by the same non-local length-scale  $\xi_{NL} = \sqrt{\ell/\kappa}$ . Thus, the criticism of what is missing in local interfacial Hamiltonian descriptions of critical wetting in Refs. [11, 12], including the size of the critical regime and also the paradoxical prediction of possible fluctuation-induced first order transitions [62, 63], remains unchanged; see Refs. [42, 43]. Nevertheless, it would be interesting to include the coupling of orientation and position into renormalization group and simulation studies of the non-local model.

Having formulated the problem exactly for the DP potential, it is possible to make extensions to more general potentials perturbatively, by using a Feynman-Hellman theorem similar to the approximate analysis of Ref. [41]. For the wall-liquid and free liquid-gas interface, this would generate further curvature corrections to the free energy, although this will not alter the diagrammatic structure only altering the values of the coefficients. However, in applications to the wetting film, the binding potential will now contain decorated versions of the  $\chi$  diagram identified in Ref. [41]. To identify the curvature corrections to this term, further re-summation of the diagrammatic series is required, similar to the decorated diagrams in the DP model discussed here. Generalizations to heterogeneous walls are also technically possible using the boundary integral approach.

Our rigorous and rather technical derivation of the non-local model, is still subject to a number of criticisms.

For example, we have assumed that the surface field  $h_1$  and enhancement  $g$  are not altered by the surface curvature of a structured wall, which is very probably an over simplification. And, of course, the continuum LGW model (2) does not in any way account for volume exclusion and local layering present when a high-density fluid is adsorbed at a wall. There are also alternative definitions of “the” interfacial position. For example, Fisher and Jin discuss integral criteria, and show that these alter the coefficients appearing in the binding potential function; see Refs. [47, 48]. Hopefully, the diagrammatic structure of the binding potential functional is not altered when using a different definition of the interfacial position, although we should expect that the values of all coefficients and curvature corrections are altered.

We should also mention that, of course, as soon as long-ranged forces are present all results here change dramatically [64]. For example, exponential terms are replaced by algebraic terms in the binding potential. Additionally, for Lennard-Jones forces the curvature expansion of the interfacial free energy fails completely, due to non-analytic logarithmic corrections.

However, there are deeper issues concerning the connection between mesoscopic and microscopic descriptions, which highlight some of the fundamental problems still open in the theory of interfacial phenomena discussed here. For example within the crossing criterion, for any potential  $\phi(m)$ , there is no escape from having a negative bending rigidity  $\kappa_B$  (the positive saddle-splay rigidity plays no part since the principal radius of curvature along the wedge is infinite). However the very meaning of having a negative bending coefficient has been questioned by Tarazona and co-workers [37], who have argued that the continuum LGW Hamiltonian is already too coarse grained to enable a direct determination of the rigidity from a constrained minimization of the model. At a microscopic level, they argue that there must be a molecular top to the capillary-wave spectrum, which leads to a positive rigidity. Whilst density functional models may be consistent with this feature when we look closely at the structure of the equilibrium density-density correlation function, a constrained minimization of any model functional will not suffice. Alternatively, they propose that the constrained minimization is replaced by a weighted convolution, which smears the interface location over a region comparable with the bulk correlation length. This means, of course, that the interface position no longer has a strict crossing-criterion interpretation. In fact, it has been shown that the crossing criterion does not distinguish correctly bulk from interfacial contributions present in the mean-field correlation function, and therefore cannot be used naively to determine any wavevector dependent corrections to the surface tension [65]. These concerns must also be married with the observation that the mean-field identification [47, 48] is, strictly speaking, only valid in the limit of low temperatures (i.e.,  $T \rightarrow 0$ ) where a saddle-point evaluation of the partial trace suffices. Finite-temperature corrections

to the interfacial free energy, interfacial Hamiltonian and binding potential must be present at some order. Indeed, these corrections are already allowed for implicitly when, in the application of the interfacial Hamiltonian, the mean-field value of the surface tension is replaced by its true thermodynamic value. These ideas, which are still under development, of course mean that the determination of the binding potential functional for wetting layers and the values, and indeed the signs, of the coefficients of all curvature correction terms, are much more difficult to determine.

### Acknowledgments

JMR-E thanks financial support from the Spanish Ministerio de Economía y Competitividad through grants no. FIS2017-87117-P and FIS2012-32455, Junta de Andalucía through grant no. P09-FQM-4938, all co-funded by the EU FEDER, and the Portuguese Foundation for Science and Technology under Contract No. EXCL/FIS-NAN/0083/2012. AS acknowledges hospitality of the University of Seville. AOP acknowledges support from the EPSRC UK grant EP/L020564/1 “Multiscale Analysis of Complex Interfacial Phenomena”. PMG gratefully acknowledges support from NSF DMR12-1207026.

### Appendix A: Perturbative solutions of the boundary integral equations

In this appendix we illustrate how to solve the integral equations which emerge in our analysis of the curvature expansion. We start with the evaluation of the first terms in the curvature expansion of the normal derivative  $q$  for a single phase in contact with a substrate  $\psi$ . After substitution of the curvature expansions of the terms which appear in (33) we find a recursive chain of equations for the  $q_n$ 's up to  $\mathcal{O}(R^{-3})$ :

$$\int_{\mathbb{R}^2} d\mathbf{r}_\perp q_0 \left[ \mathcal{K}(r_\perp) - \frac{\kappa}{g} \delta(\mathbf{r}_\perp) \right] = \kappa \left( \frac{h_1}{g} + m_b \right) \quad (\text{A1})$$

$$\int_{\mathbb{R}^2} d\mathbf{r}_\perp q_1 \left[ \mathcal{K}(r_\perp) - \frac{\kappa}{g} \delta(\mathbf{r}_\perp) \right] = -\frac{1}{g} \int_{\mathbb{R}^2} d\mathbf{r}_\perp \mathcal{W}(r_\perp) \Delta\psi(\mathbf{r}_\perp) (q_0 + h_1 + gm_b) \quad (\text{A2})$$

and

$$\int_{\mathbb{R}^2} d\mathbf{r}_\perp q_2 \left[ \mathcal{K}(r_\perp) - \frac{\kappa}{g} \delta(\mathbf{r}_\perp) \right] = \frac{1}{2} \int_{\mathbb{R}^2} d\mathbf{r}_\perp \left[ \mathcal{W}(r_\perp) \Delta\psi(\mathbf{r}_\perp) \left( q_0 \Delta\psi(\mathbf{r}_\perp) - \frac{2q_1}{g} \right) - q_0 \left( \mathcal{K}(r_\perp) (\nabla_\perp \Delta\psi(\mathbf{r}_\perp))^2 + \frac{2}{g} \mathcal{W}(r_\perp) \chi(\mathbf{r}_\perp) \right) \right] \quad (\text{A3})$$

where  $\mathcal{K}(x) = \kappa \exp(-\kappa x)/(2\pi x)$ ,  $\mathcal{W}(x) = (1 + \kappa x)\mathcal{K}(x)/x^2$  and we have extended the integral to  $\mathbb{R}^2$ ,

ignoring exponentially decaying terms on  $\kappa R$ . Note that self-consistency means that only the leading terms of  $\Delta\psi$  and  $\chi \equiv \mathbf{r}_\perp \cdot \nabla_\perp \Delta\psi - 2\Delta\psi$ , which scale as  $R^{-1}$  and  $R^{-2}$ , respectively, should be used.

For a flat interface  $q_0(\mathbf{s})$  is translationally invariant therefore it can be factorized from the integral, but since  $\int_{\mathbb{R}^2} d\mathbf{r}_\perp \mathcal{K}(r_\perp) = 1$  we have that  $q_0$  is given by Eq. (34). However it will be useful to develop a further technique to solve the above equation. We define a parallel Fourier transform, in which only the fluctuating modes parallel to the interface are considered. The kernel reads

$$K(\mathbf{s} - \mathbf{s}') = \int_{\mathbb{R}^2} \frac{d^2\mathbf{q}}{(2\pi)^2} e^{i\mathbf{q} \cdot (\mathbf{s} - \mathbf{s}')} \tilde{K}(\mathbf{q}), \quad (\text{A4})$$

and with a simple complex integration, we get the inverse Fourier transform

$$\tilde{K}(\mathbf{q}) = \int_{\mathbb{R}^2} ds e^{-i\mathbf{q} \cdot (\mathbf{s} - \mathbf{s}')} K(\mathbf{s} - \mathbf{s}') = \frac{\kappa}{\sqrt{\kappa^2 + q^2}}. \quad (\text{A5})$$

With these definitions the convolution equation for  $q_0$  becomes an algebraic equation for the Fourier modes

$$\tilde{q}_0(\mathbf{q}) = (2\pi)^2 \kappa \left( \frac{h_1}{g} + m_b \right) \frac{\delta(\mathbf{q})}{\tilde{K}(-\mathbf{q}) - \frac{\kappa}{g}}, \quad (\text{A6})$$

and transforming back to real space we find  $q_0 = -\kappa(h_1 + gm_b)/(\kappa - g)$ . Let us consider now the equations for the order  $\mathcal{O}(R^{-1})$  and  $\mathcal{O}(R^{-2})$ . If the leading contributions to  $\Delta\psi$  and  $\chi$  in powers of  $(\kappa R)^{-1}$  are used in Eqs. (A2) and (A3), the integrations over  $\mathbf{r}_\perp$  in their right-hand sides can be performed in polar coordinates. After few simple calculations we find

$$\int_{\psi} d\mathbf{r}_\perp q_1 \left[ \mathcal{K}(r_\perp) - \frac{\kappa}{g} \delta(\mathbf{r}_\perp) \right] = \left( \frac{h_1 + gm_b}{\kappa - g} \right) \left( \frac{k_1 + k_2}{2} \right) = \frac{h_1 + gm_b}{\kappa - g} H \quad (\text{A7})$$

and

$$\begin{aligned} \int_{\psi} d\mathbf{r}_\perp q_2 \left[ \mathcal{K}(r_\perp) - \frac{\kappa}{g} \delta(\mathbf{r}_\perp) \right] &= \\ \kappa \frac{h_1 + gm_b}{8(\kappa - g)} \left( \frac{k_1 - k_2}{\kappa} \right)^2 & \\ - \frac{1}{g} \int_{\mathbb{R}^2} d\mathbf{r}_\perp q_1 \mathcal{W}(r_\perp) \Delta\psi(\mathbf{r}_\perp) &= \\ \frac{h_1 + gm_b}{2\kappa(\kappa - g)} \left[ H^2 - K_G \right] & \\ - \frac{1}{g} \int_{\mathbb{R}^2} d\mathbf{r}_\perp q_1 \mathcal{W}(r_\perp) \Delta\psi(\mathbf{r}_\perp), & \quad (\text{A8}) \end{aligned}$$

Note that the results of the integrations are expressed in terms of the mean and Gaussian curvatures of the interface, both evaluated at the origin. If we denote by

$\mathcal{R}_{1,2}(\mathbf{s})$  the RHS of these equations, their formal solution reads

$$q_{1,2}(\mathbf{s}) = \int_{\mathbb{R}^2} \frac{d^2 \mathbf{q}}{(2\pi)^2} e^{i\mathbf{q}\cdot\mathbf{s}} \frac{\widetilde{\mathcal{R}}_{1,2}(\mathbf{q})}{\sqrt{1+\frac{q^2}{\kappa^2}} - \frac{\kappa}{g}}, \quad (\text{A9})$$

For our substrate  $\kappa R \gg 1$ , so the integral is dominated by the slow sector of Fourier modes. Hence it is reasonable to expand the square root in powers of the small parameter  $q/\kappa$ , thus

$$\begin{aligned} q_{1,2}(\mathbf{s}) &\approx \int_{\mathbb{R}^2} \frac{d^2 \mathbf{q}}{(2\pi)^2} \frac{e^{i\mathbf{q}\cdot\mathbf{s}}}{1 - \frac{\kappa}{g}} \left( 1 + \frac{q^2}{2\kappa^2(1 - \frac{\kappa}{g})} \right) \widetilde{\mathcal{R}}_{1,2}(\mathbf{q}) \\ &= -\frac{g}{\kappa - g} \left( \mathcal{R}_{1,2}(\mathbf{s}) + \frac{g}{2\kappa^2} \frac{\nabla_{\perp}^2 \mathcal{R}_{1,2}(\mathbf{s})}{\kappa - g} \right. \\ &\quad \left. + \mathcal{O}(\nabla_{\perp}^4 \mathcal{R}_{1,2}(\mathbf{s})) \right). \end{aligned} \quad (\text{A10})$$

The same result is obtained if we make a Taylor expansion of  $q_{1,2}$  around the origin and substitute in Eqs. (A2) and (A3). However, we note that  $\nabla_{\perp}^2 \mathcal{R}_{1,2} \sim \mathcal{R}_{1,2}/R^2$ , so the derivative terms contribute to higher order curvature terms, and thus they can be neglected. The solutions are then given by the leading contributions of Eq. (A10), which correspond to Eqs. (41) and (42).

In a similar way, the perturbative scheme for the computation of the normal derivatives  $q$  for a free interface are the following

$$\int_{\mathbb{R}^2} d\mathbf{r}_{\perp} q_0^{\pm} \mathcal{K}(r_{\perp}) = -\kappa m_0 \quad (\text{A11})$$

$$\int_{\mathbb{R}^2} d\mathbf{r}_{\perp} q_1^{\pm} \mathcal{K}(r_{\perp}) = \pm m_0 \int_{\mathbb{R}^2} d\mathbf{r}_{\perp} \mathcal{W}(r_{\perp}) \Delta \ell(\mathbf{r}_{\perp}) \quad (\text{A12})$$

and

$$\begin{aligned} \int_{\mathbb{R}^2} d\mathbf{r}_{\perp} q_2^{\pm} \mathcal{K}(r_{\perp}) &= \frac{1}{2} \int_{\mathbb{R}^2} d\mathbf{r}_{\perp} q_0^{\pm} \left[ \mathcal{W}(r_{\perp}) \Delta \ell(\mathbf{r}_{\perp})^2 \right. \\ &\quad \left. - \mathcal{K}(r_{\perp}) (\nabla_{\perp} \Delta \ell(\mathbf{r}_{\perp}))^2 \right]. \end{aligned} \quad (\text{A13})$$

These have the solutions

$$q_0^{\pm} = -\kappa m_0 \quad (\text{A14})$$

$$q_1^{\pm} = \pm \kappa m_0 \frac{k_1 + k_2}{2\kappa} = \pm m_0 H(\mathbf{s}) \quad (\text{A15})$$

and

$$\begin{aligned} q_2^{\pm} &= \frac{\kappa m_0}{8} \left( \frac{k_1 - k_2}{k} \right)^2 \\ &= \frac{m_0}{2\kappa} \left[ H(\mathbf{s})^2 - K_G(\mathbf{s}) \right]. \end{aligned} \quad (\text{A16})$$

Finally, the curvature expansion of  $\Psi$  for the single phase in contact with the substrate can be obtained from

Eq. (23). After substitution of Eq. (31) and the curvature expansions of  $q$ , the kernel  $K$  and the elementary area  $ds$  into Eq. (23), we obtain the following equations:

$$\int_{\mathbb{R}^2} d\mathbf{r}_{\perp} \Psi_0 \mathcal{K}(r_{\perp}) = -\frac{h_1 + gm_b}{g} - \frac{q_0}{g} \quad (\text{A17})$$

$$\int_{\mathbb{R}^2} d\mathbf{r}_{\perp} \Psi_1 \mathcal{K}(r_{\perp}) = -\frac{q_1}{g} \quad (\text{A18})$$

and

$$\begin{aligned} \int_{\mathbb{R}^2} d\mathbf{r}_{\perp} \Psi_2 \mathcal{K}(r_{\perp}) &= -\frac{q_2}{g} - \frac{1}{2} \int_{\mathbb{R}^2} d\mathbf{r}_{\perp} \frac{\Psi_0}{g} \\ &\times \left[ \mathcal{W}(r_{\perp}) \Delta \psi(\mathbf{r}_{\perp})^2 - \mathcal{K}(r_{\perp}) (\nabla_{\perp} \Delta \psi(\mathbf{r}_{\perp}))^2 \right] \end{aligned} \quad (\text{A19})$$

where  $\Psi_0$ ,  $\Psi_1$  and  $\Psi_2$  stand for the first terms in the curvature expansion of  $\Psi$ . The solutions of these integral equations are:

$$\frac{\Psi_0}{2\kappa} = \frac{h_1 + gm_b}{\kappa - g} \quad (\text{A20})$$

$$\frac{\Psi_1}{2\kappa} = \left( \frac{h_1 + gm_b}{\kappa - g} \right) \left( \frac{\kappa}{\kappa - g} \right) \frac{H}{\kappa} \quad (\text{A21})$$

and

$$\begin{aligned} \frac{\Psi_2}{2\kappa} &= \left( \frac{h_1 + gm_b}{\kappa - g} \right) \left[ \left( \frac{1}{2} \frac{g}{\kappa - g} + \frac{\kappa^2}{(\kappa - g)^2} \right) \left( \frac{H}{\kappa} \right)^2 \right. \\ &\quad \left. - \frac{1}{2} \frac{g}{\kappa - g} \frac{K_G}{2\kappa^2} \right] \end{aligned} \quad (\text{A22})$$

## Appendix B: Derivation of the liquid-gas interfacial self-interaction Hamiltonian

In this appendix we derive (82). Consider two points on the interface with  $\mathbf{s}_1$  as the origin and  $\mathbf{s}_2$  as in Fig. 2. We supposed that the surface  $\ell$  can be approximated, locally, as a paraboloid. Taking into account the right-hand side of Eq. (A16), the interfacial free-energy functional Eq. (67) can be written as

$$\begin{aligned} H[\ell] &\approx \sigma \mathcal{A}_{\ell g} - \frac{\sigma}{2} \int_{\ell} d\mathbf{s}_1 \int_{\mathbb{R}^2} d\mathbf{r}_{\perp} \mathcal{K}(r_{\perp}) (\nabla_{\perp} \Delta \ell(\mathbf{s}, \mathbf{r}_{\perp}))^2 \\ &\quad + \frac{\sigma}{2} \int ds_{\ell} \int_{\mathbb{R}^2} d\mathbf{r}_{\perp} \mathcal{W}(r_{\perp}) \Delta \ell(\mathbf{s}, \mathbf{r}_{\perp})^2, \end{aligned} \quad (\text{B1})$$

where  $\mathbf{r}_{\perp}$  is the projection of  $\mathbf{s}_2 - \mathbf{s}_1$  on the tangent plane  $\pi_{\mathbf{s}_1}$  to the interface at  $\mathbf{s}_1$ , and  $\Delta \ell$  is the vertical displacement from  $\pi_{\mathbf{s}_1}$

$$\Delta \ell(\mathbf{s}_1, \mathbf{r}_{\perp}) = \mathbf{n}(\mathbf{s}_1) \cdot (\mathbf{s}_2 - \mathbf{s}_1). \quad (\text{B2})$$

The last step is to convert the surface integrations in integrals over the reference plane. In order to do that we need the mapping between the charts  $\{\mathbf{x}_1, \mathbf{x}_2\}$  and  $\{\mathbf{s}, \mathbf{r}_{\perp}\}$ . The expressions of the mapping can be obtained

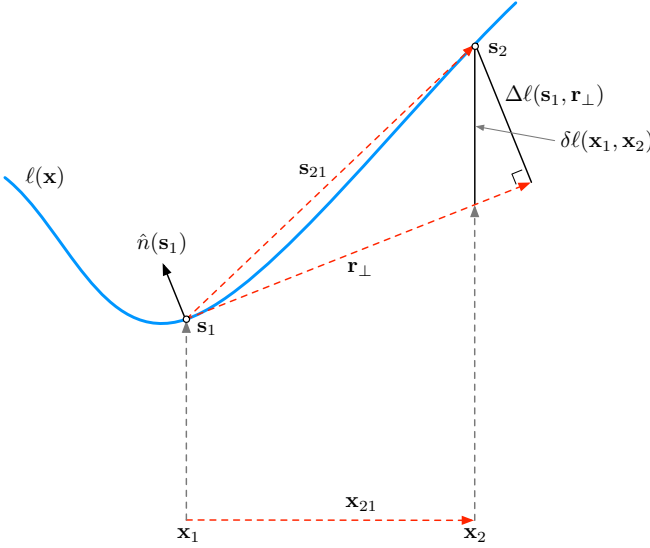


FIG. 2: Schematic illustration of the coordinates, vectors and geometry appearing in the curvature expansion for a constrained interfacial configuration. Symbols described in text.

from  $\mathbf{s}_2 - \mathbf{s}_1 = \mathbf{n}(\mathbf{s}_1)\Delta\ell(\mathbf{s}_1, \mathbf{r}_\perp) + \mathbf{r}_\perp$ , supplemented by (B2) and

$$\mathbf{n}(\mathbf{s}_1) = \frac{1}{\sqrt{1 + (\nabla\ell(\mathbf{x}_1))^2}} (-\nabla\ell(\mathbf{x}_1), 1), \quad (\text{B3})$$

where  $\nabla$  represents the 2D gradient on the reference plane coordinates.

$$J = \left| \frac{\partial(\mathbf{s}_1, \mathbf{r}_\perp)}{\partial(\mathbf{x}_1, \mathbf{x}_2)} \right|. \quad (\text{B4})$$

We can show that the mapping Jacobian  $J = 1$  if quadratic terms on the gradients are neglected. In this limit  $|\mathbf{r}_\perp| \approx |\mathbf{x}_{21}|$ , the orthogonal displacement (B2) can be replaced with the vertical displacement

$$\Delta\ell(\mathbf{s}_1, \mathbf{r}_\perp) \simeq \delta\ell(\mathbf{x}_1, \mathbf{x}_2) \equiv \ell(\mathbf{x}_2) - \ell(\mathbf{x}_1) - \mathbf{x}_{21} \cdot \nabla\ell(\mathbf{x}_1), \quad (\text{B5})$$

and taking the 2D gradient,  $\nabla_\perp\Delta\ell \simeq \nabla\ell(\mathbf{x}_1) - \nabla\ell(\mathbf{x}_1)$ . Finally,

$$\mathcal{A}_{lg} \simeq \mathcal{A}_\pi + \frac{1}{2} \int d\mathbf{x} (\nabla\ell(\mathbf{x}))^2, \quad (\text{B6})$$

where  $\mathcal{A}_\pi$  is the area of the surface obtained from the projection of the surface  $\ell$  onto the reference plane. The Hamiltonian (B1) becomes

$$\begin{aligned} H[\ell] &\simeq \sigma\mathcal{A}_\pi + \frac{\sigma}{2} \int d\mathbf{x} (\nabla\ell(\mathbf{x}))^2 \\ &- \frac{\sigma}{2} \int d\mathbf{x}_1 d\mathbf{x}_2 \mathcal{K}(x_{12}) (\nabla\ell(\mathbf{x}_1) - \nabla\ell(\mathbf{x}_2))^2 \\ &+ \frac{\sigma}{2} \int d\mathbf{x}_1 d\mathbf{x}_2 \mathcal{W}(x_{12}) (\ell(\mathbf{x}_2) - \ell(\mathbf{x}_1) - \mathbf{x}_{12} \cdot \nabla\ell(\mathbf{x}_1))^2. \end{aligned} \quad (\text{B7})$$

The expressions in (B7) can be further simplified. First we compute the squares, isolating the term proportional to the difference in vertical displacement. New terms will be created and for them we use the identities:

$$\begin{aligned} &\frac{1}{2} \int d\mathbf{x}_1 d\mathbf{x}_2 \mathcal{K}(x_{12}) (\nabla\ell(\mathbf{x}_1) - \nabla\ell(\mathbf{x}_2))^2 \\ &= \int d\mathbf{x}_1 d\mathbf{x}_2 \mathcal{K}(x_{12}) [(\nabla\ell(\mathbf{x}_1))^2 - \nabla\ell(\mathbf{x}_1) \cdot \nabla\ell(\mathbf{x}_2)] \\ &= \int d\mathbf{x} (\nabla\ell(\mathbf{x}))^2 - \int d\mathbf{x}_1 d\mathbf{x}_2 \mathcal{K}(x_{12}) \nabla\ell(\mathbf{x}_1) \cdot \nabla\ell(\mathbf{x}_2), \end{aligned} \quad (\text{B8})$$

and

$$\begin{aligned} &\int d\mathbf{x}_1 d\mathbf{x}_2 \mathcal{W}(x_{12}) (\mathbf{x}_{12} \cdot \nabla\ell(\mathbf{x}_1))^2 \\ &= \int d\mathbf{x}_1 d\mathbf{x}_{12} \mathcal{W}(x_{12}) [x_{21}^2 (\partial_{x_1}\ell(\mathbf{x}_1))^2 + y_{21}^2 (\partial_{y_1}\ell(\mathbf{x}_1))^2] \\ &= \frac{1}{2} \int d\mathbf{x}_{12} \mathbf{x}_{12}^2 \mathcal{W}(x_{12}) \int d\mathbf{x}_1 (\nabla\ell(\mathbf{x}_1))^2 \\ &= \int d\mathbf{x} (\nabla\ell(\mathbf{x}))^2. \end{aligned} \quad (\text{B9})$$

There is also a term of the form

$$\int d\mathbf{x}_1 d\mathbf{x}_2 \left[ \mathcal{K}(x_{12}) \nabla\ell(\mathbf{x}_1) \cdot \nabla\ell(\mathbf{x}_2) - \mathcal{W}(x_{12}) (\ell(\mathbf{x}_2) - \ell(\mathbf{x}_1)) (\mathbf{x}_{21} \cdot \nabla\ell(\mathbf{x}_1)) \right]. \quad (\text{B10})$$

Grouping the integral over  $\mathbf{x}_1$  we have

$$\int d\mathbf{x}_1 \nabla\ell(\mathbf{x}_1) \cdot \int d\mathbf{x}_2 \left[ \mathcal{K}(x_{12}) \nabla\ell(\mathbf{x}_2) - \mathcal{W}(x_{12}) (\ell(\mathbf{x}_2) - \ell(\mathbf{x}_1)) \mathbf{x}_{21} \right], \quad (\text{B11})$$

but since  $-\mathcal{W}(x_{12})\mathbf{x}_{21} = \nabla_{\mathbf{x}_2}\mathcal{K}(x_{12})$ , the second integrand can be written as a gradient of a scalar function

$$\int d\mathbf{x}_1 \nabla\ell(\mathbf{x}_1) \cdot \int d\mathbf{x}_2 \nabla_{\mathbf{x}_2} \left[ (\ell(\mathbf{x}_2) - \ell(\mathbf{x}_1)) \mathcal{K}(x_{12}) \right], \quad (\text{B12})$$

and so it reduces to a boundary contribution, which we can neglect. Collecting all the remaining terms we are left with (82).

### Appendix C: Wetting diagrams

In this appendix we collect the definitions for the various wetting diagrams used in the main text. The follow-



ing diagrams:

$$\text{---}\bullet\text{---} = \int ds \quad (\text{C1})$$

$$\text{---}\blacktriangle\text{---} = \int ds H(\mathbf{s})/\kappa \quad (\text{C2})$$

$$\text{---}\blacksquare\text{---} = \int ds H^2(\mathbf{s})/\kappa^2 \quad (\text{C3})$$

$$\text{---}\blacklozenge\text{---} = \int ds K_G(\mathbf{s})/\kappa^2 \quad (\text{C4})$$

involve only *local* interfacial properties. The circle represents the area element, while  $H$  denotes the local mean curvature and  $K_G(\mathbf{s})$  the Gaussian curvature. Empty symbols as the one appearing in (53) and (54) stand for the evaluation of the corresponding weight functions at a specified point  $\mathbf{s}$  on the surface.

The Ornstein-Zernike kernel of (15) is represented by a thick black line with two white circles at the extrema. For instance, if  $\mathbf{s}$  belong to the surface  $\ell$  and  $\mathbf{r}$  to the upper region we shall write

$$\text{---}\circ\text{---}\circ = \int_{\ell} ds K(\mathbf{s}, \mathbf{r}), \quad (\text{C5})$$

and similarly

$$\text{---}\blacklozenge\text{---}\circ = \kappa^{-2} \int_{\ell} ds K_G(\mathbf{s}) K(\mathbf{s}, \mathbf{r}). \quad (\text{C6})$$

Then we have the ‘‘dashed’’ and ‘‘arrow’’ diagrams

$$\text{---}\text{---}\text{---} = \text{---}\text{---}\text{---} - \delta(\mathbf{s} - \mathbf{s}') = U(\mathbf{s}, \mathbf{s}'), \quad (\text{C7})$$

$$\text{---}\text{---}\text{---} = \frac{1}{\kappa} \partial_n K(\mathbf{s}, \mathbf{s}'), \quad (\text{C8})$$

where in the latter diagram the arrow points to the position where the normal derivative is taken, as in the following example

$$\int_{\ell} ds_1 ds_2 U(\mathbf{s}, \mathbf{s}_1) \frac{1}{\kappa} \partial_{n_1} K(\mathbf{s}_1, \mathbf{s}_2) = \text{---}\text{---}\text{---}. \quad (\text{C9})$$

The arrow diagram can also span between two interfaces; for example:

$$\text{---}\text{---}\text{---} = \int_{\psi} ds_{\psi} \int_{\ell} ds_{\ell} \frac{1}{\kappa} \partial_{n_{\ell}} K(\mathbf{s}_{\ell}, \mathbf{s}_{\psi}). \quad (\text{C10})$$

The algebraic expressions for all other diagrams can be reconstructed in terms of these elementary building blocks.

#### Appendix D: Binding potential for planar, spherical and cylindrical interfacial configurations.

In this App. we will review the known form for planar, spherical and cylindrical interfacial configurations, and how they are reproduced from the non-local representations of the binding potential we have discussed in Section V.

### 1. Planar interfaces

We first consider the simplest case of a planar wall ( $\psi = 0$ ) and a planar interface of constant thickness,  $\ell(\mathbf{x}) = \ell$ . In this case,  $\mathcal{F}_{wl}[\psi] = \sigma_{wl} \mathcal{A}_{wl}$  and  $H[\ell] = \sigma \mathcal{A}_{lg}$ , where  $\mathcal{A}_{lg} = \mathcal{A}_{wl} = \mathcal{A}$  is the interfacial area, and  $\sigma_{wl} = (\kappa/2)(h_1 + gm_b)^2/[g(g - \kappa)]$  and  $\sigma = \kappa m_0^2$  are the surface tensions defined for the planar wall-liquid and liquid-gas interfaces, respectively. On the other hand, the binding potential is [40, 41, 60]

$$\begin{aligned} \frac{W[\ell, \psi]}{\mathcal{A}} &= 2\kappa m_0 \left( \frac{h_1 + gm_0}{\kappa - g} \right) \frac{e^{-\kappa\ell}}{1 - \frac{g+\kappa}{g-\kappa} e^{-2\kappa\ell}} \\ &+ \kappa \left( \frac{h_1 + gm_0}{\kappa - g} \right)^2 \frac{e^{-2\kappa\ell}}{1 - \frac{g+\kappa}{g-\kappa} e^{-2\kappa\ell}} \\ &+ \frac{g + \kappa}{g - \kappa} \kappa m_0^2 \frac{e^{-2\kappa\ell}}{1 - \frac{g+\kappa}{g-\kappa} e^{-2\kappa\ell}} \end{aligned} \quad (\text{D1})$$

The basic diagrams to obtain the decorated version of the original non-local model are

$$\text{---}\circ\text{---}\text{---} = \text{---}\text{---}\text{---} = e^{-\kappa\ell} \quad (\text{D2})$$

and

$$\text{---}\text{---}\text{---} = \text{---}\text{---}\text{---} = \text{---}\text{---}\text{---} = \text{---}\text{---}\text{---} = 0 \quad (\text{D3})$$

We note that these diagrams do not depend on the position associated to the empty circle, so any diagram can be split into the contribution of its bonds. For example

$$\text{---}\text{---}\text{---} = \left( \text{---}\text{---}\text{---} \right) \times \left( \text{---}\text{---}\text{---} \right) \times \left( \text{---}\text{---}\text{---} \right) \quad (\text{D4})$$

with

$$\text{---}\text{---}\text{---} = \text{---}\text{---}\text{---} = \mathcal{A} \quad (\text{D5})$$

Due to the expression (D3), the non-vanishing diagrams are those of the original non-local model. In particular, Eqs. (108), (109) and (110) reduce to

$$\Omega_1^1 = \frac{2g}{g - \kappa} \text{---}\text{---}\text{---} = \frac{2g}{g - \kappa} \mathcal{A} e^{-\kappa\ell} \quad (\text{D6})$$

$$\Omega_1^2 = \frac{g + \kappa}{g - \kappa} \text{---}\text{---}\text{---} = \frac{g + \kappa}{g - \kappa} \mathcal{A} e^{-2\kappa\ell} \quad (\text{D7})$$

$$\Omega_2^1 = \left( \frac{g}{g - \kappa} \right)^2 \text{---}\text{---}\text{---} = \left( \frac{g}{g - \kappa} \right)^2 \mathcal{A} e^{-2\kappa\ell} \quad (\text{D8})$$

which are consistent with the expressions in Refs. [41, 60], although our notation differs slightly from the used one in these references. The higher-order terms in the

functional can also be easily evaluated:

$$\Omega_n^n = \Omega_1^1 \left( \frac{g + \kappa}{g - \kappa} e^{-2\kappa\ell} \right)^{n-1} \quad (\text{D9})$$

$$\Omega_n^{n+1} = \Omega_1^2 \left( \frac{g + \kappa}{g - \kappa} e^{-2\kappa\ell} \right)^{n-1} \quad (\text{D10})$$

$$\Omega_{n+1}^n = \Omega_2^1 \left( \frac{g + \kappa}{g - \kappa} e^{-2\kappa\ell} \right)^{n-1} \quad (\text{D11})$$

If we substitute these expressions into Eq. (107), we obtain Eq. (D1) after a trivial resummation. Finally, the expressions obtained in Ref. [40] for fixed boundary conditions on the wall are reobtained by taking the limit  $g \rightarrow -\infty$  and  $-h_1/g - m_0 \rightarrow \delta m_1 \equiv m_1 - m_0$  in our equations, where  $m_1$  is the order parameter on the wall.

Now we turn to the new formulation for the non-local model we have introduced in this paper for fixed boundary conditions on the wall. The basic diagrams for this formulation are

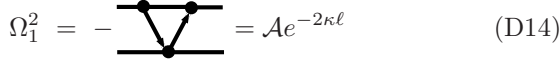


$$\text{Diagram 1} = - \text{Diagram 2} = e^{-2\kappa\ell} \quad (\text{D12})$$

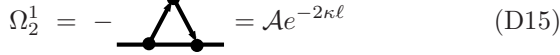
The expressions for  $\Omega_1^1$ ,  $\Omega_1^2$  and  $\Omega_2^1$  are obtained from Eqs. (137), (138) and (139) as



$$\Omega_1^1 = \text{Diagram 1} - \text{Diagram 2} = \mathcal{A}e^{-\kappa\ell} \quad (\text{D13})$$



$$\Omega_1^2 = - \text{Diagram} = \mathcal{A}e^{-2\kappa\ell} \quad (\text{D14})$$



$$\Omega_2^1 = - \text{Diagram} = \mathcal{A}e^{-2\kappa\ell} \quad (\text{D15})$$

and for higher-order contributions we get that

$$\Omega_n^n = \Omega_1^1 e^{-2(n-1)\kappa\ell} \quad (\text{D16})$$

$$\Omega_n^{n+1} = \Omega_1^2 e^{-2(n-1)\kappa\ell} \quad (\text{D17})$$

$$\Omega_{n+1}^n = \Omega_2^1 e^{-2(n-1)\kappa\ell} \quad (\text{D18})$$

Substitution of these expressions into Eq. (136) leads to the following expression

$$\frac{W[\ell, \psi]}{\mathcal{A}} = \sum_{n=1}^{\infty} \left( 2\kappa m_0 \delta m_1 e^{-(2n-1)\kappa\ell} + (\kappa(\delta m_1)^2 + \kappa(m_0)^2) e^{-2n\kappa\ell} \right) \quad (\text{D19})$$

which can be resummed as

$$\frac{W[\ell, \psi]}{\mathcal{A}} = \frac{2\kappa m_0 \delta m_1 e^{-\kappa\ell}}{1 - e^{-2\kappa\ell}} + (\kappa(\delta m_1)^2 + \kappa(m_0)^2) \frac{e^{-2\kappa\ell}}{1 - e^{-2\kappa\ell}} \quad (\text{D20})$$


which is Eq. (D1) in the limit of fixed boundary conditions on the wall.

## 2. Spherical interfaces

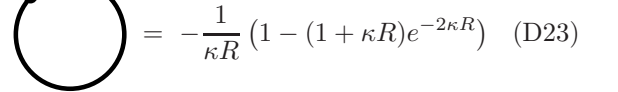
A similar calculation can be performed for the problem of wetting around a sphere. We suppose that the sphere is of radius  $R$  and consider an interfacial configuration corresponding to a concentric sphere of radius  $R + \ell$ . In this case,  $\mathcal{F}_{wl}[\psi]$  is given by [60]

$$\mathcal{F}_{wl}[\psi] = \sigma_{wl} \mathcal{A}_{wl} \left( \frac{1 + \frac{1}{\kappa R}}{1 + \frac{1}{(\kappa - g)R}} \right) \quad (\text{D21})$$

where  $\sigma_{wl}$  is the surface tension for the planar wall-liquid interface, and the area of the sphere is  $\mathcal{A}_{wl} = 4\pi R^2$ . Note that the mean curvature and the Gaussian curvature on the sphere are  $H = -1/R$  and  $K_G = 1/R^2$ , respectively. Thus Eq. (D21) satisfies Eq. (44) for large  $R$ . It is instructive to reobtain Eq. (D21) from the diagrammatic expansion Eq. (55). The relevant diagrams for this calculation are



$$\text{Diagram 1} = -e^{-2\kappa R} \quad (\text{D22})$$



$$\text{Diagram 2} = -\frac{1}{\kappa R} (1 - (1 + \kappa R)e^{-2\kappa R}) \quad (\text{D23})$$



$$\text{Diagram 3} = 4\pi R^2 \quad (\text{D24})$$

which are independent of the position of the open circle, as in the planar case. So, again each diagram is just the product of its bonds. In order to sum the contributions of the diagrams, we note that each diagram is a chain-like sequence of  $U$  and  $\partial K/\kappa$  bonds, with coefficients given by Eq. (52). We first sum the diagrams without  $\partial K/\kappa$  bonds. Their total contribution  $S_0$  to  $\mathcal{F}_{wl}$  is

$$S_0 = \sigma_{wl} \mathcal{A}_{wl} \sum_{n=0}^{\infty} \left[ \frac{g}{\kappa - g} (-e^{-2\kappa R}) \right]^n = \sigma_{wl} \mathcal{A}_{wl} \frac{1}{1 + \frac{g}{\kappa - g} e^{-2\kappa R}} \quad (\text{D25})$$

Now, we consider the diagrams with only one  $\partial K/\kappa$  bond. Their total contribution  $S_1$  to  $\mathcal{F}_{wl}$  can be written as

$$S_1 = \sigma_{wl} \mathcal{A}_{wl} \left( \sum_{n_1=0}^{\infty} \left[ \frac{g}{\kappa - g} (-e^{-2\kappa R}) \right]^{n_1} \right) \times \left( \frac{\kappa}{\kappa - g} \right) \left[ -\frac{1}{\kappa R} (1 - (1 + \kappa R)e^{-2\kappa R}) \right] \times \left( \frac{g}{\kappa} + \sum_{n_2=1}^{\infty} \left[ \frac{g}{\kappa - g} (-e^{-2\kappa R}) \right]^{n_2} \right) \quad (\text{D26})$$

which can be written as

$$S_1 = \sigma_{wl} \mathcal{A}_{wl} \frac{g}{\kappa} \frac{(1 - e^{-2\kappa R})}{1 + \frac{g}{\kappa - g} e^{-2\kappa R}} \times \frac{-\frac{1}{(\kappa - g)R} (1 - (1 + \kappa R)e^{-2\kappa R})}{1 + \frac{g}{\kappa - g} e^{-2\kappa R}} \quad (\text{D27})$$

For diagrams with  $m > 1$   $\partial K/\kappa$  bonds, their contribution  $S_m$  to  $\mathcal{F}_{wl}$  can be obtained similarly as

$$S_m = \sigma_{wl} \mathcal{A}_{wl} \frac{g}{\kappa} \frac{(1 - e^{-2\kappa R})}{1 + \frac{g}{\kappa - g} e^{-2\kappa R}} \times \left( \frac{-\frac{1}{(\kappa - g)R} (1 - (1 + \kappa R)e^{-2\kappa R})}{1 + \frac{g}{\kappa - g} e^{-2\kappa R}} \right)^m \quad (\text{D28})$$

So,  $\mathcal{F}_{wl}[\psi]$  has the expression

$$\mathcal{F}_{wl}[\psi] = \sum_{m=0}^{\infty} S_m = \frac{\sigma_{wl} \mathcal{A}_{wl}}{1 + \frac{g}{\kappa - g} e^{-2\kappa R}} \times \left[ 1 + \frac{g}{\kappa} (1 - e^{-2\kappa R}) \times \frac{-\frac{1}{(\kappa - g)R} \left( \frac{1 - (1 + \kappa R)e^{-2\kappa R}}{1 + \frac{g}{\kappa - g} e^{-2\kappa R}} \right)}{1 + \frac{1}{(\kappa - g)R} \left( \frac{1 - (1 + \kappa R)e^{-2\kappa R}}{1 + \frac{g}{\kappa - g} e^{-2\kappa R}} \right)} \right] \quad (\text{D29})$$

which after some algebra reduces to the Eq. (D21).

Similarly,  $H[\ell]$  has the following expression

$$H[\ell] = \frac{\sigma \mathcal{A}_{lg}}{1 - e^{-2\kappa(R+\ell)}} \quad (\text{D30})$$

where  $\sigma$  is the surface tension for the planar liquid-gas interface, with area  $\mathcal{A}_{lg} = 4\pi(R+\ell)^2$ . The diagrammatic expansion Eq. (78) can be evaluated explicitly [57], where now the basic diagrams are

$$\begin{aligned} \text{Diagram 1} &= -e^{-2\kappa(R+\ell)} \quad (\text{D31}) \\ \text{Diagram 2} &= -e^{-2\kappa(R+\ell)} \quad (\text{D32}) \end{aligned}$$

$$\text{Diagram 3} = 4\pi(R+\ell)^2 \quad (\text{D33})$$

leading after resummation to Eq. (D30).

We turn to the evaluation of  $W[\ell, \psi]$ , which has the following expression

$$\begin{aligned} W[\ell, \psi] &= 2\kappa m_0 \left( -\frac{h_1 + gm_0}{g - \kappa - \frac{1}{R}} \right) \frac{\sqrt{\mathcal{A}_{wl} \mathcal{A}_{lg}} e^{-\kappa \ell}}{1 - \frac{g + \kappa - \frac{1}{R}}{g - \kappa - \frac{1}{R}} e^{-2\kappa \ell}} \\ &+ \frac{g + \kappa - \frac{1}{R}}{g - \kappa - \frac{1}{R}} \left( \frac{\kappa m_0^2}{1 - e^{-2\kappa(R+\ell)}} \right) \frac{\mathcal{A}_{lg} e^{-2\kappa \ell}}{1 - \frac{g + \kappa - \frac{1}{R}}{g - \kappa - \frac{1}{R}} e^{-2\kappa \ell}} \\ &+ \kappa \left( \frac{h_1 + gm_0}{g - \kappa - \frac{1}{R}} \right)^2 \frac{\mathcal{A}_{wl} e^{-2\kappa \ell}}{1 - \frac{g + \kappa - \frac{1}{R}}{g - \kappa - \frac{1}{R}} e^{-2\kappa \ell}} \quad (\text{D34}) \end{aligned}$$

This expression reduces to Eq. (D1) for  $R \rightarrow \infty$ , and it is consistent with those reported in Refs. [40, 60] if the exponential term  $\exp(-2\kappa(R+\ell))$  in Eq. (D34) is neglected.

As in the planar case, we will reproduce this result within the non-local model. We will first consider the decorated version of the original non-local model. In this formalism, the basic diagrams for this model are the following

$$\text{Diagram 1} = 4\pi(R+\ell)^2 \quad (\text{D35})$$

$$\text{Diagram 2} = 4\pi R^2 \quad (\text{D36})$$

$$\text{Diagram 3} = \left(1 + \frac{\ell}{R}\right) (1 - e^{-2\kappa R}) e^{-\kappa \ell} \quad (\text{D37})$$

$$\text{Diagram 4} = \frac{1 - e^{-2\kappa R}}{1 + \frac{\ell}{R}} e^{-\kappa \ell} \quad (\text{D38})$$

$$\text{Diagram 5} = -e^{-2\kappa R} \quad (\text{D39})$$

$$\text{Diagram 6} = -e^{-2\kappa(R+\ell)} \quad (\text{D40})$$

$$\text{Diagram 7} = -\frac{1}{\kappa R} (1 - (1 + \kappa R)e^{-2\kappa R}) \quad (\text{D41})$$

Note that, as for the planar case, the diagrams do not depend on the position associated to the open circle, so a general diagram can be obtained as a product of its bonds contributions. In order to resum all the contributions to  $\Omega_n^n$ ,  $\Omega_{n+1}^n$  and  $\Omega_{n+1}^{n+1}$ , we have to sum the contributions of all possible segments either on the wall or on the liquid-gas interface in a similar manner as we did for the evaluation of  $\mathcal{F}_{wl}$ . The resummation of all the contributions of the segments of consecutive ( $U$ ) bonds on the liquid-gas interface is

$$I_\ell = \frac{1}{1 - e^{-2\kappa(R+\ell)}} \quad (\text{D42})$$

On the other hand, the analogous expression for a segment of consecutive bonds on the wall depends on its position in the diagram. If the segment is on an extreme of the full diagram, its contribution is

$$I_\psi^1 = \frac{g}{g - \kappa - \frac{1}{R}} \frac{1}{1 - e^{-2\kappa R}} \quad (\text{D43})$$

Otherwise, the contribution of the segment is

$$I_\psi^2 = \left( \frac{1}{1 - e^{-2\kappa R}} \right) \left( 1 + \frac{2\kappa}{g - k - \frac{1}{R}} \frac{1}{1 - e^{-2\kappa R}} \right) \quad (\text{D44})$$

With these results, Eqs. (108), (109) and (110) reduce to

$$\Omega_1^1 = 8\pi R(R + \ell) \left( \frac{g}{g - k - \frac{1}{R}} \right) \frac{e^{-\kappa\ell}}{1 - e^{-2\kappa(R+\ell)}} \quad (\text{D45})$$

$$\Omega_1^2 = 4\pi(R + \ell)^2 \left( \frac{1 - e^{-2\kappa R}}{1 - e^{-2\kappa(R+\ell)}} \right) \times \left( 1 + \frac{2\kappa}{g - k - \frac{1}{R}} \frac{1}{1 - e^{-2\kappa R}} \right) \frac{e^{-2\kappa\ell}}{1 - e^{-2\kappa(R+\ell)}} \quad (\text{D46})$$

$$\Omega_2^1 = 4\pi R^2 \left( \frac{g}{g - k - \frac{1}{R}} \right)^2 \frac{e^{-2\kappa\ell}}{1 - e^{-2\kappa(R+\ell)}} \quad (\text{D47})$$

For higher order contributions

$$\Omega_n^n = \Omega_1^1 \left[ \left( \frac{1 - e^{-2\kappa R}}{1 - e^{-2\kappa(R+\ell)}} \right) \times \left( 1 + \frac{2\kappa}{g - k - \frac{1}{R}} \frac{1}{1 - e^{-2\kappa R}} \right) e^{-2\kappa\ell} \right]^{n-1} \quad (\text{D48})$$

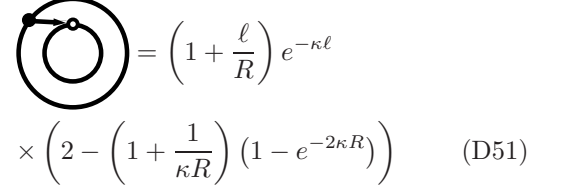
$$\Omega_n^{n+1} = \Omega_1^2 \left[ \left( \frac{1 - e^{-2\kappa R}}{1 - e^{-2\kappa(R+\ell)}} \right) \times \left( 1 + \frac{2\kappa}{g - k - \frac{1}{R}} \frac{1}{1 - e^{-2\kappa R}} \right) e^{-2\kappa\ell} \right]^{n-1} \quad (\text{D49})$$

$$\Omega_{n+1}^n = \Omega_2^1 \left[ \left( \frac{1 - e^{-2\kappa R}}{1 - e^{-2\kappa(R+\ell)}} \right) \times \left( 1 + \frac{2\kappa}{g - k - \frac{1}{R}} \frac{1}{1 - e^{-2\kappa R}} \right) e^{-2\kappa\ell} \right]^{n-1} \quad (\text{D50})$$

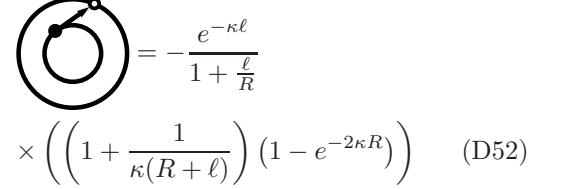
As in the planar case, the resummation of the series Eq. (136) leads to Eq. (D34).

In order to check the new formulation for the non-local model for fixed boundary conditions on the wall, we will

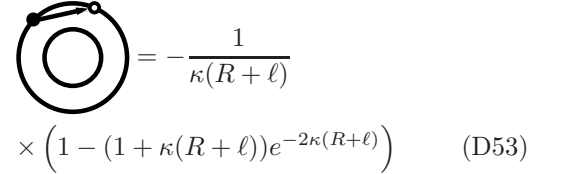
make use of the diagrams



$$\begin{aligned} & \text{Diagram} = \left( 1 + \frac{\ell}{R} \right) e^{-\kappa\ell} \\ & \times \left( 2 - \left( 1 + \frac{1}{\kappa R} \right) (1 - e^{-2\kappa R}) \right) \quad (\text{D51}) \end{aligned}$$



$$\begin{aligned} & \text{Diagram} = -\frac{e^{-\kappa\ell}}{1 + \frac{\ell}{R}} \\ & \times \left( \left( 1 + \frac{1}{\kappa(R+\ell)} \right) (1 - e^{-2\kappa R}) \right) \quad (\text{D52}) \end{aligned}$$



$$\begin{aligned} & \text{Diagram} = -\frac{1}{\kappa(R+\ell)} \\ & \times \left( 1 - (1 + \kappa(R+\ell)) e^{-2\kappa(R+\ell)} \right) \quad (\text{D53}) \end{aligned}$$

The total contribution of the segments of the diagrams on the liquid-gas interface now depends on its positions. The leftmost one is composed by  $U$  bonds, and it has a contribution  $I_\ell$  given by Eq. (D42). Otherwise, the segments are composed by  $\partial K/\kappa$  bonds, with a contribution

$$I'_\ell = \frac{1}{\left( 1 + \frac{1}{\kappa(R+\ell)} \right) (1 - e^{-2\kappa(R+\ell)})} \quad (\text{D54})$$

Similarly, the segments of the diagrams on the wall on the left extreme of the diagram contribute as

$$(I'_\psi)^1 = \frac{1}{1 - e^{-2\kappa R}} \quad (\text{D55})$$

which is the limit of Eq. (D43) when  $g \rightarrow -\infty$ , and otherwise as

$$(I'_\psi)^2 = \frac{1}{2 - \left( 1 + \frac{1}{\kappa R} \right) (1 - e^{-2\kappa R})} \quad (\text{D56})$$

Thus, the expressions from Eqs. (137), (138) and (139) for  $\Omega_1^1$ ,  $\Omega_1^2$  and  $\Omega_2^1$  can be resummed as

$$\Omega_1^1 = 8\pi R(R + \ell) \frac{e^{-\kappa\ell}}{1 - e^{-2\kappa(R+\ell)}} \quad (\text{D57})$$

$$\Omega_1^2 = 4\pi(R + \ell)^2 \left( \frac{1 - e^{-2\kappa R}}{(1 - e^{-2\kappa(R+\ell)})^2} \right) e^{-2\kappa\ell} \quad (\text{D58})$$

$$\Omega_2^1 = 4\pi R^2 \frac{e^{-2\kappa\ell}}{1 - e^{-2\kappa(R+\ell)}} \quad (\text{D59})$$

and for higher-order contributions we get that

$$\Omega_n^n = \Omega_1^1 \left[ \left( \frac{1 - e^{-2\kappa R}}{1 - e^{-2\kappa(R+\ell)}} \right) e^{-2\kappa\ell} \right]^{n-1} \quad (\text{D60})$$

$$\Omega_n^{n+1} = \Omega_1^2 \left[ \left( \frac{1 - e^{-2\kappa R}}{1 - e^{-2\kappa(R+\ell)}} \right) e^{-2\kappa\ell} \right]^{n-1} \quad (\text{D61})$$

$$\Omega_{n+1}^n = \Omega_2^1 \left[ \left( \frac{1 - e^{-2\kappa R}}{1 - e^{-2\kappa(R+\ell)}} \right) e^{-2\kappa\ell} \right]^{n-1} \quad (\text{D62})$$

which coincide with the expressions Eqs. (D45)-(D50) in the limit  $g \rightarrow -\infty$ .

### 3. Cylindrical interfaces


Finally, we will consider the problem of wetting around a cylinder of radius  $R$  and length  $L$  (large enough to neglect border effects), where the liquid-gas interfacial configuration is a concentric cylinder of radius  $R + \ell$ . In this case,  $\mathcal{F}_{wl}[\psi]$  is given by

$$\mathcal{F}_{wl}[\psi] = \sigma_{wl} \mathcal{A}_{wl} \frac{\frac{K_1(\kappa R)}{K_0(\kappa R)}}{1 - \frac{\kappa}{\kappa - g} \left(1 - \frac{K_1(\kappa R)}{K_0(\kappa R)}\right)} \quad (\text{D63})$$


where  $\sigma_{wl}$  is the surface tension for the planar wall-liquid interface,  $\mathcal{A}_{wl} = 2\pi RL$  is the area of the cylinder and  $K_0$  and  $K_1$  are the modified Bessel functions of the second kind and order 0 and 1, respectively. For large  $\kappa R$ , this expression can be approximated as

$$\mathcal{F}_{wl}[\psi] = \sigma_{wl} \mathcal{A}_{wl} \left[ 1 - \left(\frac{g}{\kappa - g}\right) \frac{1}{2\kappa R} + \left(\frac{g}{\kappa - g}\right) \left(1 + \frac{2\kappa}{\kappa - g}\right) \frac{1}{(2\kappa R)^2} + \mathcal{O}(R^{-3}) \right] \quad (\text{D64})$$

which satisfies Eq. (44) since the mean curvature and the Gaussian curvature on the cylinder are  $H = -1/2R$  and  $K_G = 0$ , respectively. Eq. (D63) can be obtained in a similar way as in the spherical case from the diagrammatic expansion Eq. (55), where the relevant diagrams are



$$= 2\kappa R I_0(\kappa R) K_0(\kappa R) - 1 \quad (\text{D65})$$



$$= 2\kappa R I_1(\kappa R) K_0(\kappa R) = 1 - 2\kappa R I_0(\kappa R) K_1(\kappa R) \quad (\text{D66})$$



$$= 2\pi R L \quad (\text{D67})$$

where  $I_0$  and  $I_1$  are the modified Bessel function of the first kind and order 0 and 1, respectively. Note that as in the planar and spherical cases, they are independent of the position of the open circle. Thus, as in these previous cases the contribution of each diagram is the product of its bonds.


Similarly,  $H[\ell]$  has the following expression

$$H[\ell] = \frac{\sigma \mathcal{A}_{lg}}{2\kappa R K_0(\kappa(R + \ell)) I_0(\kappa(R + \ell))} \quad (\text{D68})$$

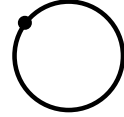
where  $\sigma$  is the surface tension for the planar liquid-gas interface, with area  $\mathcal{A}_{lg} = 2\pi(R + \ell)L$ . For large  $\kappa R$ , Eq. (D68) yields

$$H[\ell] \approx \sigma \mathcal{A}_{lg} \left(1 - \frac{1}{8(\kappa R)^2}\right) \quad (\text{D69})$$

in agreement with Eq. (68). The diagrammatic expansion Eq. (78) can be also evaluated explicitly in this case, where now the basic diagrams are



$$= 2\kappa(R + \ell) I_0(\kappa(R + \ell)) K_0(\kappa(R + \ell)) - 1 \quad (\text{D70})$$



$$= 2\pi(R + \ell)L \quad (\text{D71})$$

After resummation of Eq. (78), we recover Eq. (D68).

Finally the binding potential  $W[\ell, \psi]$  has the following expression

$$W[\ell, \psi] = \left(\frac{\pi L}{\kappa \Delta}\right) \left[ 2\kappa m_0 \left(-\frac{h_1 + gm_0}{g}\right) + \kappa \left(\frac{h_1 + gm_0}{g}\right)^2 \left(\frac{1}{1 - \frac{\kappa}{g} \frac{K_1(\kappa R)}{K_0(\kappa R)}}\right) \left(\frac{K_0(\kappa(R + \ell))}{K_0(\kappa R)}\right) + \kappa m_0^2 \frac{I_0(\kappa R)}{I_0(\kappa(R + \ell))} \left(1 + \frac{\kappa}{g} \frac{I_1(\kappa R)}{I_0(\kappa R)}\right) \right] \quad (\text{D72})$$

where  $\Delta$  is defined as

$$\Delta = I_0(\kappa(R + \ell)) K_0(\kappa R) \left(1 - \frac{\kappa}{g} \frac{K_1(\kappa R)}{K_0(\kappa R)}\right) - K_0(\kappa(R + \ell)) I_0(\kappa R) \left(1 + \frac{\kappa}{g} \frac{I_1(\kappa R)}{I_0(\kappa R)}\right) \quad (\text{D73})$$

The modified Bessel functions can be approximated asymptotically for large values of their arguments as


$$K_0(x) \sim K_1(x) \sim \sqrt{\frac{\pi}{2x}} e^{-x} \left(1 + \mathcal{O}\left(\frac{1}{x}\right)\right) \\ I_0(x) \sim I_1(x) \sim \sqrt{\frac{1}{2\pi x}} e^x \left(1 + \mathcal{O}\left(\frac{1}{x}\right)\right) \quad (\text{D74})$$

Thus, Eq. (D72) reduces for large  $\kappa R$  to

$$W[\ell, \psi] = 2\kappa m_0 \left(-\frac{h_1 + gm_0}{g - \kappa}\right) \frac{\sqrt{\mathcal{A}_{wl} \mathcal{A}_{lg}} e^{-\kappa \ell}}{1 - \frac{g + \kappa}{g - \kappa} e^{-2\kappa \ell}} + \frac{g + \kappa}{g - \kappa} \kappa m_0^2 \frac{\mathcal{A}_{lg} e^{-2\kappa \ell}}{1 - \frac{g + \kappa}{g - \kappa} e^{-2\kappa \ell}} + \kappa \left(\frac{h_1 + gm_0}{g - \kappa}\right)^2 \frac{\mathcal{A}_{wl} e^{-2\kappa \ell}}{1 - \frac{g + \kappa}{g - \kappa} e^{-2\kappa \ell}} \quad (\text{D75})$$

up to corrections of order of  $(\kappa R)^{-1}$  and  $(\kappa(R + \ell))^{-1}$ . This expression is consistent with the expression reported in Ref. [60], and it reduces to Eq. (D1) for  $R \rightarrow \infty$ .


This result can be also obtained within the non-local model. We will first consider the decorated version of the original non-local model. In this formalism, the basic diagrams model are the following




$$= 2\pi(R + \ell)L \quad (\text{D76})$$




$$= 2\pi RL \quad (\text{D77})$$




$$= 2\kappa(R + \ell)I_0(\kappa R)K_0(\kappa(R + \ell)) \quad (\text{D78})$$




$$= 2\kappa RI_0(\kappa R)K_0(\kappa(R + \ell)) \quad (\text{D79})$$



$$= 2\kappa RI_0(\kappa R)K_0(\kappa R) \quad (\text{D80})$$



$$= 2\kappa(R + \ell)I_0(\kappa(R + \ell))K_0(\kappa(R + \ell)) \quad (\text{D81})$$



$$= 2\kappa RI_1(\kappa R)K_0(\kappa R) - 1 \quad (\text{D82})$$

Again these diagrams do not depend on the position associated to the open circle. We proceed as in the spherical case to obtain the expressions of  $\Omega_n^n$ ,  $\Omega_{n+1}^n$  and  $\Omega_n^{n+1}$ . The resummation of all the contributions of the segments of consecutive ( $U$ ) bonds on the liquid-gas interface is

$$I_\ell = \frac{1}{2\kappa(R + \ell)I_0(\kappa(R + \ell))K_0(\kappa(R + \ell))} \quad (\text{D83})$$

On the other hand, segments on the wall contribute as

$$I_\psi^1 = \left( \frac{1}{1 - \frac{\kappa K_1(\kappa R)}{g K_0(\kappa R)}} \right) \frac{1}{2\kappa RI_0(\kappa R)K_0(\kappa R)} \quad (\text{D84})$$

if the segment is at any of the extremes of the diagram, and otherwise

$$I_\psi^2 = \left( \frac{1 + \frac{\kappa I_1(\kappa R)}{g I_0(\kappa R)}}{1 - \frac{\kappa K_1(\kappa R)}{g K_0(\kappa R)}} \right) \frac{1}{2\kappa RI_0(\kappa R)K_0(\kappa R)} \quad (\text{D85})$$

With these results, Eqs. (108), (109) and (110) reduce to

$$\Omega_1^1 = \frac{2\pi L}{\kappa K_0(\kappa R)I_0(\kappa(R + \ell))} \left( \frac{1}{1 - \frac{\kappa K_1(\kappa R)}{g K_0(\kappa R)}} \right) \quad (\text{D86})$$

$$\Omega_1^2 = \frac{\pi L}{\kappa K_0(\kappa R)I_0(\kappa(R + \ell))} \left( \frac{I_0(\kappa R)}{I_0(\kappa(R + \ell))} \right) \times \left( \frac{1 + \frac{\kappa I_1(\kappa R)}{g I_0(\kappa R)}}{1 - \frac{\kappa K_1(\kappa R)}{g K_0(\kappa R)}} \right) \quad (\text{D87})$$

$$\Omega_2^1 = \frac{\pi L}{\kappa K_0(\kappa R)I_0(\kappa(R + \ell))} \left( \frac{K_0(\kappa(R + \ell))}{K_0(\kappa R)} \right) \times \left( \frac{1}{1 - \frac{\kappa K_1(\kappa R)}{g K_0(\kappa R)}} \right)^2 \quad (\text{D88})$$

For higher order contributions

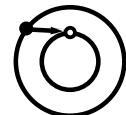
$$\Omega_n^n = \Omega_1^1 \left[ \left( \frac{I_0(\kappa R)K_0(\kappa(R + \ell))}{I_0(\kappa(R + \ell))K_0(\kappa R)} \right) \times \left( \frac{1 + \frac{\kappa I_1(\kappa R)}{g I_0(\kappa R)}}{1 - \frac{\kappa K_1(\kappa R)}{g K_0(\kappa R)}} \right) \right]^{n-1} \quad (\text{D89})$$

$$\Omega_n^{n+1} = \Omega_2^1 \left[ \left( \frac{I_0(\kappa R)K_0(\kappa(R + \ell))}{I_0(\kappa(R + \ell))K_0(\kappa R)} \right) \times \left( \frac{1 + \frac{\kappa I_1(\kappa R)}{g I_0(\kappa R)}}{1 - \frac{\kappa K_1(\kappa R)}{g K_0(\kappa R)}} \right) \right]^{n-1} \quad (\text{D90})$$


$$\Omega_{n+1}^n = \Omega_2^1 \left[ \left( \frac{I_0(\kappa R)K_0(\kappa(R + \ell))}{I_0(\kappa(R + \ell))K_0(\kappa R)} \right) \times \left( \frac{1 + \frac{\kappa I_1(\kappa R)}{g I_0(\kappa R)}}{1 - \frac{\kappa K_1(\kappa R)}{g K_0(\kappa R)}} \right) \right] \quad (\text{D91})$$

which lead to Eq. (D72) after resummation of the series Eq. (136).


For the new formulation of the non-local model for fixed boundary conditions on the wall, we consider the diagrams



$$= 2\kappa(R + \ell)I_1(\kappa R)K_0(\kappa(R + \ell)) \quad (\text{D92})$$



$$= -2\kappa RI_0(\kappa R)K_1(\kappa(R + \ell)) \quad (\text{D93})$$



$$= 2\kappa(R + \ell)I_1(\kappa(R + \ell))K_0(\kappa(R + \ell)) - 1 \quad (\text{D94})$$

The contributions of segments on the liquid-gas interface are given by Eq. (D83) if the segment is on the left extreme, and otherwise by

$$I'_\ell = \frac{1}{2\kappa(R+\ell)I_0(\kappa(R+\ell))K_1(\kappa(R+\ell))} \quad (\text{D95})$$

Similarly, the segments of the diagrams on the wall on the left extreme of the diagram contribute as

$$(I')^1_\psi = \frac{1}{2\kappa R I_0(\kappa R) K_0(\kappa R)} \quad (\text{D96})$$

and otherwise as

$$(I')^2_\psi = \frac{1}{2\kappa R I_1(\kappa R) K_0(\kappa(R+\ell))} \quad (\text{D97})$$

The expressions from Eqs. (137), (138) and (139) for  $\Omega_1^1$ ,  $\Omega_1^2$  and  $\Omega_2^1$  are

$$\Omega_1^1 = \frac{2\pi L}{\kappa K_0(\kappa R) I_0(\kappa(R+\ell))} \quad (\text{D98})$$

$$\Omega_1^2 = \frac{\pi L}{\kappa K_0(\kappa R) I_0(\kappa(R+\ell))} \left( \frac{I_0(\kappa R)}{I_0(\kappa(R+\ell))} \right) \quad (\text{D99})$$

$$\Omega_2^1 = \frac{\pi L}{\kappa K_0(\kappa R) I_0(\kappa(R+\ell))} \left( \frac{K_0(\kappa(R+\ell))}{K_0(\kappa R)} \right) \quad (\text{D100})$$

and for higher order contributions

$$\Omega_n^n = \Omega_1^1 \left( \frac{I_0(\kappa R) K_0(\kappa(R+\ell))}{I_0(\kappa(R+\ell)) K_0(\kappa R)} \right)^{n-1} \quad (\text{D101})$$

$$\Omega_n^{n+1} = \Omega_1^2 \left( \frac{I_0(\kappa R) K_0(\kappa(R+\ell))}{I_0(\kappa(R+\ell)) K_0(\kappa R)} \right)^{n-1} \quad (\text{D102})$$

$$\Omega_{n+1}^n = \Omega_2^1 \left( \frac{I_0(\kappa R) K_0(\kappa(R+\ell))}{I_0(\kappa(R+\ell)) K_0(\kappa R)} \right)^{n-1} \quad (\text{D103})$$

which correspond to Eqs. (D86)-(D91) in the limit  $g \rightarrow -\infty$ .

- 
- [1] R. Evans, *Adv. Phys.* **28**, 143 (1979).  
[2] S. Dietrich, in *Phase Transitions and Critical Phenomena*, edited by C. Domb and J. L. Lebowitz (Academic Press, New York, 1988), vol. 12.  
[3] M. Schick, in *Liquids at Interfaces*, edited by J. F. J. J. Charvolin and J. Zinn-Justin (Elsevier, Amsterdam, 1990).  
[4] G. Forgacs, R. Lipowsky, and T. M. Nieuwenhuizen, in *Phase Transitions and Critical Phenomena*, edited by C. Domb and J. L. Lebowitz (Academic Press, New York, 1991), vol. 14.  
[5] J. K. Lee, J. A. Barker, and G. M. Pound, *J. Chem. Phys.* **60**, 1976 (1974).  
[6] L. A. Rowley, D. Nicholson, and N. G. Parsonage, *Mol. Phys.* **31**, 365 (1976).  
[7] R. Evans, in *Fundamentals of Inhomogeneous Fluids*, edited by D. Henderson (Dekker, New York, 1992).  
[8] F. P. Buff, R. A. Lovett, and F. H. Stillinger, *Phys. Rev. Lett.* **15**, 621 (1965).  
[9] J. D. Weeks, *J. Chem. Phys.* **67**, 3106 (1977).  
[10] D. Bedeaux and J. D. Weeks, *J. Chem. Phys.* **82**, 972 (1985).  
[11] E. Brézin, B. I. Halperin, and S. Leibler, *Phys. Rev. Lett.* **50**, 1387 (1983).  
[12] D. S. Fisher and D. A. Huse, *Phys. Rev. B* **32**, 247 (1985).  
[13] G. Delfino and A. Squarcini, *J. Stat. Mech. Theory Exp.* **2013**, P05010 (2013).  
[14] A. O. Parry, C. Rascón, and A. J. Wood, *Phys. Rev. Lett.* **83**, 5535 (1999).  
[15] A. O. Parry, C. Rascón, and A. J. Wood, *Phys. Rev. Lett.* **85**, 345 (2000).  
[16] A. O. Parry, A. J. Wood, and C. Rascón, *J. Phys.: Condens. Matter* **12**, 7671 (2000).  
[17] A. O. Parry, A. J. Wood, and C. Rascón, *J. Phys.: Condens. Matter* **13**, 4591 (2001).  
[18] J. M. Romero-Enrique and A. O. Parry, *EPL* **72**, 1004 (2005).  
[19] J. M. Romero-Enrique and A. O. Parry, *J. Phys.: Condens. Matter* **17**, S3487 (2005).  
[20] J. M. Romero-Enrique and A. O. Parry, *New J. Phys.* **9**, 167 (2007).  
[21] J. M. Romero-Enrique, A. Rodríguez-Rivas, L. F. Rull, and A. O. Parry, *Soft Matter* **9**, 7069 (2013).  
[22] A. Rodríguez-Rivas, J. M. Romero-Enrique, L. F. Rull, and A. Milchev, *EPL* **108**, 26003 (2014).  
[23] G. Delfino and A. Squarcini, *Phys. Rev. Lett.* **113**, 066101 (2014).  
[24] J. S. Rowlinson and B. Widom, *Molecular Theory of Capillarity* (Clarendon, Oxford, 1982).  
[25] E. Chacón and P. Tarazona, *Phys. Rev. Lett.* **91**, 166103 (2003).  
[26] P. Tarazona and E. Chacón, *Phys. Rev. B* **70**, 235407 (2004).  
[27] E. Chacón and P. Tarazona, *J. Phys.: Condens. Matter* **17**, S3493 (2005).  
[28] E. Chacón, P. Tarazona, and J. Alejandre, *J. Chem. Phys.* **125**, 014709 (2006).  
[29] E. Chacón, P. Tarazona, and L. E. González, *Phys. Rev. B* **74**, 224201 (2006).  
[30] P. Tarazona, R. Checa, and E. Chacón, *Phys. Rev. Lett.* **99**, 196101 (2007).  
[31] R. Delgado-Buscalioni, E. Chacón, and P. Tarazona,

- Phys. Rev. Lett. **101**, 106102 (2008).
- [32] E. M. Fernández, E. Chacón, and P. Tarazona, Phys. Rev. B **84**, 205435 (2011).
- [33] P. Tarazona, E. Chacón, and F. Bresme, J. Phys.: Condens. Matter **24**, 284123 (2012).
- [34] E. M. Fernández, E. Chacón, and P. Tarazona, Phys. Rev. B **86**, 085401 (2012).
- [35] E. M. Fernández, E. Chacón, P. Tarazona, A. O. Parry, and C. Rascón, Phys. Rev. Lett. **111**, 096104 (2013).
- [36] E. M. Fernández, E. Chacón, L. G. MacDowell, and P. Tarazona, Phys. Rev. E **91**, 062404 (2015).
- [37] E. Chacón and P. Tarazona, J. Phys.: Condens. Matter **28**, 244014 (2016).
- [38] J. Hernández-Muñoz, E. Chacón, and P. Tarazona, Phys. Rev. E **94**, 062802 (2016).
- [39] A. O. Parry, J. M. Romero-Enrique, and A. Lazarides, Phys. Rev. Lett. **93**, 086104 (2004).
- [40] A. O. Parry, C. Rascón, N. R. Bernardino, and J. M. Romero-Enrique, J. Phys.: Condens. Matter **18**, 6433 (2006).
- [41] A. O. Parry, C. Rascón, N. R. Bernardino, and J. M. Romero-Enrique, J. Phys.: Condens. Matter **19**, 416105 (2007).
- [42] A. O. Parry, C. Rascón, N. R. Bernardino, and J. M. Romero-Enrique, Phys. Rev. Lett. **100**, 136105 (2008).
- [43] A. O. Parry, J. M. Romero-Enrique, N. R. Bernardino, and C. Rascón, J. Phys.: Condens. Matter **20**, 505102 (2008).
- [44] A. O. Parry, C. Rascón, N. R. Bernardino, and J. M. Romero-Enrique, J. Phys.: Condens. Matter **20**, 494234 (2008).
- [45] N. R. Bernardino, A. O. Parry, C. Rascón, and J. M. Romero-Enrique, J. Phys.: Condens. Matter **21**, 465105 (2009).
- [46] K. Binder, D. P. Landau, and D. M. Kroll, Phys. Rev. Lett. **56**, 2272 (1986).
- [47] M. E. Fisher and A. J. Jin, Phys. Rev. B **44**, 1430 (1991).
- [48] A. J. Jin and M. E. Fisher, Phys. Rev. B **47**, 7365 (1993).
- [49] H. Nakanishi and M. E. Fisher, Phys. Rev. Lett. **49**, 1565 (1982).
- [50] P. Bryk and K. Binder, Phys. Rev. E **88**, 030401 (2013).
- [51] L. Pang, D. P. Landau, and K. Binder, Phys. Rev. Lett. **106**, 236102 (2011).
- [52] C. A. Brebbia and J. Domínguez, *Boundary Elements: an Introductory Course* (Computational Mechanics Publications, Southampton, 1992), 2nd ed.
- [53] J. T. Katsikadelis, *Boundary Elements: Theory and Applications* (Elsevier, Amsterdam, 2002).
- [54] R. Balian and C. Bloch, Ann. Phys. **60**, 401 (1970).
- [55] R. Balian and C. Bloch, Ann. Phys. **64**, 271 (1971).
- [56] R. Balian and C. Bloch, Ann. Phys. **69**, 76 (1972).
- [57] A. O. Parry and C. Rascón, J. Phys.: Condens. Matter **23**, 015004 (2011).
- [58] P.-M. König, R. Roth, and K. R. Mecke, Phys. Rev. Lett. **93**, 160601 (2004).
- [59] E. M. Blokhuis, Phys. Rev. E **87**, 022401 (2013).
- [60] A. O. Parry, C. Rascón, and L. Morgan, J. Chem. Phys. **124**, 151101 (2006).
- [61] W. Helfrich, Z. Naturforsch C **28**, 693 (1973).
- [62] M. E. Fisher and A. J. Jin, Phys. Rev. Lett. **69**, 792 (1992).
- [63] A. J. Jin and M. E. Fisher, Phys. Rev. B **48**, 2642 (1993).
- [64] K. R. Mecke and S. Dietrich, Phys. Rev. E **59**, 6766 (1999).
- [65] A. O. Parry, C. Rascón, G. Willis, and R. Evans, J. Phys.: Condens. Matter **26**, 355008 (2014).